이학박사 학위논문

Position-controlled growth of ZnO nanostructure array on large-area CVD-graphene for flexible piezoelectric pressure sensors

대면적 그래핀 위에 성장한 위치 제어된 산화아연 나노구조 배열 및 이를 이용한 압전 압력센서 응용

2018 년 8 월

서울대학교 물리천문학부 대학원

박 준 범

Doctoral Thesis

Position-controlled growth of ZnO nanostructure array on large-area CVD-graphene for flexible piezoelectric pressure sensors

Jun Beom Park

Department of Physics and Astronomy

Seoul National University

2018

Position-controlled growth of ZnO nanostructure array on large-area CVD-graphene for flexible piezoelectric pressure sensors

대면적 그래핀 위에 성장한 위치 제어된 산화아연 나노구조 배열 및 이를 이용한 압전 압력센서 응용

지도교수 이 규 철

이 논문을 이학박사학위논문으로 제출함

2018 년 6 월

서울대학교 대학원
물리·천문학부
박 준 범

박준범의 박사학위논문을 인준함

2018 년 6 월

위 원 장 김 기 훈 (인)

부 위 원 장 이 규 철 (인)

위 원 노 태 원 (인)

위 원 홍 승 훈 (인)

위 원 이 철 호 (인)

DMS 201020367 박준범 Jun Beom Park, Position-controlled growth of ZnO nanostructure array on large-area CVD-graphene for flexible piezoelectric pressure sensors, 대면적 그래핀 위에 성장한 위치 제어된 산화아연 나노구조 배열 및 이를 이용한 압전 압력센서 응용, Department of Physics and Astronomy, 2018, 155P, Advisor: Prof. Gyu-Chul Yi, Text in English

Abstract

Semiconductor nanostructures fabricated by bottom-up approach have been considered as ideal building blocks for electronic and optoelectronic device applications due to their own easy miniaturization of nanodevices and high crystallinity of the materials. Catalyst-free metal-organic vapor phase epitaxy (MOVPE) growth of ZnO nanostructures demonstrated their high purity and crystallinity with a few crystal defects, thus the method provides the desirable way for nano- and micrometer scale devices. In particular, individually position-controlled and vertically-aligned one-dimensional (1D) nanostructures are desirable for the practical manipulation of these nanodevices. While this can be achieved with a number of specific materials on single-crystalline substrates such as sapphire and silicon wafers, expanding this to more general material/substrate

combinations remains challenging due to limitations in growth compatibility.

To overcome the narrow combination of material/substrate, recently, the growth of 1D nanostructures on two-dimensional (2D) semiconductor layers such as graphene and h-BN has been studied as a method to allow the preparation of vertically aligned 1D nanostructures on traditionally incompatible substrates. There, the 2D layers act as a growth buffer layer that can be easily attached to, and also mechanically/chemically detached from, arbitrary substrates. However, while position-controlled and vertically aligned growth has been performed on mechanically exfoliated 2D layers, this approach cannot allow scalability to a wafer area. This thesis presents the position-controlled selective growth of ZnO nanostructures on CVD-graphene films and demonstrated piezoelectric pressure sensor as a representative device application.

This thesis consists of 7 parts. Chapter 1 decribes general introduction and chapter 2 reviews previous research activities for growing 1D nanostructures on graphene and spatial controlling trials. In chapter 3, the experimental set-ups and procedures for growing nanomaterials and device fabrication using them are described. Chapter 4 describes two different growths of wide bandgap semiconductor nanostructures on graphene films and their characteristics. Chapter 5 propose a way to controlling spatial position and shape of individual ZnO nanostructures on CVD-graphene films. Using the nanostructures grown in a controlled manner, Chapter 6 describes a preparation method for flexible

nanomaterials and demonstration of piezoelectric pressure sensors as a representative application. Finally, chapter 7 summarizes this thesis with a suggestion for future works.

Table of contents

List of figures

List of tables

Introduction

1

1.1. Motivation: Current research status in one-dimensional nanostructures and effort to use various substrates

Bottom-up grown one-dimensional (1D) semiconductor nanostructures have attracted great interest for their potential use for fabricating electronic and optoelectronic nanodevices due to their own easy miniaturization of nanodevices and high crystallinity of the materials.[1-6] Since the bottom-up approach enables to synthesis efficiently high-quality nanomaterials and their heterostructures with only a few crystal defects,[7-9] this has been expected for the potentially ideal way to fabricate functional components for various device applications.[3,4,10,11] In particular, individually position-controlled and vertically aligned 1D nanostructures grown by bottom-up method do not require the conventional lithography and etching process

for shaping or scaling-down the devices toward nanoscale use in integrated circuits.[10,11]

With the advantages of 1D nanostructures to manufacture nanoscale template for device applications, various kinds of nanostructures, such as nanorod, nanowire, nanotube, and so on, have been studied for use in various device applications.[4,12,13] Moreover, the 1D nanostructures could have either large surface-to-volume or aspect ratio, which could enhance the sensitivity of chemical sensors,[14-16] the performance of optoelectronic devices,[17-19] and even piezoelectric response for an energy converting and pressure sensing devices.[4,20-22] Besides, fabrication of quantum heterostructures realizes a way of exploiting the advantages of nanostructures as already predicted in quantum theory, such as ZnO/MgZnO nanorod quantum structures,[23,24] GaP/GaAs superlattice nanowires,[1] and even GaN/ZnO heterostructure nanorod light-emitting-diodes array.[25,26] The novel applications using 1D nanostructures have recently been studied for high-density integration with electronic circuitries, based on silicon technology,[27,28] or wearable

devices for human interfaces as a counterpart of thinfilm devices.[29]

Recent studies to take the advantages of nanostructures have successfully advanced for demonstrating the predictions using individually position-controlled and vertically aligned 1D nanostructures in a desire for the practical nanodevices.[30-32] Nanostructure growth methodology has improved with superior control in shape, dimension, and spatial arrangement that makes it possible to realize various applications.[10,33-36] However, while these can be achieved with many specific materials on single-crystalline substrates such as sapphire and silicon wafers, expanding this to more general material/substrate combinations remain challenging due to limitations in growth compatibility.[34-36] For example, a direct growth on amorphous oxides or metals can often benefit nanoelectronic or optoelectronic applications,[37] but it is difficult to achieve in a well-controlled manner.[16,38,39]

1.2. Objective and approach

The use of 2D layered materials as an interlayer on arbitrary substrates can provide a method to overcome substrate limitation for preparing single-crystalline nanomaterials.[40,41] Although the growth of 1D nanostructures on two-dimensional (2D) semiconductor layers such as graphene and h-BN has been studied on traditionally incompatible substrates,[40,42] such as amorphous oxide, shape- and position-controlled growth of 1D nanomaterials has rarely been reported. Furthermore, the scalability by using CVD-grown 2D layered materials has not been addressed yet. There are some issues to be developed before the growth of nanomaterials on 2D layered materials can be applied into practical use: (1) Which 2D layered material is suitable for growing 1D nanostructures on it? (2) How can we control the position, interdistance, and shape of 1D nanostructures? (3) Can we fabricate heterostructure nanomaterials as like single-crystalline substrate? (4) Can the 1D-2D hybrid nanosystem really overcome substrate limitation as we desire?

These questions have been remained as unsolved challenges and they may be solved by employing the well-established experiments. To resolve the issues as

mentioned above, metal-organic vapor-phase-epitaxy is adopted for growth of nanostructures on CVD-graphene layer in this dissertation. The morphology and positions of the ZnO nanostructures were controlled by changing the growth controlling layer deposited onto CVD-graphene films. The nanostructure growth on graphene layer performed on various substrates including single-crystalline silicon wafer, poly-crystalline metal film, and even on amorphous glass. Interestingly, the graphene layer also served as a buffer for mechanical lift-off to allow the transfer of nanostructures obtained by MOVPE onto the layer. In addition, to address potential application of the nanostructures on graphene layer, piezoelectric pressure sensing applications have been demonstrated to exploit these materials as building blocks.

1.3. Thesis outline

This thesis is composed of seven chapters. Chapter 2 reviews current research activities and history on the growth of one-dimensional semiconductor nanostructure on graphene films and their applications, such as LEDs. Chapter 3

describes experimental procedures including growth, characterization, and device fabrication process. Chapters 4 and 5 describe growth results of wide bandgap semiconductor nanostructures, including ZnO and GaN, on graphene films, and presents position- and shape-controlled growth method of ZnO nanostructure arrays on graphene films, respectively. In Chapter 6, fabrication and characterization of piezoelectric nanotube pressure sensors are presented as an example application using the ZnO nanotube arrays grown on graphene films. Chapter 7 summarizes the conclusion of this thesis with suggestions for future works.

Literature review

2

This chapter reviews the current research activities on the growth of one-dimensional (1D) semiconductor nanostructures on graphene. Recently, the growth of 1D nanostructures on graphene has attracted many researchers as a method to allow the preparation of vertically aligned 1D nanostructures on traditionally incompatible substrates exploiting their layered crystal structures. However, it is an obstacle that position- and shape-controlling of the 1D nanostructures for practical nanoscale applications. While position-controlled and vertically aligned growth has been performed on mechanically exfoliated graphene, this approach is not scalable to a wafer-sized area. There, this chapter begins with an overview of 1D nanostructures grown on graphene that have high electrical characteristics as well as optical transparency and mechanical flexibility & stretchability. In the following section, research activities to control the shape and positions of individual 1D

nanostructures, and the ones on graphene films for practical use of the hybrid dimension nanomaterials.

2.1. One-dimensional semiconductor nanostructure growth on graphene

Graphene has emerged as an ideal material for the next generation flexible electronics for its excellent material characteristics that can provide superior electrical and thermal conductivities,[43-45] optical transparency,[46] and mechanical flexibility, transferability, and endurance. This special material could be prepared using a chemical vapor deposition (CVD) method on metal foils.[47,48] In particular, large-scale roll-to-roll production of graphene has been successfully demonstrated.[49] Bottom-up approach 1D semiconductor nanomaterials including nanorod, nanowire, and nanotubes have attracted due to their easy manipulation and fabrication of various nanodevices,[50] such as light emitting diodes,[26,51] lasers,[52] solar cells,[53] transistors,[29,54] and even piezoelectric applications.[29] In addition, their

small footprint allows the growth of nanomaterials on a large variety of substrates because of the smaller constraints in lattice matching between the nanomaterial and the substrate. Recently, the small contact area between nanostructures and the beneath substrate enabled direct growing 1D nanostructures on graphene.[40,41] This heteroepitaxial growth of 1D semiconductor nanostructures on graphene opened up a new field of nanomaterials by providing a novel way to connect between nanostructures to two-dimensional (2D) molecular science.

2.1.1. ZnO nanostructure growth on graphene

At the early stage, ZnO nanostructures were grown on mechanically exfoliated graphene films using catalyst-free metal-organic vapor phase epitaxy (MOVPE).[40] The graphene sheets were transferred onto SiO_2/Si substrate, and became a growth interlayer for ZnO nanostructures. The grown nanowires were vertically aligned on the graphene layers, while the ones deposited on SiO_2 surface was randomly tilted (Fig. 2.1a). The 1D nanostructures showed not only the high

aspect ratio and the vertical alignment, but also had excellent optical characteristics (Fig. 2.1b). This excellent optical property suggests the high crystallinity of ZnO nanowires. The surface morphology and density of the ZnO nanostructures on the graphene layers were dependent on the growth temperature. Increasing growth temperature lowers the density of nanostructures and makes them longer and thinner. Moreover, the morphology and density of nanostructures are possibly influenced by the surface difference on the graphene substrate; step edge and middle area (Fig. 2.1c).

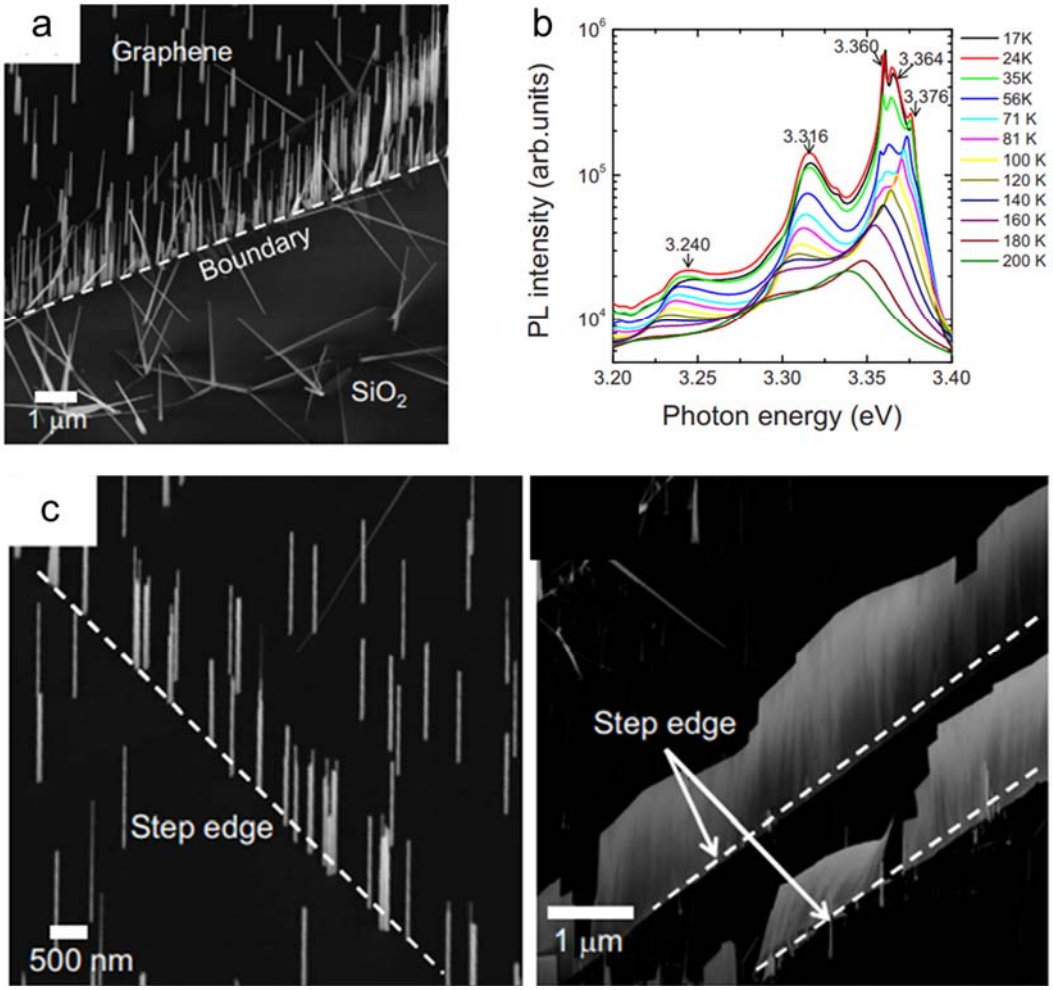

Fig. 2.1. (a) An SEM image of ZnO nanorods grown on mechanically exfoliated graphene films transferred onto SiO_2/Si substrate and (b) corresponding temperature dependent photoluminescence spectra. (c) SEM images of ZnO nanostructures near the step edges of graphene.

The catalyst-assisted CVD growth method was also employed to grow ZnO nanostructures on graphene layers.[31] The authors reported that the surface morphology of the nanostructures could be controlled by tuning the thickness of Au catalyst layer. Figure 2.2 depicts the effect of Au thickness for growing ZnO nanostructures; thin Au layer (0.5 nm) occurs low nucleation density that leads nanorod growth, while thick (2.0 nm) Au layer provides high-density nucleations that motivate nanowall growth. Moreover, the hydrothermal growth of ZnO nanostructures was also successfully demonstrated on mechanically exfoliated graphene layers. The ZnO nanorods were grown only on graphene sheets, while they were not grown on SiO_2 substrate regions (Fig. 2.3a), due to a heteroepitaxial relationship between ZnO and the growth surface. The microstructural investigation proved the heteroepitaxial growth of ZnO nanorod while the crystal orientation of the nanostructures was highly-oriented (0001) direction (Fig. 2.3b).

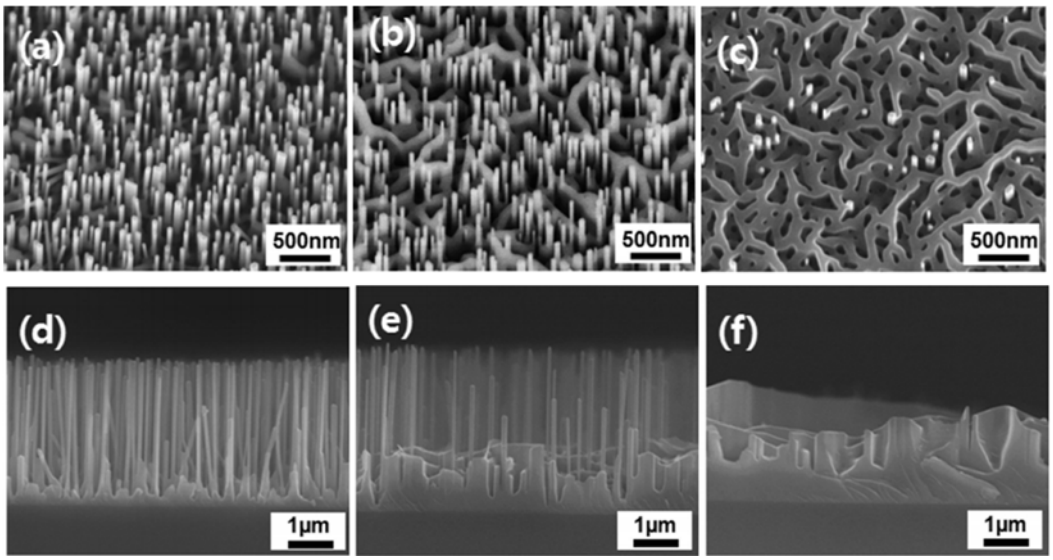

Fig. 2.2. Tilted-view FE-SEM images of ZnO (a) nanowires, (b) nanowire-nanowall hybrid, and (c) nanowall structures. Cross-sectional FE-SEM images of ZnO (d) nanowire, (e) nanowire-nanowall hybrid, and (f) nanowall structures on a graphene/ Al_2O_3 substrate.

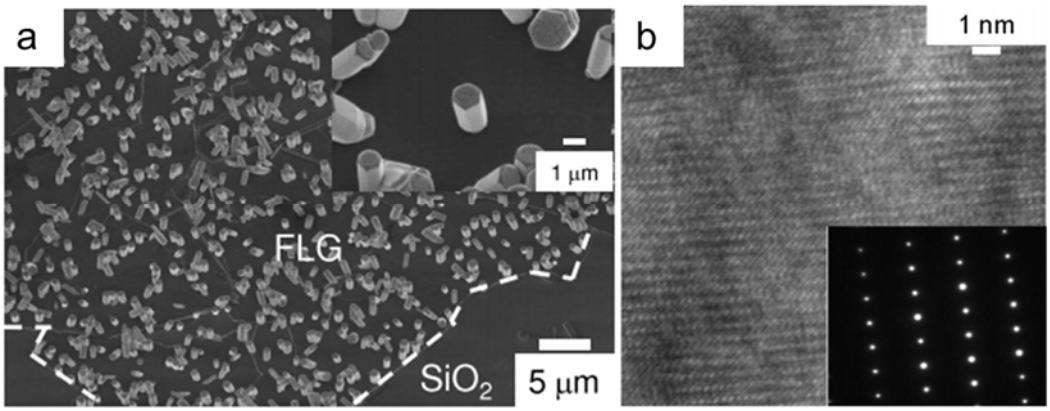

Fig. 2.3. (a) FE-SEM images of ZnO nanostructures on FLG grown using the hydrothermal method. Inset: ZnO nanostructures grew only on FLG sheets; no ZnO grew on the SiO_2 region. (b) High-resolution TEM image of a ZnO nanorod. Inset; SAED pattern of the ZnO nanorod.

2.1.2. III-V compound semiconductor nanostructure growth on graphene

III-V materials have been researched extensively for its various applications, including light emitting devices,[55] power transistors,[56] and photovoltaic cells.[57] However, most of the research has been conducted on a single crystal substrate and thus have a limitation in flexibility and size. To overcome these limitations, a method to grow III-V materials on graphene has been proposed to circumvent the problems by exploiting their layered structure and large-area scalability.

Initial reports have used ZnO nanostructures on graphene as a buffer layer to grow GaN films (Fig. 2.4).[58] Although GaN nucleation would not occur on the basal plane of pristine graphene, it could be heteroepitaxially grown onto ZnO nanostructures, while high-density zinc oxide (ZnO) nanowalls could be grown on oxygen-plasma–treated graphene layers. The nitride thin films grown on graphene layers showed excellent light emitting diode (LED) characteristics during transferring onto foreign substrates such as glass, metal, or plastic. Evolving the

concept of heteroepitaxy growth of GaN on ZnO nanostructures, *Lee et al.* proposed GaN/ZnO heterostructure nanorod LEDs on graphene films (Fig. 2.5).[59] ZnO nanorods grown on graphene layer was employed as a core structure for making the 1D nanostructured shape, and GaN and InGaN layers were radially coated onto the core to provide quantum structure for fabricating LEDs. Thanks to the excellent electric characteristics of graphene films, the LED showed reliable light emission after transfer and bending process.

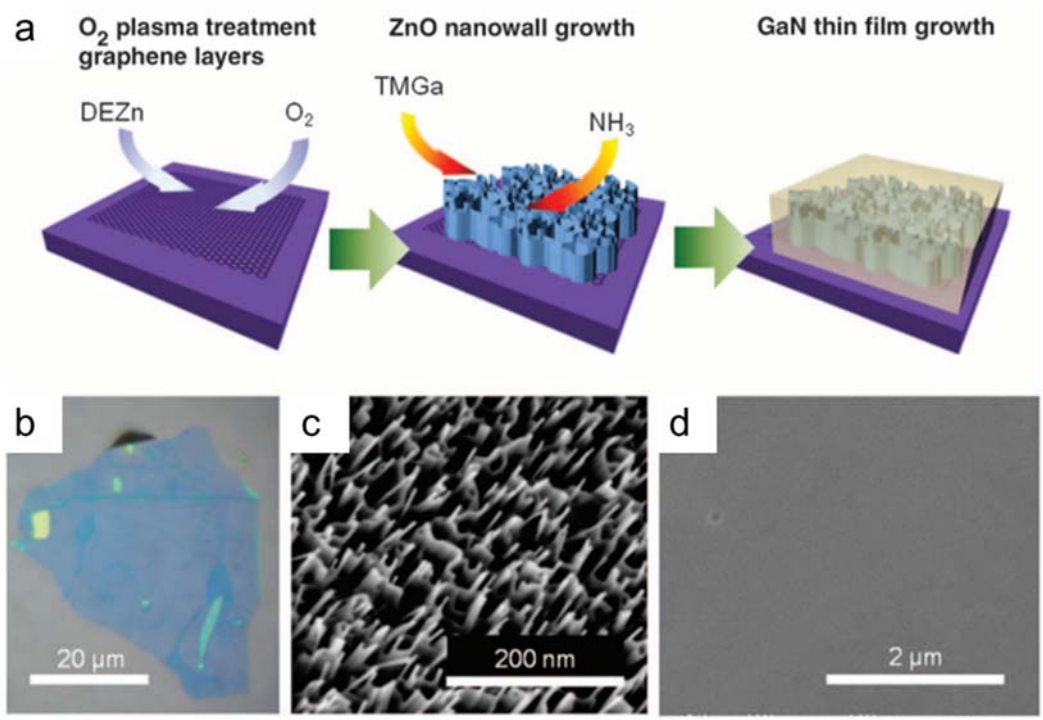

Fig. 2.4. (a) Schematic illustrations of fabrication processes for epitaxial GaN thin films. (b) Optical microscopic image of oxygen-plasma–treated graphene layers. (c and d) SEM images of (c) ZnO nanowalls grown on plasma-treated graphene layers and (d) GaN thin film grown on ZnO nanowalls on plasma-treated graphene layers.

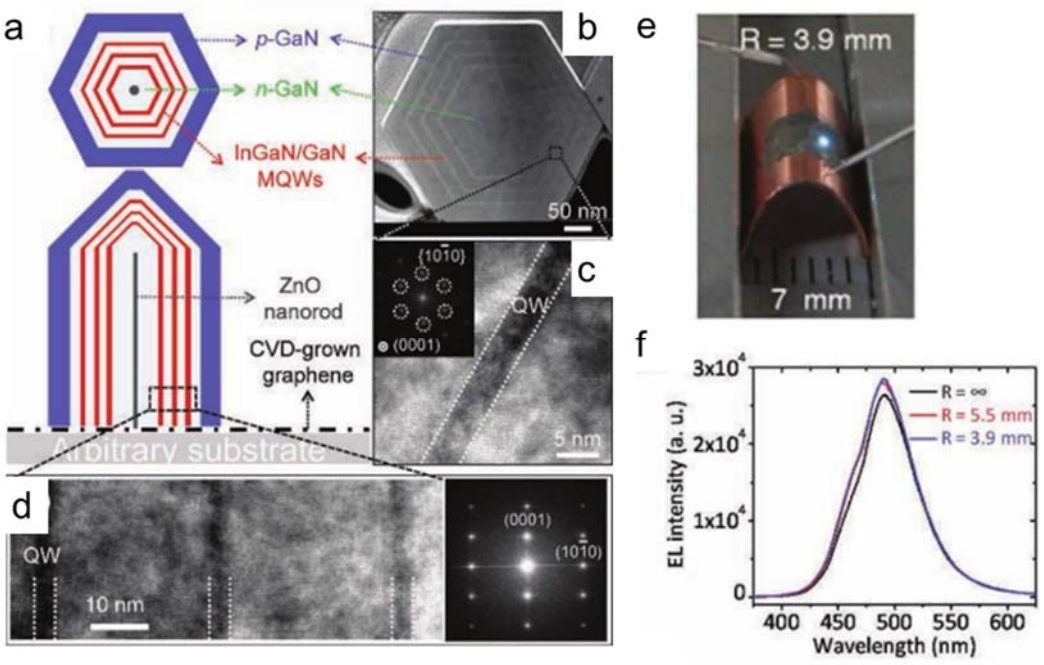

Fig. 2.5. (a, b) Cross-sectional schematic views and STEM image of the coaxially formed GaN-based LED structures. (c, d) High-resolution TEM images of the $In_xGa_{1-x}N$/GaN MQW layers and corresponding diffraction patterns obtained via fast Fourier transform. (e,f) Demonstration of flexible inorganic nanostructure LEDs. (e) A light emission photograph at bending radii of 3.9 mm. c) *I–V* characteristic curves as a function of the bending radius.

There have been reports of III-V nanostructure growth on graphene. GaAs nanowires have been grown using a Ga self-catalyzed VLS technique using a MBE. (Fig. 2.6)[57] The nanowires were grown by predepositing Ga droplets on graphene followed by a subsequent Ga and As flux to form VLS type nanowires. Using this method, vertically aligned GaAs nanowires were obtained while the density of nanowires could be controlled by tuning process temperature. Additionally, the growth of InAs and InGaAs was also performed on the graphene layers using the Au-catalyst assisted MOCVD method. (Fig. 2.7)[60]

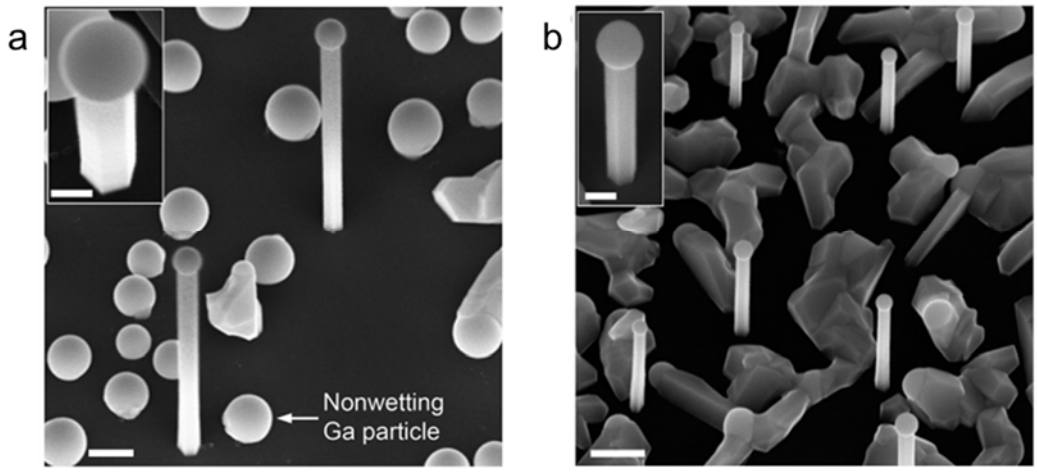

Fig. 2.6. (a) SEM image of nanowires grown on graphite at 610 °C for 10 min with an As flux of 6 × 10^{-6} Torr. The inset shows a near top-view image here the uniform hexagonal side-facets of the nanowire can be seen. (b) SEM image of nanowires grown on graphite by a two-temperature growth technique where the nanowires are nucleated at 540 °C during 10 s of growth under an As flux of 3 × 10^{-6} Torr with further nanowire growth under conditions as in part b but for 5 min. In the inset, a tilted-view image of one of the nanowires shows a uniform hexagonal cross section. The scale bars are 200 nm in the main figures and 100 nm in the insets.

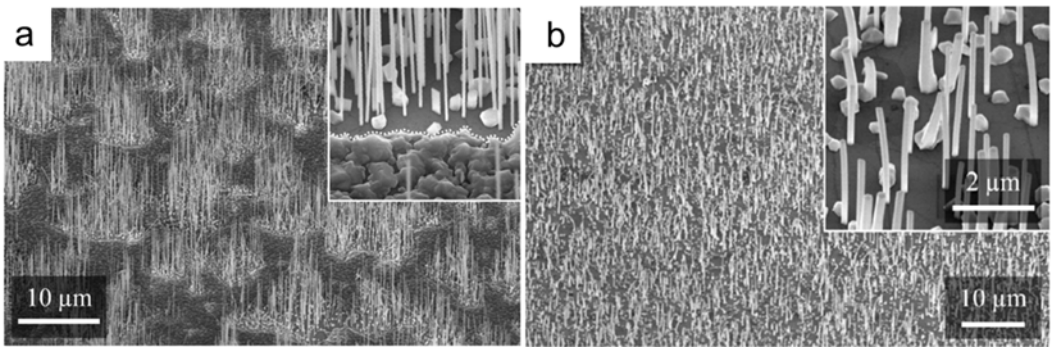

Fig. 2.7. (a) . Selective-area vdW Epi of InAs NWs on graphene. 45° tilted-view SEM image of InAs NWs grown on a discontinuous graphene film. NW growth occurs exclusively on the graphene islands. The inset shows a higher magnification image of the graphene (top)/SiO_2 (bottom) boundary, delineated by the white dotted line. (b) Tilted view of Group 4 $In_xGa_{1-x}As$ NWs ($\xi = 0.52$), with a higher magnification image shown in the inset.

2.2. Position-controlled growth of one-dimensional semiconductor nanostructure growth on graphene films.

Selective growth of semiconductor nanostructures provides an opportunity for the practical manipulation of various device applications since the spatially separated nanostructure arrays enable to fabricate the complex 3D device architectures, such as LED and piezoelectric pressure sensor arrays. Furthermore, the position-controlled selective growth of nanostructures is essential to develop the nano- or microscale integrated devices. While this can be achieved with a number of specific materials on single-crystalline substrates such as sapphire and silicon wafers,[34-36] expanding this to more general material/substrate combinations remains challenging due to limitations in growth compatibility. A few cases have been reported to address this problem. Position-controlled and vertically aligned growth has been performed on mechanically exfoliated graphene, (Fig. 2.8)[61] this approach is not scalable to a wafer-sized area. On the other hand, previous reports of growth on graphene deposited by chemical vapor deposition (CVD-graphene)

have shown poor growth controllability, with a lack of individual position control (i.e., a bundled growth), low growth selectivity, or poor vertical alignment (Fig. 2.9).[62]

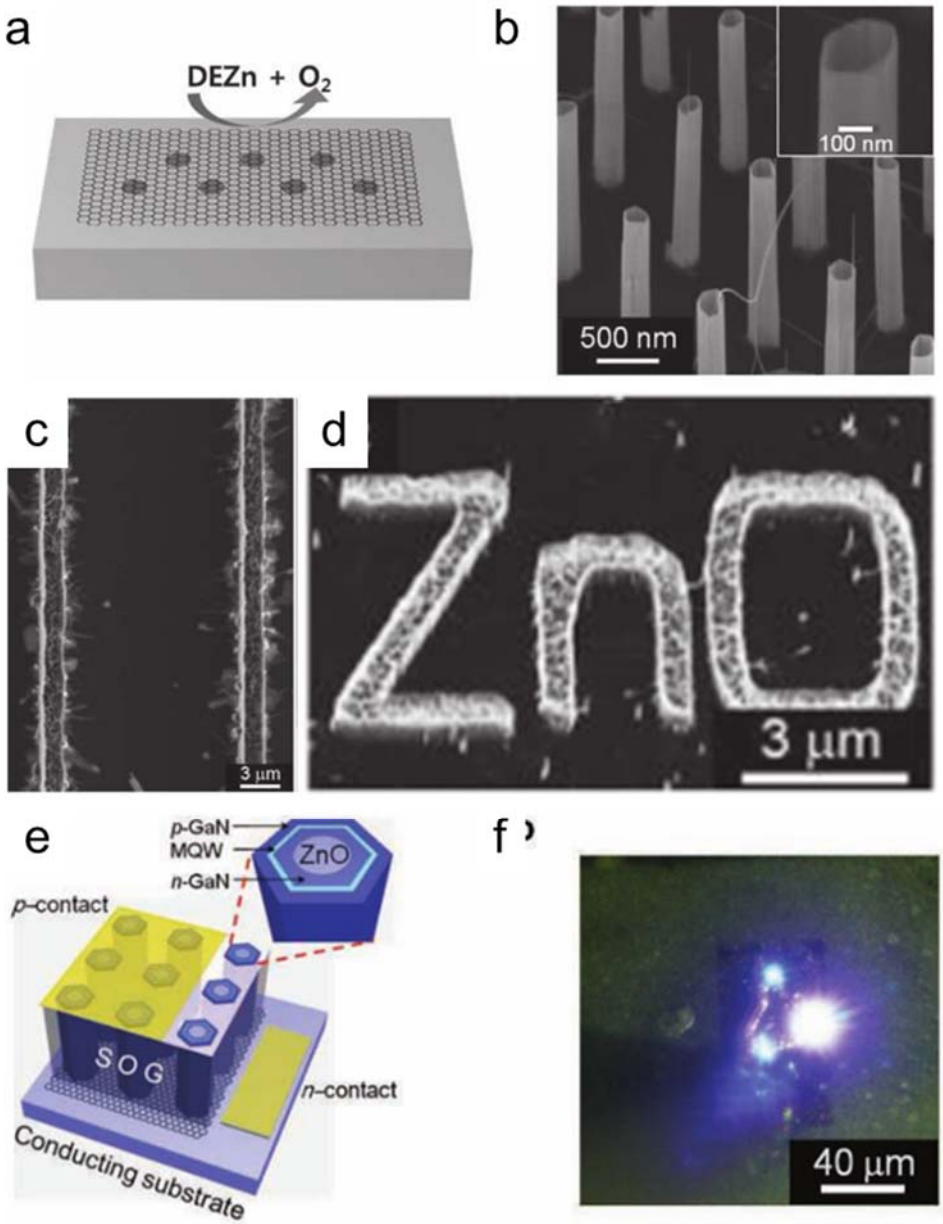

Fig. 2.8. (a) An SEM image of ZnO nanorods grown on mechanically exfoliated graphene films transferred onto SiO_2/Si substrate and (b) corresponding temperature dependent photoluminescence spectra. (c) SEM images of ZnO

nanostructures grown on the graphene at different process temperatures. (d) SEM images of ZnO nanostructures near the step edges of graphene. (e) Schematic image of GaN/$In_xGa_{1-x}N$/GaN/ZnO coaxial quantum nanostructure LEDs with GaN/$In_xGa_{1-x}N$ MQW layers. (f) An optical image of light emission from the LEDs fabricated on the graphene layers.

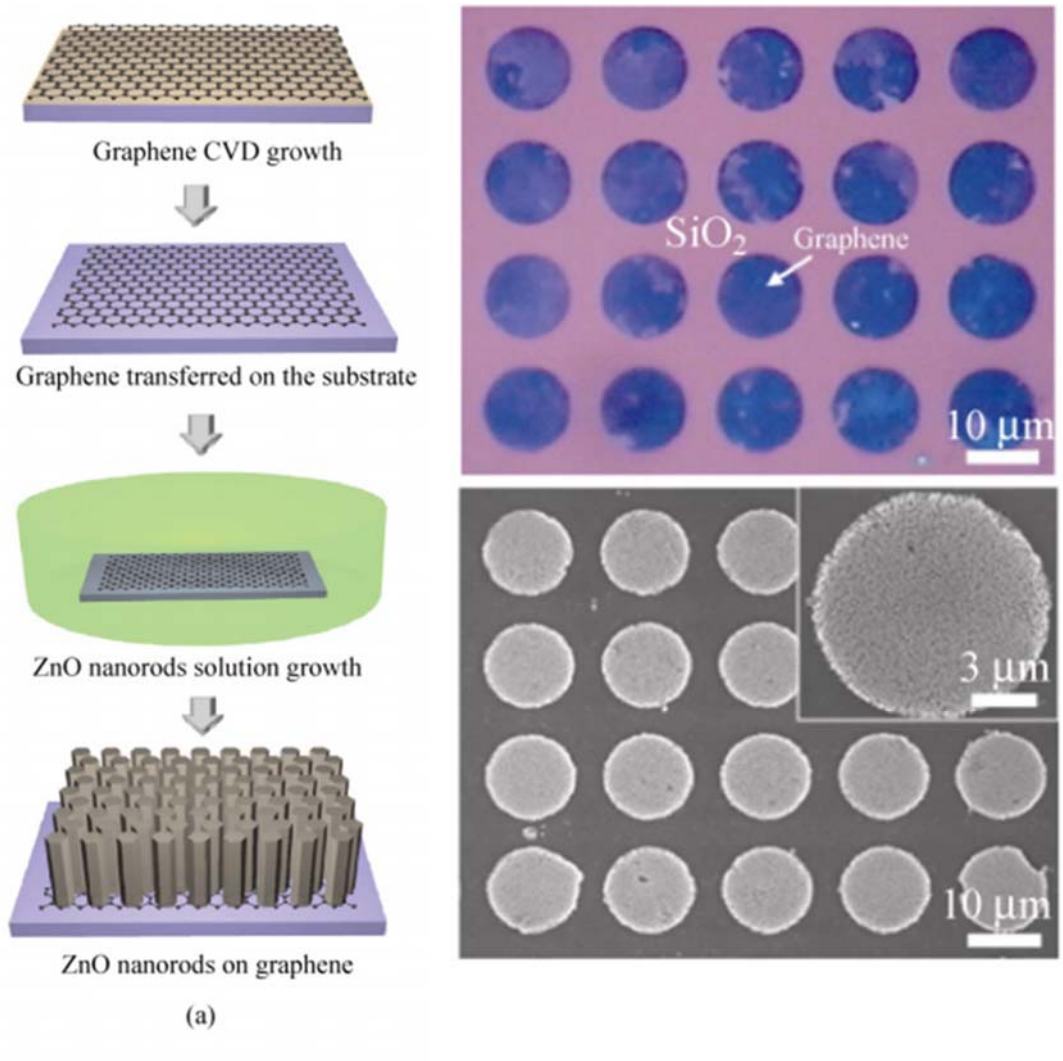

Fig. 2.9. (a) A schematic illustration of ZnO nanorod growth on graphene. (b) An optical microscope image showing the periodic arrays of patterned graphene on the SiO_2/Si substrate. (c) An FE-SEM image of ZnO nanorods selectively grown mask-free on the graphene pattern arrays.

Experimental methods

3

3.1. Material growth

This chapter describes apparatus and methods to fabricate ZnO/graphene heterostructures. Catalyst-free metal-oragnic chemical vapor deposition (MOCVD) was employed for the growth of ZnO nanostructures, including ZnO nanowalls, nanotubes, and nanoneedle arrays. MOCVD method had been widely used for fabrication of the epitaxial growth of semiconductor materials on the substrates and the growth of 1D semiconducting nanostructure has been reported using MOCVD method. Compared with other vapor-phase growth method, catalyst-free MOCVD method is appropriate to grow high-quality semiconductor materials by excluding the impurity incoporation and contamination. Furthermore, accurate control of flow rate, pressure, and temperature of MOCVD system can ensure the reproduciblity and reliability of the material growth process.

3.1.1. Metal-organic vapor-phase epitaxy system

This section describes apparatus used to grow ZnO nanostructures on graphene layer and GaN/ZnO heterostructures for device applications. Four MOCVD systems were employed for the growth of ZnO nanostructures, where three have precursors of Zn and oxygen for the ZnO synthesize, and the other MOCVD has precursors of Ga, In, Mg, Si, and ammonia for GaN/ZnO heterostructures growth. All MOCVDs consist of gas delivery system, growth chamber, radio-frequency induction heater for substrate heating system, and low pressure pumping with exhaust system.

3.1.1.1. Gas delivery system

Figure 3.1 shows gas delivery system of ZnO MOCVD. The gas delivery system consists of gas regulators (Tescom Co. 44-2263-241, Concoa Co. 4324311-580), mas flow control (MFC) controller (DFC4000), pneumatic gas manifold control card (Clippard Instrument Laboratory Inc., No. EMC-08-24-30), and pneumatic air actuator valves connected with 1/4″ electro-polished (denoted as ep

grade) 316-stainless steel (SS) tubing). All connections except reactor were made with stainless steel tungsten inert gas welding fitting or stainless steel gasket (Swagelok Inc., SS-4-VCR-2) components. All gas fluxes were controlled by individual MFCs (Tylan Co. FC-280S Celerity Co. TN 280 or Mycrolis Co. FC-280S) and after passing through MFCs, the gas directed to the reactor or vent using pneumatic air actuator (TK-FUJIKIN Inc. normally close-type for precursors and normally open-type for ambient gas, D4PDVN-VF-C-PX or FPR-UDDF-71-6.35) two-way diaphragm valves. Individual delivery line pressures for MO-source were kept higher than reactor using bellows-shield metering valves (Swagelok Inc., SS-4BMG-VCR) and line pressure was measured by mini-baratron pressure gauge (Setra Systems Inc., 225G-025P-A-D4-2C-06).

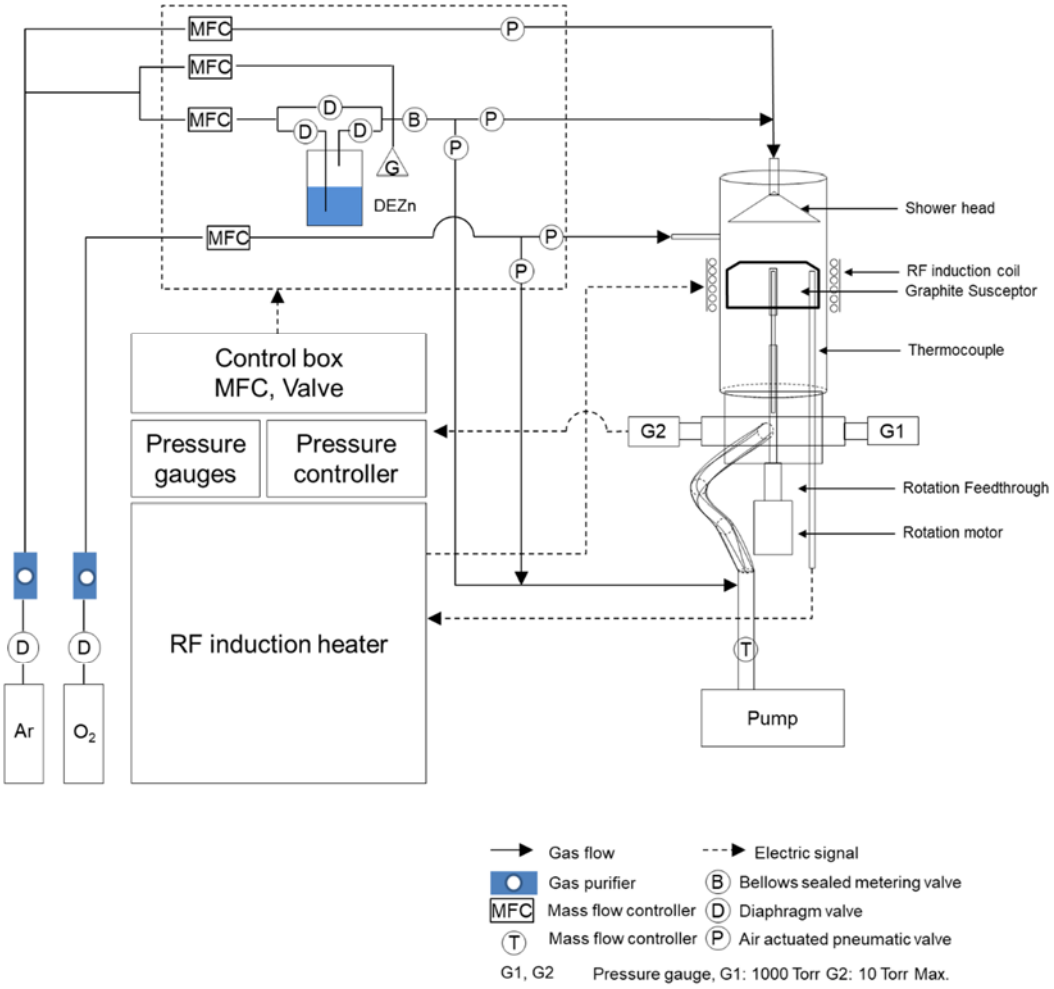

Fig. 3.1. Gas delivery system of ZnO MOCVD.

3.1.1.2. Growth chamber and substrate heating

Three kinds of reactor were employed in the MOVPE system, as shown in Fig. 3.2. The ZnO chamber is vertical type reactor which consists of a fire polished quartz tube (material grade: GE-214) with 90 mm-diameter and 300 mm-length, a quartz tube branch with 6.35 mm-diameter (compatible with 1/4″ ultratorr fitting) and 30 mm length, and two 304-stainless steel ultratorr fitting flanges on both ends. ZnO nanostructures were grown in these chamber using susceptor and induction heating system. The susceptor is made of SiC-coated-graphite with a 2-inch wafer size pocket, and it is heated by a custom radio-frequency (RF) induction heater (Eltek Inc., 80kHz, 10 kW). A high frequency copper coil was surrounded the reqctor with inter-distance of 10 mm, and temperature above 900℃ was obtained. The growth temperature depends on the type of nanostructure grown. The temperature of graphite susceptor is measured by thermocouple (Omega Co., K-type), sheathed by 1/4-inch quartz tube inserted into the graphite susceptor. The growth temperature was controlled by a proportional-integral-derivative (PID) type

temperature controller (Chino Co., KP2000). In addition, the chamber contains showerhead and susceptor rotation parts which is to improve the uniformity of composition and growth rate over the entire 2-inch wafer-scale substrate. The showerhead is connected to the precursor delivering line within gas delivery system by using O-ring sealed ultratorr fitting. Oxygen gas line of is separately connected to the chamber through branched quartz tube to prevent pre-reaction.

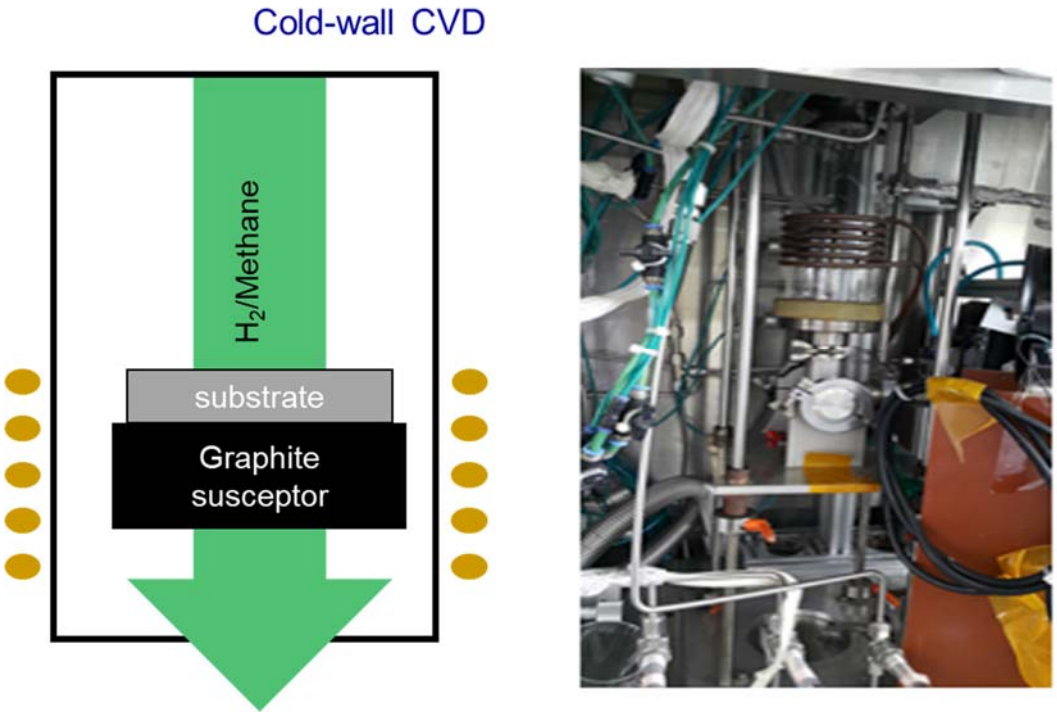

Fig. 3.2. A schematic diagram and photograph of MOCVD chamber.

3.1.1.3. Low pressure pumping and exhaust system

The by-product gas-phase chemicals were blown out through the exhaust tubing lines, which part corresponds to downstream of reactor, and were disposed by a scrubber system. The exhaust tubing lines were connected to a series of vaccum component of a throttle valve (MKS Co., No. 253B) for reactor pressure control, a manual angle valve, and a rotary pump (Kodivac Co., GHP-660K, pumping capacity: 660 L/min). Two Baratron pressure gauges (MKS Co., No. 628B-11TBE1B capacitance manometer type and 850B-13TCD2GA) were located very close to the reactor. The former one and the throttle valve control the reactor pressure in the range of zero to 10 Torr by PID pressure controller (MKS Co., 651C), and adjust the reactor pressure. The latter one was connected to voltameter panel to check the reactor pressure up to 1000 Torr. The exhaust gas from pump passes through heating and wet scrubber system where the harmful and explosive gases and particles are burnt then washed out in water.

3.1.1.4. Gas and reactants

For ZnO growths, diethylzinc (DEZn) and O_2 (99.9995 %) were used as reactants, and high purity Ar (99.9995 %) was used as an ambient and carrier gas. Sin the vapor pressure of metal-organic source was changed by the source temperature, metal-organic source kept constant temperature using refrigerated and heating bath circulators (JEIO Tech Co., RW-1025G). Typical bath temperatures of DEZn were in the rage of -15℃ to -10℃ with different target growth rate.

3.1.2. Growth techniques

Graphene films, as a growth substrate of semiconductor nanostructures, have many advantages have many advantages compared to typical single-crystalline wafers, such as sapphire or silicon, for device applications including flexibility, transferability, and even transparency. For the reason, the growth of 1D nanostructures on graphene has been studied as a method to allow the preparation way of vertically aligned 1D nanostructures on traditionally incompatible substrates. Nevertheless, the challenges of growing position-controlled 1D nanostructures on graphene had remained unresolved. This section describes growth conditions and details of ZnO nanostructures, such as nanorods, nanotubes, and nanowalls on different substrates, including GaN thinfilm-coated sapphire (*c*-Al_2O_3) and graphene, both mechanically exfoliated graphene layers from graphite flakes and CVD-graphene synthesized with copper foil. This dissertation introduces a method to grow position- and shape-controlled nanostructures on graphene substrates, including mechanically exfoliated graphene layers and CVD-graphene

films.

3.1.2.1. ZnO nanostructures on GaN thinfilms

ZnO nanostructures were grown by low-pressure catalyst-free MOVPE on GaN thinfilm-coated sapphire wafer for preliminary research. Growth of high quality ZnO nanostructures have already been studied by senior members and become a base technique for selective growth on different substrates. Therefore, ZnO nanostructures have been periodically grown on GaN thinfilm-coated sapphire wafer in order to confirm status of MOCVD system.

DEZn and oxygen were used as the reactants, and high-purity argon as the carrier gas. The flow rates of DEZn and oxygen were ranged of 5 to 30 and 20 to 100 sccm, respectively, for different shape of nanostructures. During growth, argon flowed into the reactor through the bubbler, containing DEZn, with a temperature in range of -10 to -15°C. To prevent premature reaction, the oxygen gas line was separated from the main gas manifold system. The reactor pressure and temperature during growth were typically kept at 0.5 Torr and 660°C, respectively, but the

pressure and temperature were changed in range of 0.3 to 9 Torr and 400 to 700°C for growing different morphologies of nanostructures. Table 3.1 shows typical conditions for ZnO nanostructure growth.

Conventional lithography was used to create a patterned amorphous film mask, such as SiO_2 or SiN_x, on a GaN thinfilm for the shape- and position-controlled growth of ZnO nanostructures. Before position-controlled growth of the ZnO nanowalls and nanotubes, SiO_2 or SiN_x amorphous thinfilm was deposited onto the GaN/sapphire substrates using plasma-enhanced chemical vapor deposition (STS Inc., 310PC). Electron-beam lithography, which consists of a nanometer pattern generation system (J.C. Nabity Lithography Systems) and a field-emission scanning-electron-microscopy (Tescan Inc., Mira3) or or nano imprint lithography system (Obducat, EITRE-8) was employed to make nanoscale pattern array. Electron-beam lithography was usually employed to form hole patterns with nanoscale diameter and pitches in microscale, or to form text patterns, which are composed of lines and dots (see Fig. 3.3). Nano imprint lithography

system was employed to form patterns on a large area over millimeter-scale, with a hole diameter over 500 nm and pitches over 5 μm (see Fig. 3.4). Subsequently, dry- and wet-etching using reactive ion etching (Oxford Instrument, 80 plus) and buffered oxide etchant (J.T. Baker), respectively, were used to define the patterns at the amorphous thinfilm growth masks.

Table 3.1. Typical conditions for MOVPE growth of ZnO nanostructures.

	ZnO nanorods	ZnO nanowalls (nanotubes)
Substrate temperature	400–580 °C	600−700 °C
Reactor pressure	0.5−1.0 Torr	0.5–10 Torr
Growth rate (height)	2–4 μm/hr	2–6 μm/hr
O_2 flow rate	20–100 sccm	
Ar flow rate	1500 sccm	
DEZn flow rate	5−30 sccm	
DEZn dilute flow rate	10–35 sccm (total 40 sccm with DEZn flow)	
DEZn line pressure	300 Torr	
Bubbler temperature of DEZn	-15 to -10 °C	

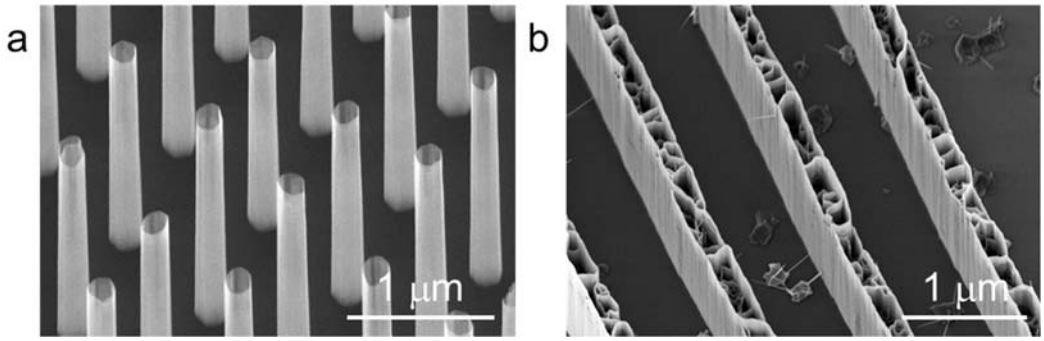

Fig. 3.3. Bird's eye-view FE-SEM images of ZnO nanostructures grown with an electron-beam lithography patterned growth mask on GaN thinfilm deposited on sapphire wafer. (a) nanotube array and (b) line array.

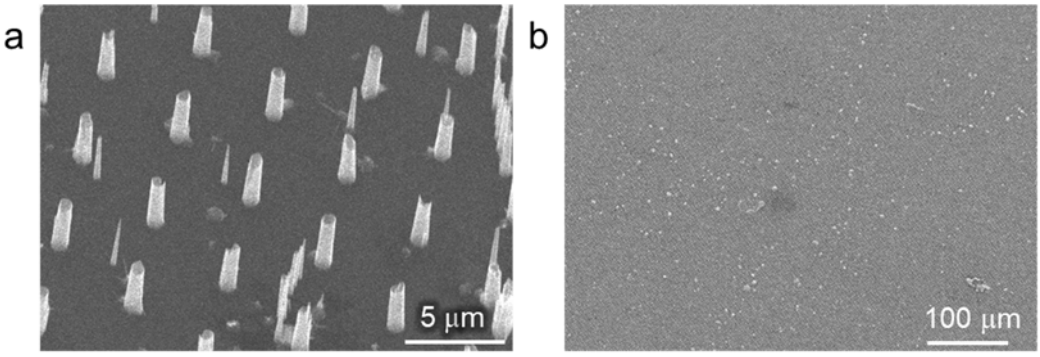

Fig. 3.4. Bird's eye-view SEM images of ZnO nanostructures grown with an nano imprint patterned growth mask on GaN thinfilm deposited on sapphire wafer. (a) high magnituge and (b) lower magnitude image.

3.1.2.2. Nanostructures on mechanical exfoliated graphene

ZnO and GaN nanostructures were position-selectively grown by using MOVPE on mechanically exfoliated graphene films from single-crystalline graphite powder. The clue of growth position controlling method of ZnO nanostructures on exfoliated graphene films was already developed, however, it had not been established. This dissertation introduces a development of shape- and position-controlling method of GaN and ZnO nanostructures on exfoliated graphene films.

First, graphene layers were mechanically exfoliated from natural graphite flake and transferred to a Si substrate with 300-nm-thick SiO_2 layer. The SiO_2/Si substrates only do the role of mechanically supporting the graphene layers in the growth process, therefore any type of substrates which are able to endure high temperature growth condition of 600 °C can be used. Micro-Raman spectroscopy or optical microscopy was employed to confirm the successful preparation of the graphene layers and was used to determine the number of graphene layers.

Second, for the morphology- and position-controlled growth of the nanostructures on graphene layers, additional steps were introduced prior to O_2 plasma treatment. Transferred graphene layers were spin-coated with electron-beam resist and text shapes or hole arrays were patterned by conventional e -beam lithography. After development, the graphene layers were selectively exposed to O_2 plasma under at 30 mA for 10 s under 100 mTorr (SPI Plasma Prep II). Then, the remaining resist layer was removed by rinsing in acetone, followed by drying by N_2 gas blowing. After preparing the graphene layers, nanostructures were grown selectively using MOVPE with the reactants of TMGa and ammonia or DEZn and oxygen for GaN and ZnO, respectively.

3.2.1.3. ZnO nanotubes on CVD-graphene films

Large-area, multi-layered graphene films were synthesized on Cu foil using the CVD method.[49] First, the Cu foil surface was cleaned using acetone and IPA and inserted into a tubular quartz tube and heated to 1030°C with an H_2 flow at 100 standard cubic centimeters per minute (sccm) at 200 Torr. After reaching 1030 °C, the Cu foil was annealed for 15 min to coarsen the grain, while maintaining the flow rate and reactor pressure. Then, graphene films were grown on the Cu foil for 130 min under a mixture of CH_4 and H_2 at flow rates of 10 and 100 sccm, respectively. During growth, the reactor pressure was maintained at 220 Torr. Finally, the sample was cooled to room temperature under flowing H_2 at a pressure of 200 Torr.

The graphene films were transferred onto a Si wafer with 300-nm-thick SiO_2 layer. Same with exfoliated graphene films, the SiO_2/Si substrates act as a mechanically supporting plate of graphene layer for growth process, therefore various types of substrates were used including metal-coated wafer, amorphous quartz and even glass (Corning Inc., Eagle glass) substrates. A thin SiO_2 layer was

deposited onto the as-transferred CVD-graphene layer using a commercial system PECVD (STS Co., LTD.). The thickness of the oxide film was typically 10–200 nm, and the experiments reported herein were performed with a 50-nm-thick film. The oxide layer was annealed at 600°C in N_2 before the patterning process to reduce the number of defects in the as-deposited SiO_2 film that would cause undesired growth and reduce growth selectivity. Next, hole-patterns at the growth-mask were defined by either NIL or EBL, where NIL readily allows a wafer-scale process and EBL enables growth of fine-diameter nanostructures. After lithography, the SiO_2 film was etched using dry-etching, followed by wet etching using CF_4 plasma and BOE. The residual oxide layer on the graphene after dry etching was completely removed using BOE.

ZnO nanotubes were selectively grown on a graphene layer using catalyst-free MOVPE.[8] Diethylzinc (DEZn) and high-purity O_2 (>99.9999%) were used as reactants, and high-purity Ar (>99.9999%) as the carrier gas. The flow rates of DEZn and O_2 were 15–30 and 70–90 sccm, respectively. During growth, Ar flowed

into the quartz reactor through the bubbler with a DEZn bubbler temperature of –15°C. To prevent premature reaction, the O_2 gas line was separated from the main gas manifold line. The reactor pressure was kept at 0.3 Torr during growth, and the temperature ranged from 580–700°C.

3.2. Structural characterization

Surface morphology was investigated using JEOL scanning electron microscopy (SEM) and TESCAN field-emission SEM (FE-SEM). Typical acceleration voltage and working distance were 5–30 kV and 10–15 mm, respectively.

The crystal structure and growth orientations were investigated using PANalytical X'pert PRO X-ray diffraction (XRD) with Ni-filtered Cu K_α radiation. The θ-2θ scan and rocking curve measurement were performed.

The microstructural characterization was performed using a transmission electron microscopy; specifically, Tecnai F20 for selective area electron diffraction

(SAED) pattern mapping, JEM-2100F equipped with ASTAR (NanoMEGAS SPRL) for electron back-scattered diffraction (EBSD) analysis and Titan 80-300TM (FEI) for high resolution imaging and analysis. Cross-sectional TEM samples were prepared by focused ion beam technique (Helios 650, FEI).

3.3. Optical characterization

Optical characteristics of ZnO nanostructures were investigated using photoluminescence (PL) spectroscopy system. A continuouse He-Cd laser (325 nm) was employed as an optical excitation source. The PL emissions from the samples were focused into the spectrometer, consisted of a monochrometer (Dongwo Optron Co. DM320i) and a charge-coupled device (CCD, Andor Inc. DUO401A). The resolution of the monochromator was 0.5 nm. For low temperature study, a cryostat with a helium displex system (Ebara technologies Inc., 531-120) was used to cooling the samples as low as 11K.

3.4. Fabrication procedures for flexible piezoelectric sensors

The basic strategy for the fabrication of flexible piezoelectric pressure

sensors using ZnO nanotubes is illustrated in Fig. 3.5. First, the nanotubes were grown with precisely controlled dimension and positions, such as 10 μm of mean length, 200 nm of diameter, and 4-μm-pitched hexagonal array. After preparing the nanotube array, the gap between the nanotubes was filled with an insulating flexible polymer layer, polyimide (PI, VTEC PI-080-051), as shown in Fig. 3.5b. Then, the PI layer was cured at 300 °C for 3 min in nitrogen mood, to enhance the mechanical strength and chemical resistance of the layer. After curing process, short oxygen plasma ashing was processed onto the nanostructures to expose the tip of ZnO nanotubes, and a 100-nm-thick gold film was deposited as a top electrode to form Schottky junction with ZnO nanotubes (Fig. 3.5c).[63]

The flexible pressure sensor is prepared by mechanical lift-off of the nanosystems from the host substrate (Fig. 3.5d), by exploiting the weak bonding between graphene and the host substrate, Si wafer. The freestanding form of ZnO/graphene hybrid dimension nanomaterials, supported by PI film, enabled the deposition of a metal electrode at the bottom graphene layer. Finally,

chromium/gold bilayer metal electrode was deposit at the graphene films to form Ohmic electrode junction (Fig. 3.5e), then the flexible piezoelectric nanostructure pressure sensor was formed as Fig. 3.5f.

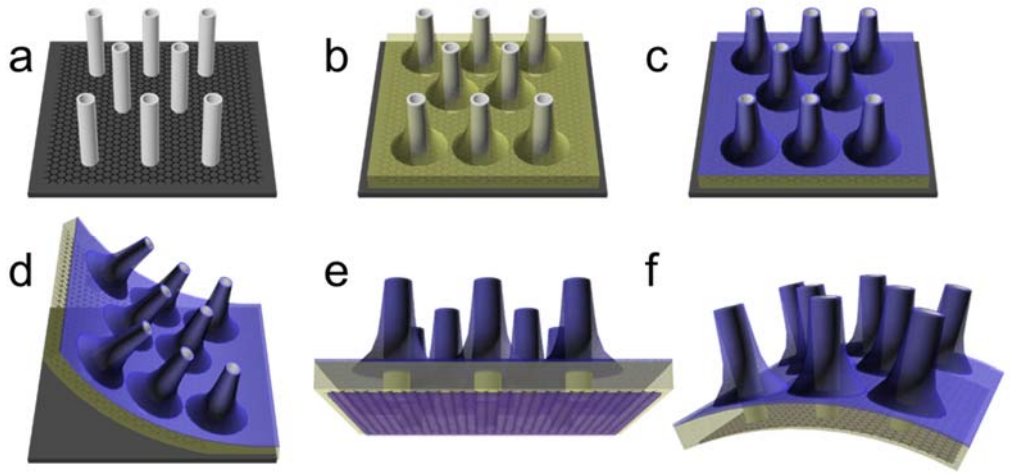

Fig. 3.5. Schematics of the overall process for piezoelectric pressure sensor using ZnO nanotubes grown on CVD-graphene films. (a) preparation of position-selectively grown ZnO nanotubes on CVD-graphene film. (b) Spin-coating of polyimide layer coating onto the nanostructures and (c) deposit top metal electrode layer onto the nanostructure surface after oxygen plasma ashing to expose the tip of ZnO nanotubes. (d) Mechanical lift-off the ZnO nanotubes to expose the bottom graphene layer and to give flexibility to the nanosystem. (e) Deposit bottom electrode (commonly Cr/Au) to form an Ohmic junction and (f) a concept image of the flexible pressure sensor.

Growth of wide-bandgap semiconductor nanostructures on graphene films

4

4.1. Introduction

Bottom-up growth of one-dimensional (1D) semiconductor nanostructures has been extensively studied for fabricating high-density and high-aspect-ratio nanodevices including sensors, light-emitting diodes, transistors, and photovoltaic cells. While this have been achieved with a number of specific materials on single-crystalline substrates such as sapphire and silicon wafers,[34-36] expanding this to more general material/substrate combinations remains challenging due to limitations in growth compatibility. Meanwhile, graphene is an attractive substrate material for the inorganic semiconductors because of its superior electric thermal conductivities, flexibility, and large-area usability with two-dimensional single-crystal structure. Recently, the growth of 1D semiconductor Here, the growth and

characterization of GaN and ZnO nanostructures on graphene films are described. In particular, two different ways, vapor-solid-liquid (VLS) and metal-organic vapor-phase-epitaxy (MOVPE) were employed to grow nanostructures. Surface morphology, structural, and optical characteristics of the nanostructures were investigated.

4.2. Catalyst-assisted growth of GaN nanowires

4.2.1. Growth method and general morphology

GaN nanowires were grown on graphene films using a low-pressure metal-organic chemical vapor deposition (MOCVD) system.[64] As show Fig. 4.1, prior to the growth of the GaN nanowires, high-quality graphene films were grown on Cu foil using CVD and transferred onto 300-nm-thick SiO_2/Si substrates using standard metal etching and layer-transfer methods.[49] Ni films with thicknesses in the range of 0.5–2 nm were deposited on the CVD-grown graphene films to form Ni droplets.[65] The Ni droplets were used as sites for metal catalyst-assisted vapor-

liquid-solid growth of GaN nanowires. For GaN nanowire growth, high-purity trimethyl-gallium (TMGa) and ammonia (NH_3) were employed as the precursors for the Ga and N, respectively, and high-purity nitrogen (N_2) and hydrogen (H_2) were used as the carrier gas and ambient gas, respectively. During the growth of the GaN nanowires, the TMGa, NH_3, and H_2 flow rates were 20, 2000, and 2000 sccm, respectively, and the reactor pressure and temperature during the growth were maintained at 200 Torr and 800 °C, respectively.

Figure 4.1b and c show the general surface morphology GaN nanostructures obtained without and with a Ni thin film as a growth-catalyst layer on CVD-graphene films. The figures reveal clearly different surface morphology of the nanowires grown on the graphene films with and without the Ni layer. The GaN grown directly on the graphene films (i.e., with no Ni layer) formed dense particles, which were typically 2–3 μm across, and nanowires were not observed. In contrast, the use of the Ni layer deposited on graphene films allowed us to obtain a large areal density of nanowires, which exhibited aspect ratios of a few hundred. The

areal density of the nanowires was in the range of 5–7 x $10^9/cm^2$, and the typical diameter was 50 nm. Gold is another well-known metal catalyst for the VLS growth of GaN nanowires; however, GaN nanowires were not observed when gold was used instead of Ni in this work.

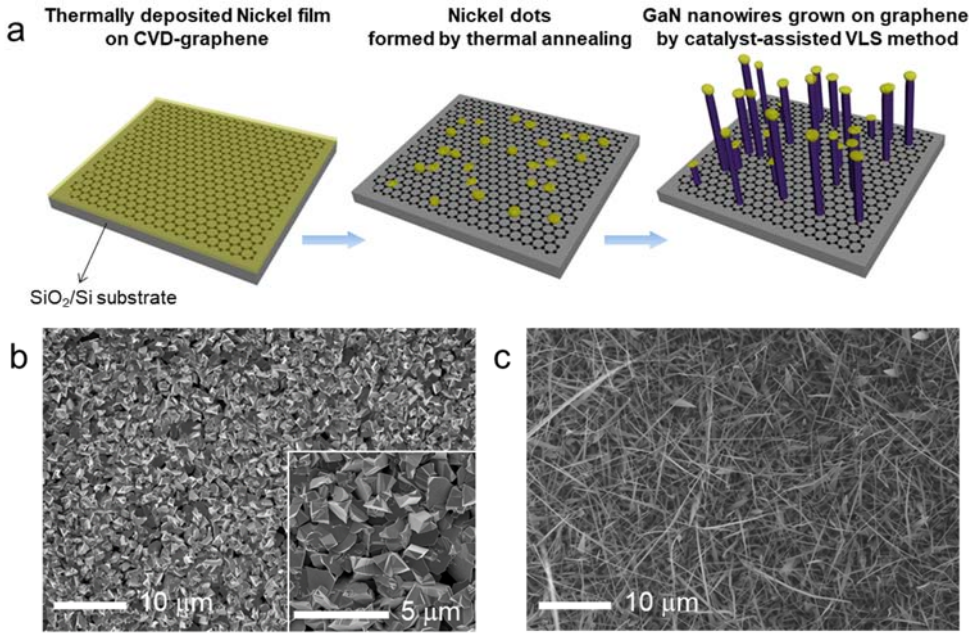

Fig. 4.1. (a) A schematic diagram illustrating of the process used to grow GaN nanowires on the large-area graphene films using the Ni catalyst. (b and c) FE-SEM images of GaN nanostructures grown on graphene without (a) and with (b) a nickel thin film growth-catalyst layer. Inset shows a high-magnification image of the nanostructures.

4.2.2. Effect of catalyst thickness to the morphology of GaN nanowires

As briefly described in section 4.2.1, GaN nanowires were grown on graphene films with nickel film, which are catalyst for the VLS process. Surface morphology of GaN nanowires were further investigated to know how the morphology of GaN nanowires depended on the thickness of the Ni layer. As shown in Fig. 4.2, when we used a 0.5-nm-thick Ni layer, pyramidal GaN particles a few microns across were formed, as well as thick submicron tapered wires with diameters in the range of 500e600 nm, with lengths in the range of 4e6 mm. When the thickness of the Ni layer was increased to 2 nm, the average diameter of the wires decreased to several tens of nanometers, and the length of the structures increased to a few tens of microns. Furthermore, the areal density of the pyramidal structures decreased as the thickness of Ni layer increased, as can be seen from Fig. 4.2. When a 5-nm-thick Ni layer was used, the resulting GaN structures were less than 1 μm thick, and triangular structures that were a few microns long were formed, rather than nanowires.

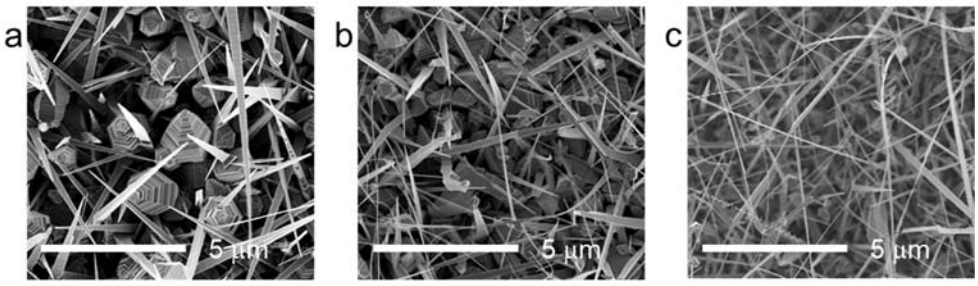

Fig. 4.2. FE-SEM images of GaN nanostructures grown on graphene with various thicknesses of the nickel layer. (a) 0.5, (b) 1.0, (c) 2.0 nm-thick of nickel film-assisted grown GaN nanostructures.

4.2.3. Structural characteristics

The crystal structure and phase of the nanowires were investigated using X-ray diffraction (XRD) and high-resolution transmission electron microscopy (HR-TEM). For the XRD measurements, the GaN nanowires grown on graphene were transferred onto amorphous-fused-silica substrates. As shown in Fig. 4.3a, XRD θ–2θ scans reveal eight sharp peaks, which were indexed to a hexagonal wurtzite structure. The HR-TEM images shown in Figures 4.3b and c provide further insight into the structure of the nanowires. Figure 4.3b reveals the presence of a spherical Ni particle located at the tip of the nanowire, which suggests that the GaN nanowires were grown via the VLS mechanism. In addition, the high-resolution image shown in Figure 4.3c confirms that the nanowires are of high crystallinity. Furthermore, an interplanar spacing of 0.244 nm observed from the image indicates that the stacking direction of the nanowires was perpendicular to the (101) plane.

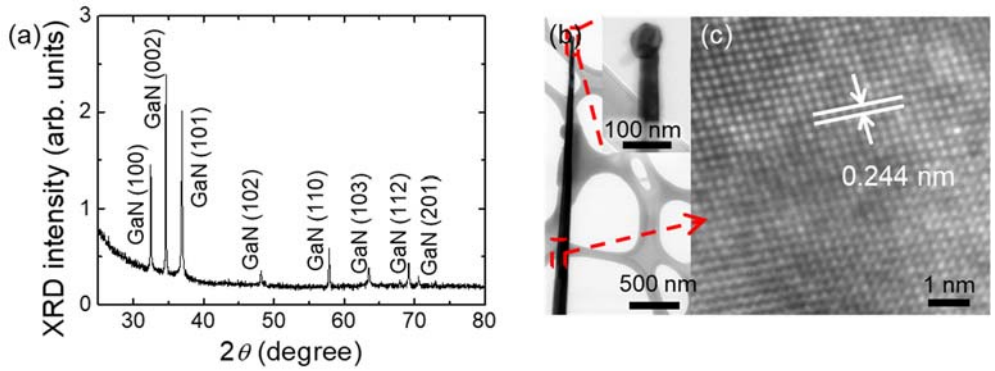

Fig. 4.3. (a) XRD θ–2θ measurements of the GaN nanowires. (b) Low- and (c) high-magnification TEM images of a GaN nanowire. The inset of (b) shows a Ni droplet at the tip of the GaN nanowire.

4.2.4. Optical characteristics

The optical characteristics of the GaN nanowires were investigated by measuring photoluminescence (PL) spectra of the nanowires at 11 K. The low-temperature PL spectrum of the GaN nanowires shown in Fig. 4.4 reveals three strong near-band-edge (NBE) emission features in the range of 3.2–3.5 eV, in addition to relatively weak deep-level emission in the range of 2–2.5 eV, which is attributed to the presence of structural defects or impurities. The sharp and strong NBE peaks and the weak deep-level emission suggest that the GaN nanowires were of good structural quality. The NBE emission was clearly resolved into three peaks at 3.375, 3.425, and 3.471 eV. In accordance with previously reported PL peak positions from GaN nanowires, thin films, and bulk crystals, the peaks at 3.471 and 3.375 eV were assigned to a neutral-donor-bound exciton and to a donor-acceptor-pair (DAP), respectively.[66,67] It has been reported that the peak at 3.425 eV results from Ni-related defects.[65] During the VLS growth of the GaN nanowires, Ni atoms are incorporated into the nanowires as impurities, which generate an acceptor state

and also result in formation of acceptor-bound excitons.

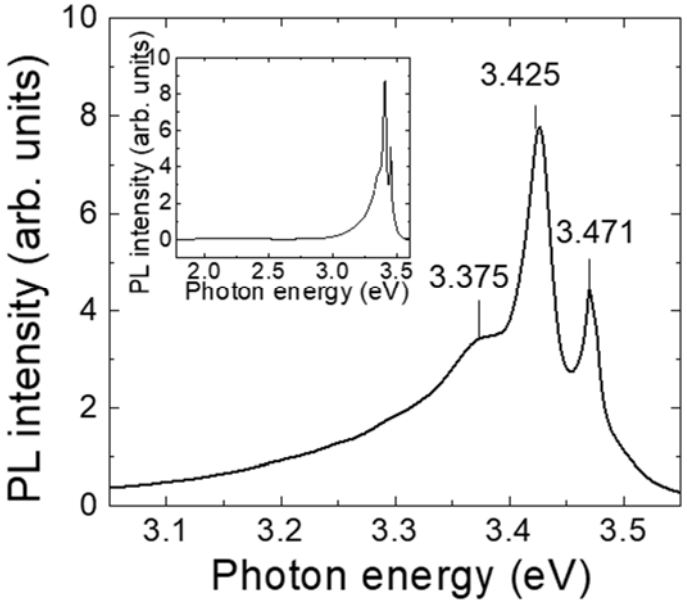

Fig. 4.4. PL spectra of the GaN nanowires measured at 11 K. NBE emission was clearly resolved into three PL peaks at 3.471, 3.425, and 3.375 eV.

4.3. Catalyst-free growth of ZnO nanostructures

The vapor-phase-epitaxy growth of ZnO nanostructures on single-crystalline substrates has already been reported. However, the growth of nanostructures on other kinds of substrates, such as conductive metal films or transparent glass, has not been achieved due the less compatibilities, including crystal structure, lattice constants, and thermal expansion coefficients for crystal growing process. In this subsection, the growth of ZnO nanostructures on graphene films is demonstrated using MOCVD.

4.3.1. Growth method

Large-area, multi-layered graphene films were synthesized on Cu foil using the CVD method.[49] First, the Cu foil surface was cleaned using acetone and IPA and inserted into a tubular quartz tube and heated to 1030°C with an H_2 flow at 100 standard cubic centimeters per minute (sccm) at 200 Torr. After reaching 1030 °C, the Cu foil was annealed for 15 min to coarsen the grain, while maintaining the flow rate and reactor pressure. Then, graphene films were grown on the Cu foil for 130

min under a mixture of CH_4 and H_2 at flow rates of 10 and 100 sccm, respectively. During growth, the reactor pressure was maintained at 220 Torr. Finally, the sample was cooled to room temperature under flowing H_2 at a pressure of 200 Torr.

ZnO nanotubes were selectively grown on a graphene layer using catalyst-free MOVPE.[8] Diethylzinc (DEZn) and high-purity O_2 (>99.9999%) were used as reactants, and high-purity Ar (>99.9999%) as the carrier gas. The flow rates of DEZn and O_2 were 15–30 and 70–90 sccm, respectively. During growth, Ar flowed into the quartz reactor through the bubbler with a DEZn bubbler temperature of –15°C. To prevent premature reaction, the O_2 gas line was separated from the main gas manifold line. The reactor pressure was kept at 0.3 Torr during growth, and the temperature ranged from 580–700°C.

4.3.2. Effect of growth temperature to the morphology of ZnO nanostructures

The surface morphology of ZnO nanostructures grown on CVD-graphene

films depends significantly on the substrate temperature during the growth process. Figure 4.5 shows SEM images of ZnO nanostructures grown at 500, 600, 700, and 800°C for 30 min on CVD-graphene films transferred onto SiO_2/Si substrates. At a low growth temperature of 500°C, the resulting nanostructures were a mixture of 20-nm-high nanowall structures and nanodots with a diameter of 20 ± 3 nm. The morphology of the nanostructures significantly changed with increasing growth temperature. At 600°C, the ZnO products consisted of 60-nm-high nanowall structures, and no nanodots. Nanostructures grown at 700°C comprised 120-nm-high nanowall structures mixed with 120 ± 30-nm-high nanoneedles. When the growth temperature was further increased to 800°C, nanoneedles with a wide range of diameters of 20–100 nm were obtained. These results indicate that lower growth temperatures yielded nanowalls, and the general shape of the nanostructures slowly changed into nanoneedles with increasing growth temperature. This result was presumably due to an inhomogeneous nucleation rate at higher temperatures caused by the rough surface of the CVD-graphene films.

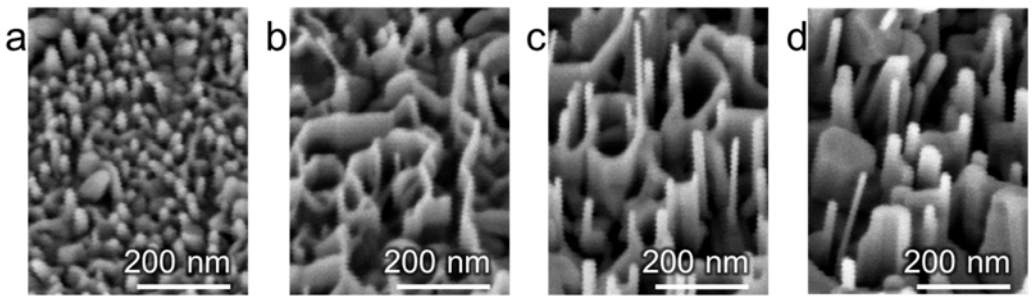

Fig. 4.5. 30° tiled SEM images of ZnO nanostructures grown on CVD-graphene films at different growth temperatures of (c) 500, (d) 600, (e) 700, and (f) 800°C.

4.3.3. Structural characteristics

The microstructural characteristics of ZnO nanowalls grown on CVD-graphene films and the interface between them were examined by cross-sectional transmission electron microscopy (TEM). For this analysis, a TEM specimen was fabricated from a ZnO nanowall/graphene/SiO_2/Si sample using a focused-ion beam (FIB). The crystallographic orientation of the ZnO nanostructures was investigated using high-resolution (HR) TEM imaging and fast Fourier transform (FFT) patterns. Figure 4.6a shows an HR-TEM image of the interfacial region indi; an ordered atomic structure was observed for ZnO in the initial stage of growth on CVD-graphene. Its corresponding FFT pattern (Fig. 4.6b) reveals a (0002) crystal orientation of ZnO parallel to the (0002) plane of graphene (Fig. 4.6c). The FFT pattern at the interface shown in the inset of Fig. 4.7a also supports the c-aligned vertical growth.

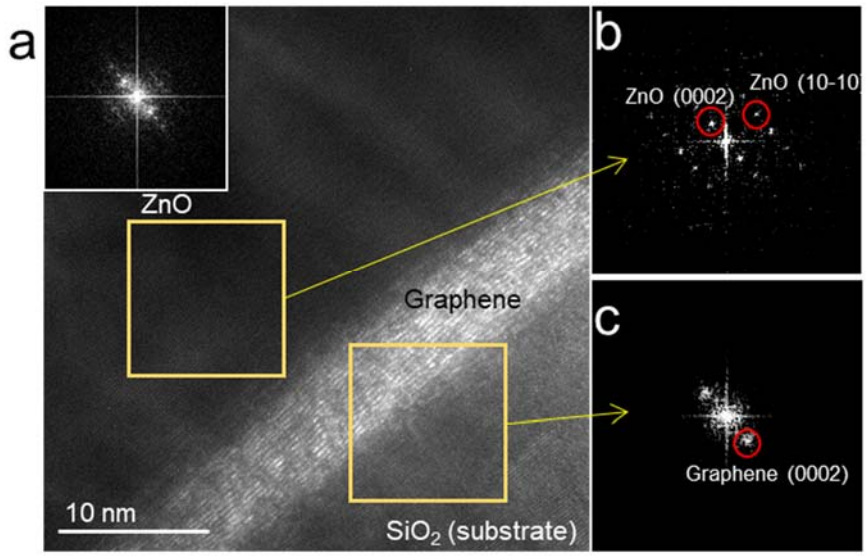

Fig. 4.6. Microstructural characteristics of ZnO nanowall. (a) HR image of the ZnO nanonanowall and (c, d) FFT obtained from HR image in the regions indicated with boxes in (a). Inset of (a): FFT obtained from whole HR image.

4.3.4. Optical characteristics

The optical characteristics of the ZnO nanotubes grown on CVD-graphene layer were investigated using photoluminescence (PL) and transmittance spectroscopy. Figure 4.7 shows a series of variable-temperature PL spectra at temperatures of 11–300 K of ZnO nanotubes grown on graphene layers. The PL spectrum at 11 K typically shows five near-band-edge (NBE) emission peaks at 3.367, 3.361, 3.318, 3.298, and 3.250 eV with full with at half maximum (FWHM) values of 3–15 meV. The NBE peaks indicate that the ZnO nanotubes grown on graphene layers have high optical quality and no carbon-impurities-related exciton peak was observed. Meanwhile, a room-temperature PL spectrum shows a weak deep level emission in visible light range with only a strong ultra-violet emission as shown in the inset of Fig. 4.7.

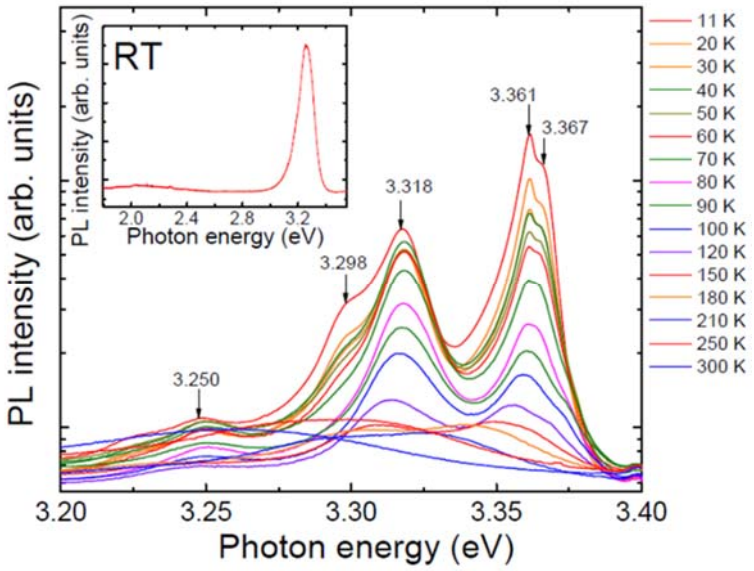

Fig. 4.7. Temperature-dependent PL spectra of ZnO nanostructures grown on CVD-graphene films. The inset shows low deep-level emission intensity at room temperature.

4.4. Summary

This chapter described successful growth results of one-dimensional nanostructures of both GaN and ZnO, and investigation of their structural and optical characteristics. The shape of GaN nanostructures was controlled by employing different thicknesses of nickel films as catalyst layer for VLS process, while the same of ZnO nanostructures was controlled by tuning process temperature. Structural analysis using TEM reveals that both nanostructures have highly-ordered atomic structures without defects. However, Optical investigation using a low temperature photoluminescence revealed different defect density of the two nanostructures synthesized by different methods.

Shape-controlled selective growth of ZnO nanostructures on CVD-graphene

5

5.1. Introduction

The growth of 1D nanostructures on two-dimensional (2D) nanomaterials such as graphene has been studied as a method to allow the preparation of vertically aligned 1D nanostructures on traditionally incompatible substrates.[60,68,69] There, the 2D nanomaterial acts as a growth buffer layer that can be mechanically attached to, and also detached from, arbitrary substrates. However, while position-controlled and vertically aligned growth has been performed on mechanically exfoliated graphene, this approach is not scalable to a wafer-sized area.[61] On the other hand, previous reports of growth on graphene deposited by chemical vapor deposition (CVD-graphene) have shown unsatisfactory growth controllability, with a lack of individual position control (i.e., a bundled growth), low growth selectivity, or poor

vertical alignment.[41,62] This chapter describes a method to significantly enhance the growth controllability on CVD-graphene, enabling a wafer-scale preparation of individually position-controlled and vertically aligned 1D ZnO nanostructure arrays on arbitrary substrates including amorphous, metallic, or flexible substrates.

5.2. Selective-area growth of ZnO on graphene films with a locally-confined oxygen plasma treatment

5.2.1. Growth method and general morphology

The typical process for selective-area growth of ZnO nanostructures on graphene films with a locally-confined oxygen plasma treatment is schematically illustrated in Fig. 5.1a.[61] For the selective area growth of ZnO nanostructures on graphene films, locally-confined oxygen-plasma treatment was performed on each graphene film, covered with a patterned polymer layer. First, graphene films were transferred onto a supporting substrate; 300-nm-thick SiO_2 covered Si substrates were typically used. For the graphene preparation, both the mechanical exfoliation

method using a 3M Scotch tape from graphite flakes[70] and wet-chemical transfer method for CVD-graphene synthesized on the surface of Cu foil.[49] Next, the conventional lithography technique and oxygen plasma treatment process were conducted to create artificial step edges for designing selective growth area. After spin-coating of a PMMA layer onto both graphene films, hexagonal hole array was formed at the resist layer using an e-beam lithography. Then, oxygen-plasma treatment was performed at the area exposed to the graphene surface. The substrates were then immersed into acetone solution to remove the protecting polymer layer on the graphene sheets.

ZnO nanostructures ZnO nanotubes were selectively grown on a graphene layer using catalyst-free MOVPE.[8] Diethylzinc (DEZn) and high-purity O_2 (>99.9999%) were used as reactants, and high-purity Ar (>99.9999%) as the carrier gas. The flow rates of DEZn and O_2 were 15–30 and 70–90 sccm, respectively. During growth, Ar flowed into the quartz reactor through the bubbler with a DEZn bubbler temperature of –15°C. To prevent premature reaction, the O_2 gas line was

separated from the main gas manifold line. The reactor pressure was kept at 0.3 Torr during growth, and the temperature ranged from 580–700°C.

The general surface morphology of ZnO nanostructure arrays grown on exfoliated and CVD-graphene following the above procedures are different as shown in Figs. 5.1b and c. On exfoliated graphene films, we can observe distinguishing ZnO nanotube arrays with some undesired ZnO nanostructures, such as short width nanowalls or nanowires. In contrast, on CVD-graphene films, we can observe only short root of nanotubes, surrounded by a highly-dense rough film. This difference in ZnO nanostructures grown on mechanically exfoliated graphene films and on CVD-graphene films are presumably originated from the density of step edges the surface of graphene films.

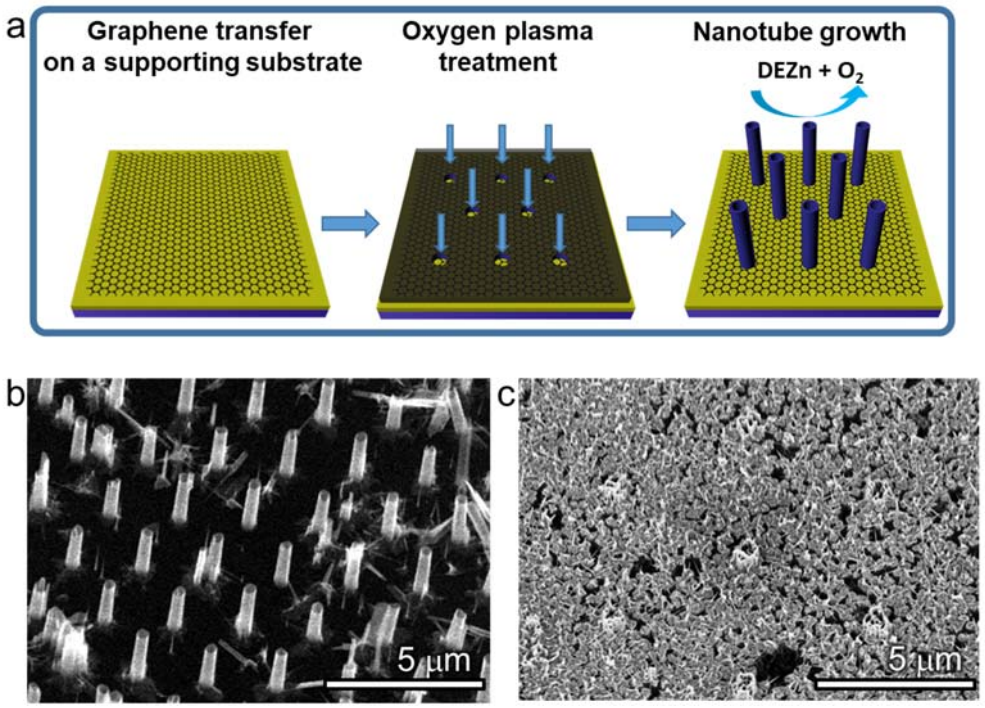

Figure 5.1. (a) Schematic illustration of the process for selective growth of ZnO nanostructures using selective oxygen-plasma treatment on graphene films. (b, c) 30° tiled SEM images of ZnO nanostructure arrays grown on different graphene films after selective oxygen plasma treatment. (b) on mechanical exfoliated graphene and (c) on CVD-graphene film.

5.2.2. Growth behavior of ZnO nanostructures on CVD-graphene and mechanically exfoliated graphene

The different growth result described above may come from the different nucleation densities on the surface of the two different graphene films. Figure 5.2 reveals the drastically different general surface morphology of ZnO nanostructures grown on exfoliated and CVD-graphene. In previous work reporting ZnO nanotube arrays grown using metal-organic vapor-phase epitaxy (MOVPE) on exfoliated graphene,[61] the mechanically cleaved surface of graphene was shown to exhibit a small density of nucleation sites, with slight growth occurring presumably along the step edges of the graphene films (Fig. 5.2a). Hence, nucleation sites were artificially introduced by selective oxygen (O_2) plasma treatment to grow the nanomaterial with a desired density.[40] On the other hand, the same growth conditions applied to CVD-graphene led to a significantly different growth behavior (Fig. 5.2b). Comparing the SEM images of ZnO nanostructures grown at 600°C on the two graphene films, the density and morphology of ZnO

nanostructures were both affected, with a row of ZnO nanoneedles on the exfoliated graphene film (Fig. 5.2a) and ZnO nanowall structures on the entire surface of the CVD-graphene film (Fig 5.2b).

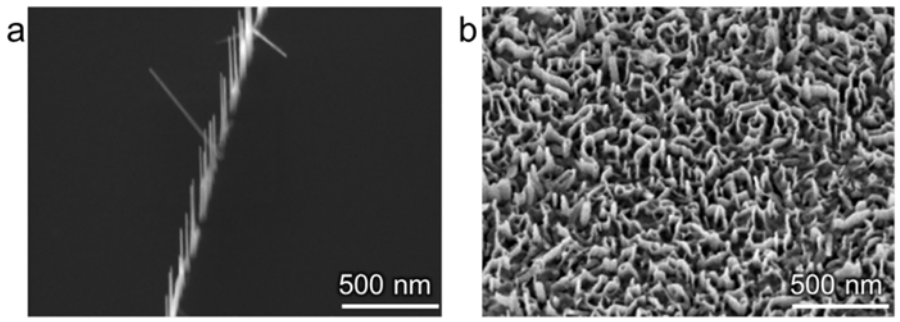

Fig. 5.2. 30° tiled SEM images showing different nucleation density of ZnO nanostructures grown with a same condition on (a) mechanically exfoliated-graphene and (b) CVD-graphene films.

The different growth behaviors of ZnO nanostructures on mechanically exfoliated graphene films and on CVD-graphene films presumably come from the different surface status of the two of graphene films. Figure 5.3 shows AFM topology images of different kinds of graphene films and SEM surface morphology images of ZnO nanostructures grown on the different graphene films. As shown in Fig. 5.3a, the topology image of CVD-graphene shows highly-dense wrinkles and a large surface roughness of 3.5 nm. In contrast, the AFM surface image of a mechanically exfoliated graphene film shows only a few strips on the surface with a small surface roughness under 0.1 nm, meanwhile, the AFM image of oxygen-plasma-treated exfoliated graphene films shows increased surface roughness over 6 times without any significant strips on the surface.

SEM images in Fig. 5.3b reveal significantly different growth behavior of ZnO nanostructures on a CVD-graphene and a mechanically exfoliated graphene film. The ZnO nanostructures were densely grown on CVD-graphene and plasma-treated graphene flake, which have rougher surfaces than untreated graphene flake,

while Only a few nanowires and several nanowall lines grew on non-treated graphene flake. Furthermore, the density of ZnO nanostructures, grown on mechanically exfoliated graphene after oxygen-plasma-treatment, was increased and surface morphology was also changed like CVD-graphene films. The surface roughnesses of these substrates presumably affected the nucleation behavior of ZnO nanostructures.

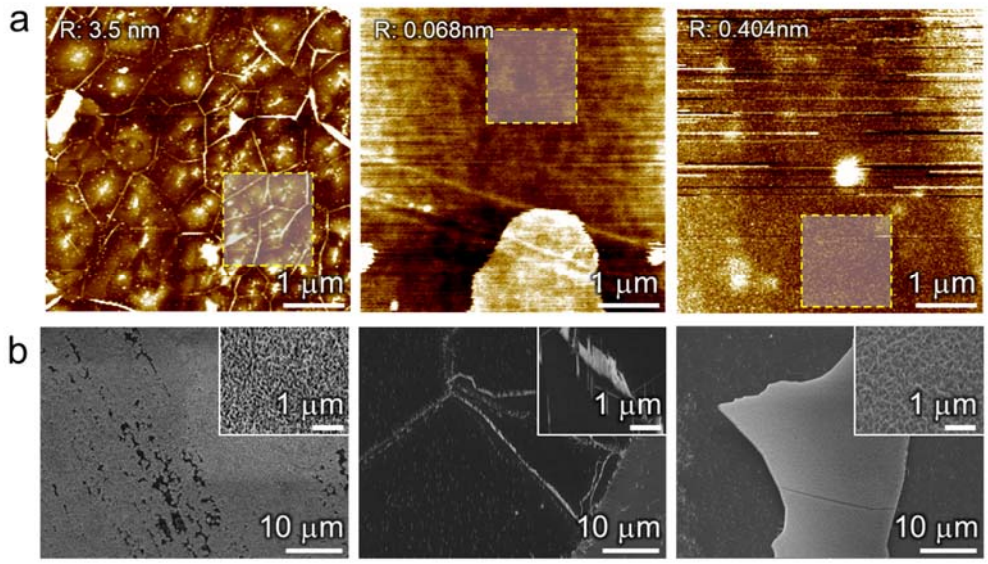

Fig. 5.3. (a) Atomic force microscopy (AFM) topology profile images of chemical vapor deposition (CVD)-graphene, exfoliated graphene, and oxygen-plasma-treated exfoliated graphene films. Inset values indicate the surface roughness of each graphene calculated at the indicated area (red), while wrinkles on CVD-graphene films were removed before calculating surface roughness. (b) 30° tiled SEM images of ZnO nanostructures grown on the three kinds of graphene films.

5.3. Selective growth of ZnO nanostructure array on CVD-graphene

ZnO nanostructures were grown selectively on CVD-graphene layers using low-pressure, catalyst-free metal-organic vapor-phase epitaxy (MOVPE). To control both the shape and position of ZnO nanostructures, a patterned SiO_2 thinfilm was prepared as a growth-mask layer on the graphene films using a conventional electron-beam lithography and both dry- and wet-chemical etching techniques. The nanowalls were then grown using diethylzinc and oxygen reactant gases at 580–700°C of process temperature.

5.3.1. Growth method for position-controlled ZnO nanostructures

Position- and dimension-controlled growth of ZnO nanotubes was performed by selectively suppressing the nucleation of ZnO using a growth mask (Figs. 5.4a–d). First, a few-layered CVD-graphene film was transferred onto a supporting substrate. As the supporting substrate, arbitrary substrates with sufficient

thermal tolerance can be employed, such as metallic, ceramic, or glass substrates. Next, a thin SiO_2 film was deposited onto the graphene films using plasma-enhanced CVD (PECVD). The thickness was typically 10–200 nm; I typically used a 50-nm-thick film. Importantly, the oxide layer was annealed at 600 °C in oxygen (O_2) before

the patterning process to reduce the defects in the as-deposited SiO_2 film that caused undesired growth and reduced the growth selectivity. Figures 5.4e and f show the effect of thermal annealing on the position-selective growth of ZnO nanostructures. We note that this step was not required when the same SiO_2 film was used for selective growth on GaN films, implying that the defects may have originated from the deposition of the SiO_2 film on a defect-rich CVD-graphene film.

Hole patterns on the growth mask were defined by either nanoimprint lithography (NIL) or e-beam lithography (EBL). The typical diameters and pitches of the holes were 100–500 nm and 1–8 μm, respectively. After lithography, the SiO_2 film was first etched by reactive-ion etching (RIE) using CF_4 plasma until a very

thin oxide film was left to prevent damage to the graphene by the plasma. The residual oxide layer was then completely removed by a brief wet etch using buffered oxide etchant (BOE). This mixed etching process provided better reproducibility for the preparation of a patterned oxide growth mask on the CVD-graphene films, as opposed to using a dry- or wet-etch alone. Then, ZnO nanotube arrays were selectively grown on SiO_2-mask-patterned CVD-graphene films by catalyst-free MOVPE.

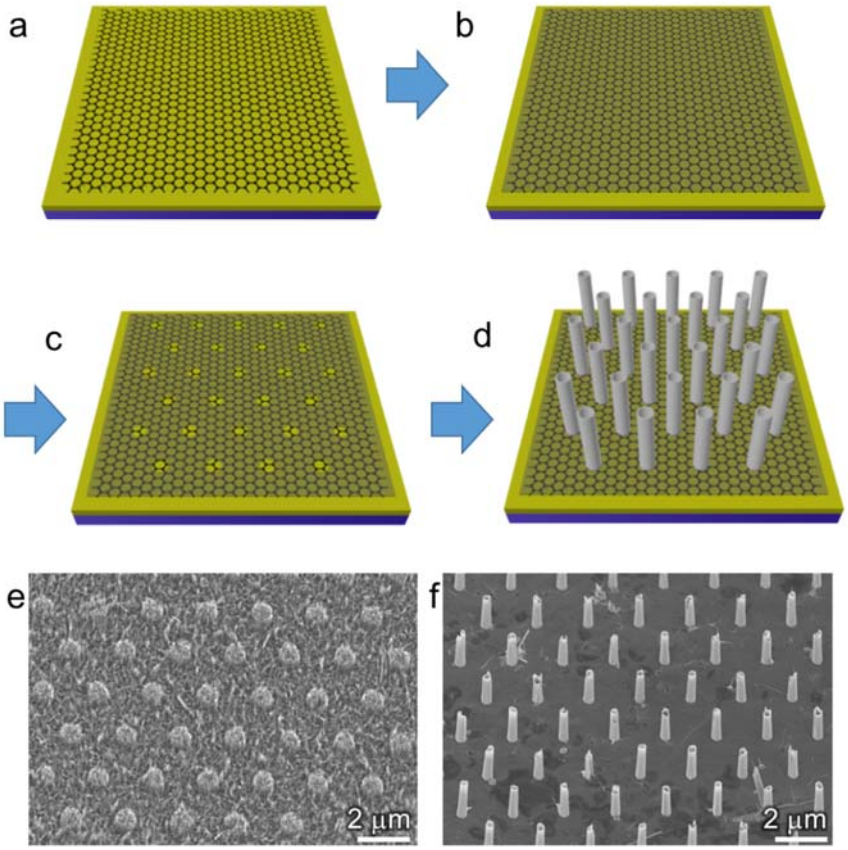

Fig. 5.4. Schematic illustrations of the process for selective growth of ZnO nanostructures on CVD-graphene films. (a) Graphene transfer on a supporting substrate, (b) SiO_2 mask covering onto the graphene, (c) patterning the SiO_2 mask to form growth mask, and (d) nanotube growth. Surface morphologies of ZnO nanostructures grown on SiO_2 growth-mask patterned CVD-graphene films (a) without thermal annealing and (b) with thermal annealing.

5.3.2. Growth behavior of ZnO nanotube arrays on CVD-graphene

Main parameters of ZnO MOVPE process such as flow rates of diethylzinc (DEZn) and oxygen, process pressure and temperature were varied to investigate the growth behavior of ZnO nanostructure arrays on CVD-graphene film. The effect of growth temperature for ZnO nanotubes was investigated by changing the growth temperatures from 500 to 660 °C. Figure 5.5 displays the SEM images of ZnO nanostructures grown at different temperatures. The morphology and growth selectivity of ZnO nanostructures grown on CVD-graphene films remarkably changed depending on the process temperature. At low process temperature of 500 °C, ZnO nanowall was grown on the whole area of SiO_2 growth-mask covered region. We can see a hexagonal array of short tubular nanostructures among the nanowall structure. By increasing growth temperature, the nanowall grown on the growth mask layer rapidly diminished, growth selectivity increased, and the average aspect ratio of ZnO nanostructures grown at designed positions was increased. At 550 °C of growth temperature, cone-shaped nanostructure hexagonal

array was observed with some lumps on the void between each nanotube. The cone-shaped nanostructures altered to straight tubular structures as shown in Fig. 5.5. At 640 °C of process temperature, the SEM image shows a clearly defined hexagonal array of ZnO nanotubes. When the process temperature reached 660 °C, the tips of ZnO nanotubes were split.

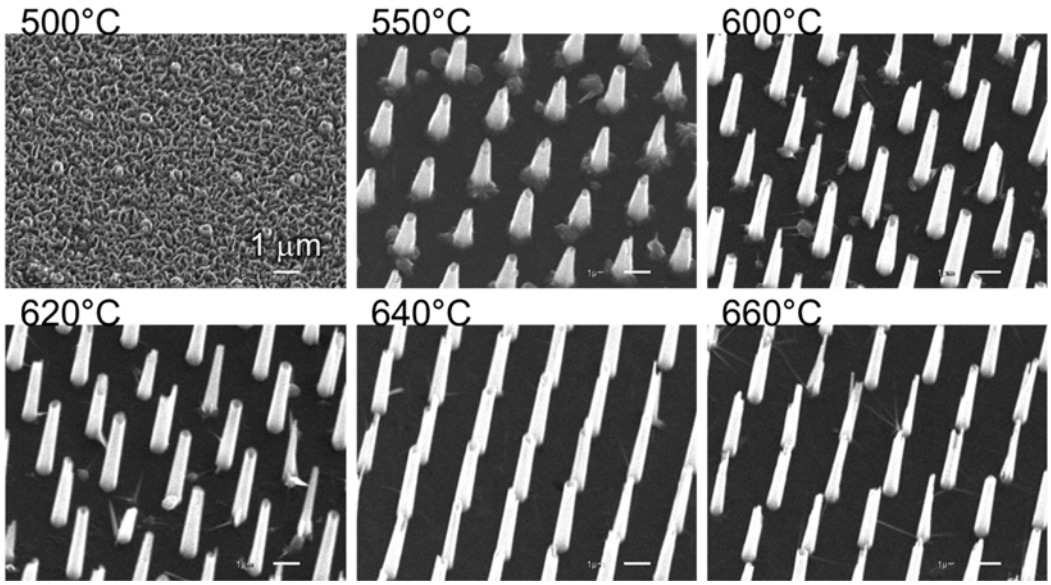

Fig. 5.5. 30° tilted Scanning electron microscopy images of ZnO nanotubes grown on CVD-graphene films at different process temperatures.

5.3.3. Shape controlled ZnO nanostructures

As mentioned in 5.3.1 and 5.3.2, ZnO nanostructures with a uniform height grew along the patterned SiO_2 growth mask. This selective-growth of ZnO nanostructures can be applied to various kinds of shape-controlled nanostructures. For example, nanostructures with a uniform width and height grew along the line patterned SiO_2 mask as shown in Fig. 5.6a. This method could be also applied to more complex shape, such as a text pattern as shown in Fig. 5.6b. These results indicate that the shape of ZnO nanostructures is freely controlled by the SiO_2 growth mask on CVD-graphene films.

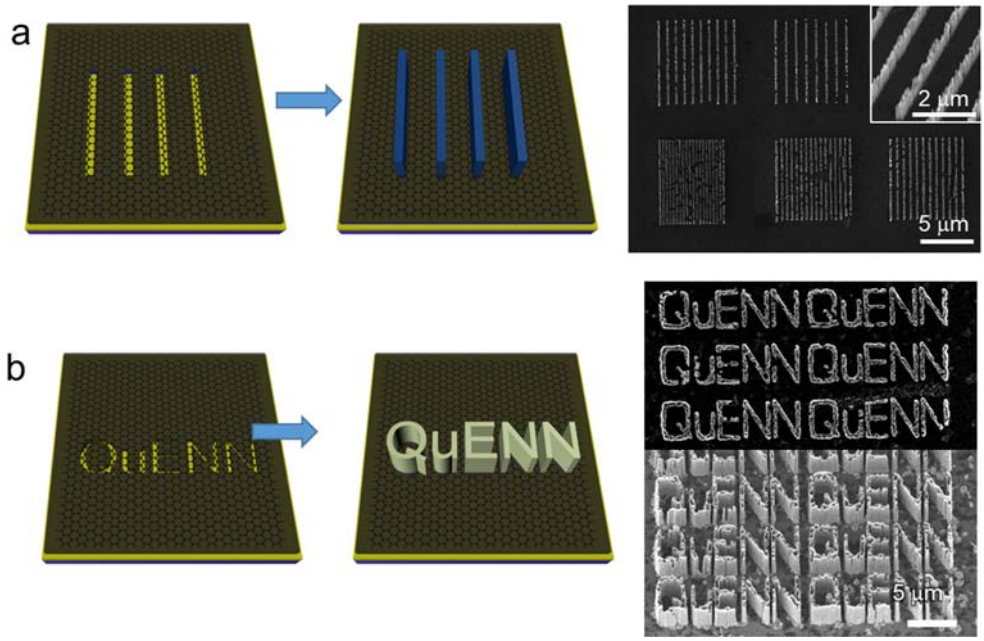

Fig. 5.6. Schematics of the process for obtaining shape-controlled ZnO nanostructures using selective growth along patterned SiO_2 growth mask, and the corresponding SEM images of the shape-controlled ZnO nanostructures. (a) Shape-controlled selective growth of ZnO nanostructures with line-patterned SiO_2 growth mask. (b) Shape-controlled selective growth of ZnO nanostructures with text-patterned SiO_2 growth mask.

5.3.4. Position- and diameter-controlled ZnO nanotube arrays

The diameter and pitch of these selectively grown nanotubes were controlled precisely by changing the geometry of patterns at oxide film as shown in Fig. 5.7. Figures 5.7a–c show SEM images of regular hexagonal arrays of ZnO nanotubes with different spacings of 8, 4, and 2 μm with a fixed diameter and Figs. 5.7 d–e show controlled diameters of 500, 200, and 100 nm with a fixed spacing. Since the diameter and length of the ZnO nanotubes are determined by the hole diameter and the growth time, respectively. The typical growth rate of ZnO nanotubes with diameters of a few hundred nanometers is approximately 80 nm/min.

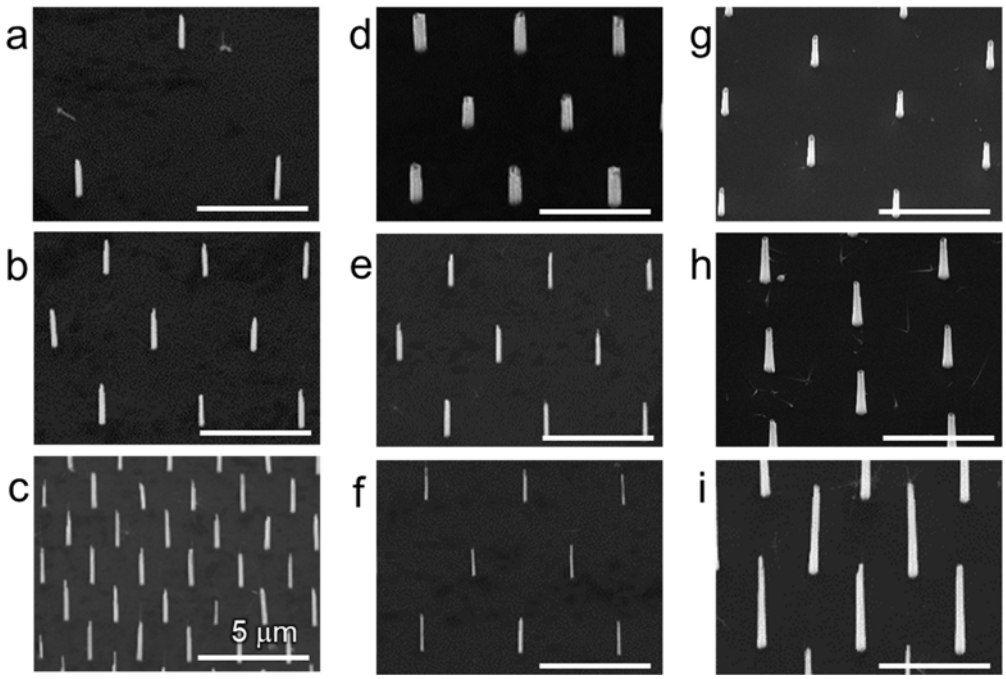

Fig. 5.7. 30° tiled SEM images of position- and dimension-controlled ZnO nanotube arrays. (a–c) Hexagonal nanotube array with spacings of (a) 8, (b) 4, and (c) 2 μm and (d–f) array with varying diameters of (d) 500, (e) 200, and (f) 100 nm. The position and diameter of the nanotubes can be controlled by changing the hole patterns of SiO_2 thin film mask layer. (g–i) Array with different tube lengths of (g) 2.1, (h) 4.3, and (i) 8.6 mm grown in 30, 60, and 120 mins of growth time, respectively.

5.3.5. Selective growth of ZnO nanostructure array on diverse substrates

The growth of ZnO nanostructures arrays on 2D graphene layer was successfully achieved as the above. In this subsection, the growth results of 1D ZnO nanotube arrays on diverse substrates and their applications are described.

5.3.5.1. ZnO nanostructure array on different substrates

Figure 5.8 shows SEM images of selectively grown ZnO nanostructure arrays on different substrates (glass, tungsten, and TiN) prepared with the CVD-graphene interlayer. As shown in the figures, vertically well-aligned ZnO nanotube arrays were grown on graphene layer regardless of the underlying substrate, where ZnO nanotubes of uniform heights were grown only on the position-controlled hexagonal sites under the same growth condition. Interestingly, the morphology of the vertical nanotubes is exactly the same whether on amorphous glass (Fig. 5.8a), metal (Fig. 5.8b), and conductive ceramic (Fig. 5.8c) substrates. These results indicate that the CVD-graphene film provides a growth seed layer for vertically-

aligned ZnO nanotube arrays on arbitrary substrates using a simple MOVPE process.

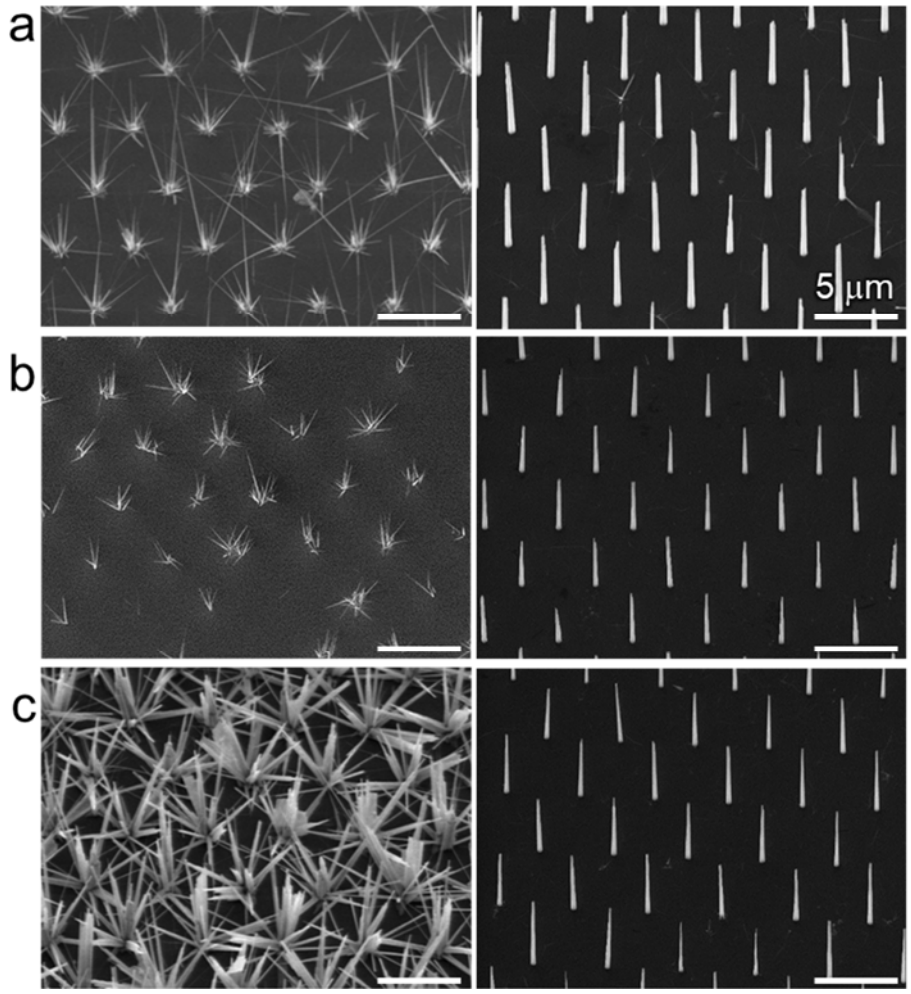

Fig. 5.8. Effect of CVD-graphene film as an interlayer for growth of ZnO nanotubes on different substrates. The morphologies of ZnO nanotubes grown with CVD-graphene films (left) and without graphene films (right) on different substrates; (a) glass, (b) tungsten, and (c) TiN.

The effect of CVD-graphene layer as a growth-buffer on crystal structure and growth orientation of the ZnO nanostructures was also examined by X-ray diffraction (XRD). Figure 5.9 shows θ–2θ scan results for ZnO nanotubes grown on various substrates using a CVD-graphene interlayer as well as ZnO products without using the graphene interlayer. A diffraction peak for the ZnO nanotubes grown on the substrates covered with graphene films was observed only at 34.4°. The peak corresponds to the (002) orientation of wurtzite ZnO. The directly grown ZnO products without the graphene interlayer showed no or weak *c*–aligned ZnO peak in the measured range (20—60°), because of the lattice mismatch between ZnO crystal and the amorphous or poly-crystalline substrate.

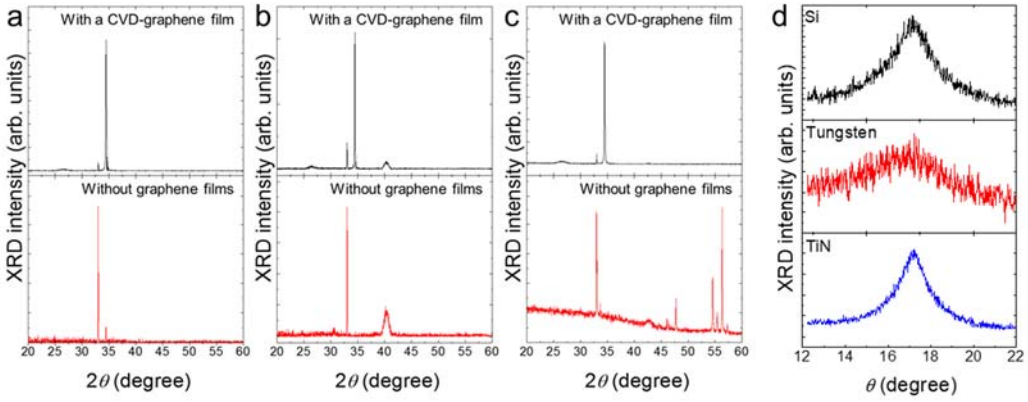

Fig. 5.9. X-ray diffraction (XRD) θ–2θ spectra of ZnO nanostructures grown with (black line) and without (red line) a graphene interlayer on (a) silicon, (b) tungsten and (c) TiN substrate. (d) Rocking curves of ZnO nanotubes grown on different substrates with a graphene interlayer.

5.3.5.2. A wafer-scale process of ZnO nanotube array growth

The resulting product was a wafer-scale array of position-controlled and vertically aligned ZnO nanotubes. Figure 5.10 shows a photograph and corresponding SEM images of ZnO nanotube arrays prepared on the entire area of a 2-inch-diameter SiO_2/Si wafer. Position-controlled nanostructures with designed dimensions were grown by varying the lithographic pattern and the growth duration. In this way, nanotubes of various dimensions, line arrays of nanowalls or complex-shaped letters formed by nanowalls were prepared. Combined with the diverse choice of substrates (section 5.3.5.1.), CVD-graphene films may provide a universal seed layer for large-area growth of individually position-controlled and vertically aligned ZnO nanotube arrays for various applications.

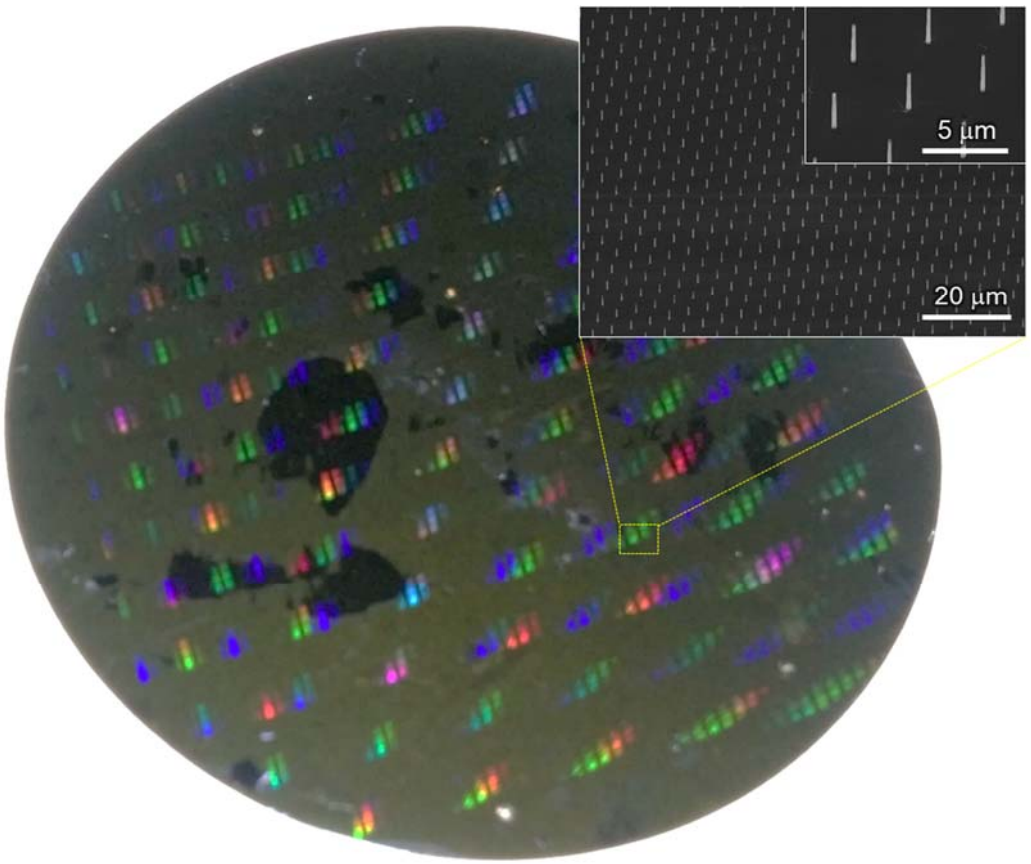

Fig. 5.10. A photograph of ZnO nanotube arrays grown on a 2-inch SiO_2/Si wafer and (inset) the corresponding SEM images of ZnO nanotubes with different magnitude.

5.3.5.3. Mechanical lift-off the flexible nanosystems

The graphene growth buffer layer also served as a buffer for mechanical lift-off[71] to allow the transfer of 1D nanostructures obtained by MOVPE to thermally unstable substrates, for instance, to create flexible nanodevices. This is illustrated in Fig. 5.11a, in which a thick polymeric polyimide (PI) film, spin-coated as a supporting layer, is detached from the surface together with ZnO nanotubes and graphene using punched a Kapton tape. The ZnO nanotubes on graphene can then be attached to arbitrary substrates including plastic films, after which the nanostructures are exposed by O_2 plasma etching of the supporting PI layer to a depth of a few micrometers. Figure 5.11b shows a photograph of ZnO nanotubes on graphene after the mechanical lift-off from the original substrate. The punched tape was used for detaching and attaching the nanomaterials and to provide a mechanical handle for the freestanding 1D/2D hybrid system; the freestanding nanomaterial was supported by a 3-μm-thick polymeric film and was handled using the tape (ca. 50-μm-thick). The thin supporting layer allowed extremely bent ZnO

nanotube arrays at a radius of curvature of 0.5 mm as shown in Figs. 5.11c and d. The images suggest that no mechanical damage or fracture occurred during the bending test. This exfoliation method to fabricate a flexible nanosystem may provide a template for individually position-controlled and vertically aligned nanodevice arrays, which can be directly applied to flexible LEDs or touch sensors.[29,59]

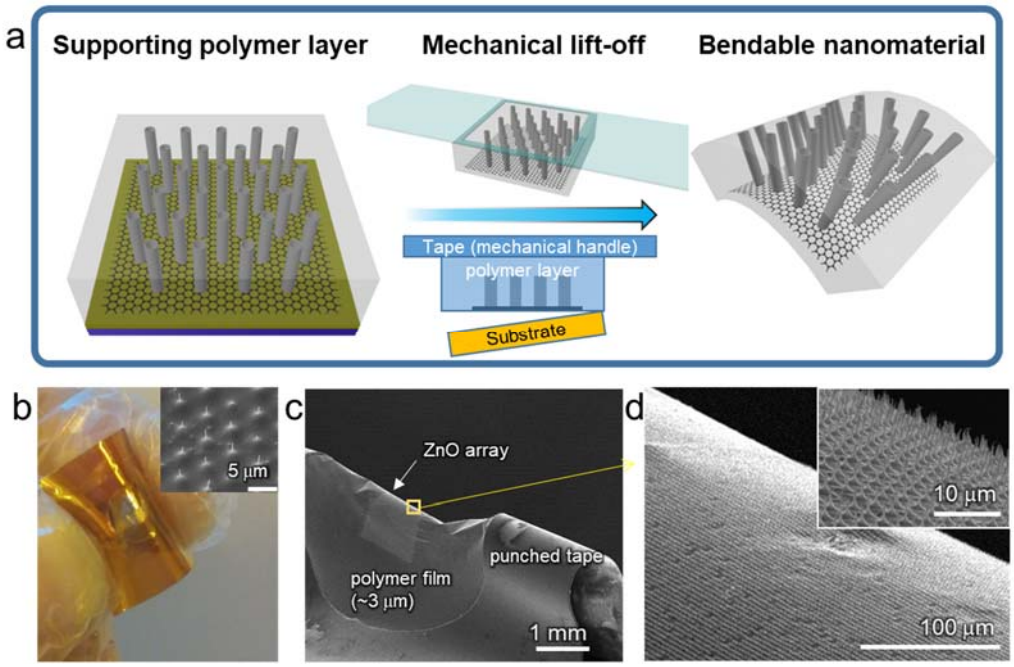

Fig. 5.11. (a) Schematic illustration of the lift-off procedure of nanotube arrays through a simple exfoliation using the conventional polymer tape. (b) A photograph of bent nanotube arrays. ((c) and (d)) SEM images of transferred ZnO nanotubes at a bending radius of 0.5 mm (c) over a wide view and (d) at high magnification at the indicated area.

5.4. Structural and optical characteristics of ZnO nanotubes

5.4.1. Structural characteristics

To understand the selective growth mechanism of ZnO nanostructures on CVD-graphene films and the interface between them, cross-sectional scanning transmission electron microscopy (STEM) was employed. For this analysis, a TEM specimen was fabricated from a ZnO nanotube/graphene/SiO_2/Si sample using a focused-ion-beam (FIB). Figure 5.12 shows a bright field (BF) cross-sectional image of a ZnO nanotube grown on a CVD-graphene film with a SiO_2 mask, revealing the selective growth mechanism. The patterned SiO_2 mask film was not only used to define the positions of the ZnO nanostructure array but also to effectively control undesired lateral growth at the bottom edge of the nanotubes. There was an undercut in the SiO_2 mask, presumably formed by wet etching, and ZnO also grew in this region. However, further growth of this ZnO product was blocked by the upper SiO_2 layer as shown in the TEM image, resulting in sharply defined nanostructures without undesired basal structures. This is in contrast to

nanotubes grown on exfoliated graphene following selective O_2 plasma treatment,[61] where lateral tailing of ZnO reaching micrometer scales was observed at the base.

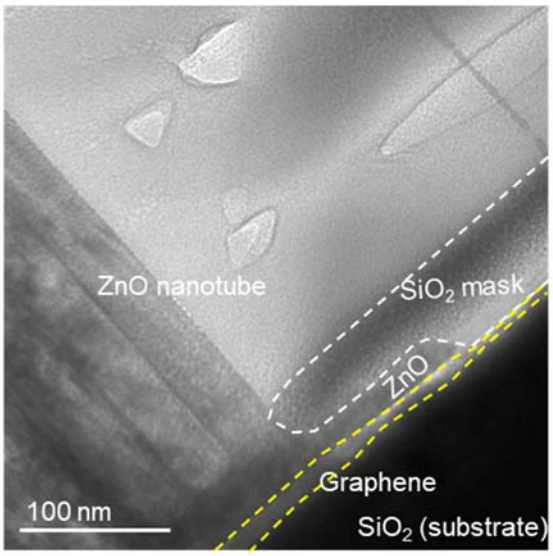

Fig. 5.12. Microstructural characteristics of ZnO nanotubes. (a) Cross-sectional transmission electron microscopy (TEM) bright-field (BF) image of ZnO nanotubes on CVD-graphene films. The white and yellow dashed lines indicate SiO_2 mask and CVD-graphene regions, respectively.

We also investigated the crystal structure of the ZnO nanotubes grown on graphene layers using a TEM as Fig. 5.13. Figure 5.13a showsa bright field (BF) image of the ZnO nanotubes dispersed onto TEM grid by using EtOH dispersion, and Fig. 5.13b shows a higher magnification image showing investigation area. The crystal orientation was investigated using the selected-area electron diffraction (SAED) technique. The SAED pattern in the Fig. 5.13c indicates that the ZnO nanostructures had the wurtzite crystal structure, with their c-axis growth orientation, and No distinct streaks in the SAED pattern was observed. It indicates that the ZnO nanotubes have high crystallinity. The atomic arrangement of the ZnO nanotube was further investigated using high-resolution (HR) TEM imaging and its fast Fourier transform (FFT). Figure 5.13d shows the HR image of the region indicated in Fig. 5.13b. It shows a highly ordered atomic arrangement of the ZnO nanotube grown on the graphene layers and the corresponding FFT confirmed this order.

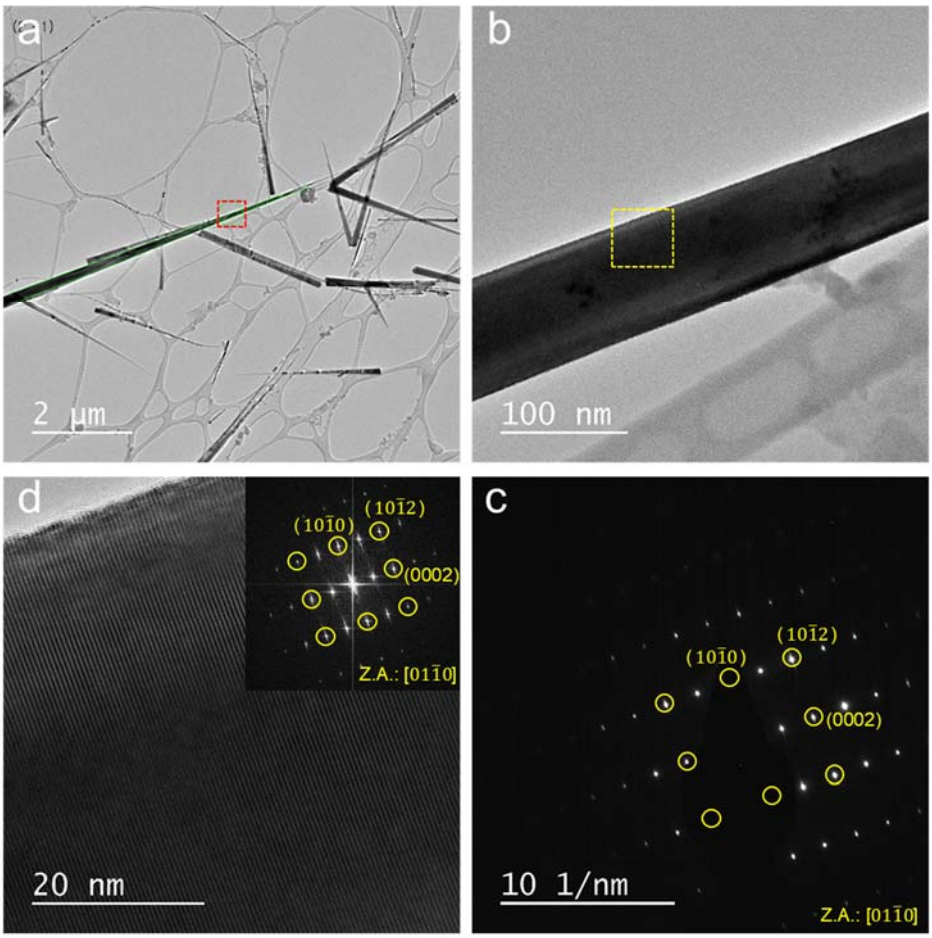

Fig. 5.13. Microstructural characteristics of the ZnO nanotube. (a and b) TEM BF images of (a) nanotubes dispersed onto TEM grid and (b) higher magnification image of indicated with red box, and (c) corresponding SAED pattern. (d) HR image of the ZnO nanotube taken from yellow box in (b). The inset represents the corresponding FFT pattern indicates the crystal orientation.

5.4.2. Optical characterizations

To use ZnO nanotubes grown on graphene films for optoelectronic devices, we investigated the optical characteristics of the ZnO nanotubes using an Nd:YAG pluse laser (355 nm) as an optical excitation source. Before measuring the lasing properties, lateral overgrowth onto the ZnO nanotubes, because the wall thickness of the as-grown ZnO nanotubes was too thin to sustain laser oscillation. Figures 5.14a schematically illustrates before and after of lateral coating on ZnO nanotubes.

Figure 5.14b shows field-emission scanning electron microscopy (FE-SEM) images of the position-controlled and vertically aligned ZnO nanotube arrays grown on graphene films. Uniform ZnO nanotubes were grown and regularly spaced, at distances of 4 μm, with a diameter of 420 ± 20 nm at the base and of 250 ± 40 nm at the top and a length of 8.2 ± 0.5 μm. The wall thickness was about 20 nm. 5.14c shows FE-SEM images after the lateral growth. During this process, an overgrowth of ZnO took place at the surface of the ZnO nanotubes, increasing the wall thickness to 140 nm at the base and to 190 nm near the tip, as indicated by the

SEM images. Additionally, the outer shape of the nanotube changed from a smooth circle-like polygon, as shown in the inset of Fig. 5.14b, to a hexagon, as shown in the inset of Fig. 5.14c. Figure 5.14d shows FE-SEM images of the nanotubes before and after lateral growth times of 1 and 3 h. As the growth time increased, the shape of the nanotube transformed from tapered to straightened. Also, the inner core at the end-tip of the nanotube was modified from an open hole to closed solid during lateral growth. We inferred that the inner core of the remaining nanotube remained open due to its long aspect ratio. The lateral growth rate was estimated to be 1.3 nm/min at the base and 1.8 nm/min near the tip, as shown in Fig. 5.13e.

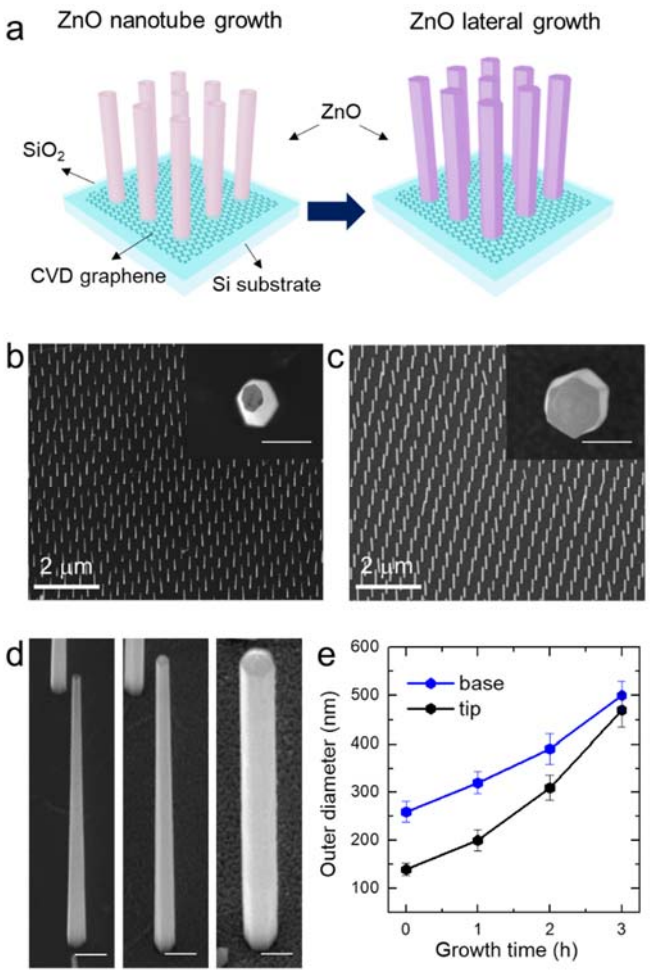

Fig. 5.14. (a) A schematic diagram of the ZnO nanotubes on graphene films. (b,c) FESEM images of ZnO nanotubes grown on CVD graphene/Si substrates before (b) and after (c) lateral growth. FESEM images were obtained at a tilt angle of 30°. Insets show the nanotubes from above. The scale bars of the insets are 500 nm. (d) FESEM images of ZnO nanotubes before and after lateral

growth times of 1 and 3 h. The scale bar is 500 nm. (e) Plot of the outer diameter of a nanotube as a function of growth time. Diameters were measured at the base and the tip of a nanotube.

The ZnO nanotubes grown on graphene films exhibited excellent lasing characteristics. We investigated these using confocal micro-photoluminescence (μ-PL) spectroscopy. The frequency-tripled output (355 nm) of a Nd:YAG laser (10 Hz, 6 ns pulse width) was focused using a ×39 UV objective lens (NA=0.50). The direction of the incident laser beam was normal to the end facets of the nanotubes. Figure 5.15a shows the power-dependent PL spectra of a nanotube with a wall thickness of 160 nm at the center. At excitation densities below 40 kW/cm^2, a broad spontaneous emission centered at 383 nm was observed. However, as the excitation density was increased beyond 40 kW/cm^2, sharp peaks appeared within the broad emission spectra. With further increases in the excitation density, the sharp peaks dominated the spectra. Sharp emission lines and a dramatic increase in the emission intensity indicated that lasing action was occurring in the ZnO nanotube. The plot of the output PL emission intensity against the input excitation density (*i.e.*, light–light curve) in the inset of Fig. 5.15a shows that the lasing threshold was 50 kW/cm^2, which is comparable to that of high-quality ZnO nanowires grown on single crystalline substrates.[72] This low threshold density suggests that the ZnO

nanotubes grown on CVD graphene films were of high optical quality. No laser emission was observed in nanotubes where the additional lateral growth stage had been omitted as shown in Fig. 5.15b. This was due to the thin wall thickness. In the case of nanotubes with a wall thickness of 50 nm, lasing emissions were observed. The lasing intensity was lower in these thin tubes than in thicker tubes due to lower levels of light confinement.

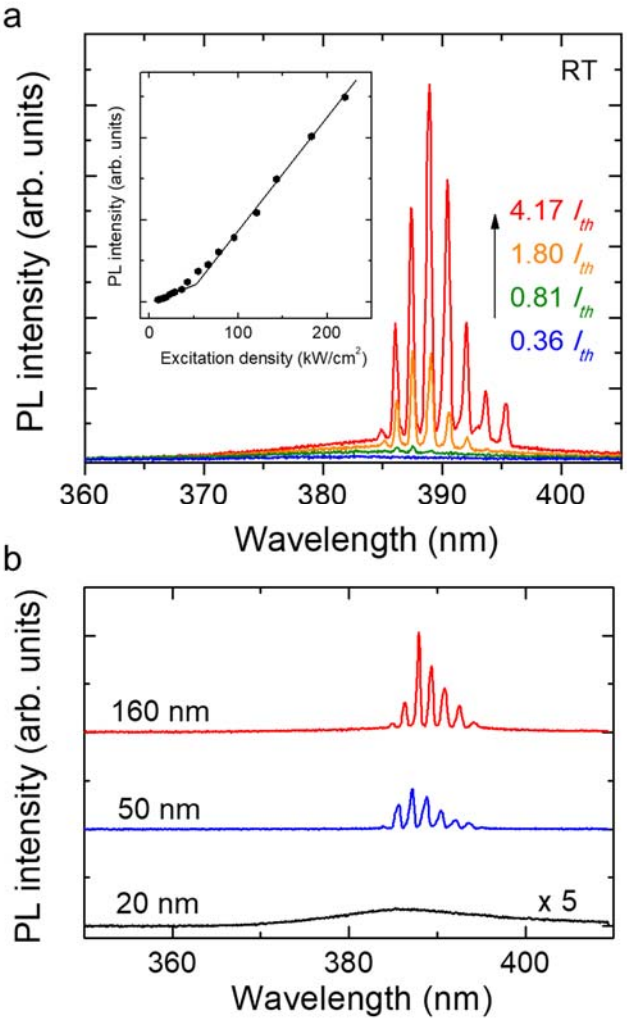

Fig. 5.15. (a) Power-dependent PL spectra of ZnO nanotubes. The inset shows the output PL intensity against the input excitation density. (b) Lasing spectra of nanotubes with thicknesses of 160, 50, and 20 nm at an excitation density of 180 kW/cm^2.

5.5. Summary

This chapter described the catalyst-free growth of individually position-controlled and vertically aligned ZnO nanotube array on CVD-graphene films. Graphene films were grown on Cu-foil by chemical vapor deposition, transferred onto SiO_2/Si substrates, and used as substrates for the selective growth of ZnO nanotube array. The ZnO nanostructures had precisely controlled shapes and highly crystalline structures as examined by SEM and TEM. The ZnO nanotubes exhibited promising optical characteristics for lasing device applications. Additionally, the nanostructures were easily detached with negligible damage from the host substrate using a simple mechanical lift-off to form flexible nanomaterial systems. This method presents a versatile means for the preparation of one-dimensional (1D) nanostructures as functional components in various applications by allowing vertically aligned growth of 1D nanostructures even on amorphous, metallic, or flexible substrate materials, with individually controlled positions and designed dimensions over a wafer-scale area. All these features show that ZnO nanotubes

grown on CVD-graphene films are desirable for fabricating three-dimensional integrated nanodevices.

Flexible piezoelectric pressure sensor using ZnO nanostructure array

6

6.1. Introduction

Piezoelectric materials have attracted great attention for use in sensors or power generators since they can directly convert mechanical energy into electric energy without additional components.[20,73] Amongst various piezoelectric material system, ZnO- or GaN-based one-dimensional nanorod/nanowires are considered to be highly advantageous for piezoelectronic devices.[73-75] ZnO and GaN have both semiconducting and piezoelectric properties that make possible to combine sensors and transducer monolithically. Additionally, they are biocompatible to be used as biomedical applications without additional treatment. Moreover, one-dimensional (1D) structure gives further advantage since its nanoscale diameter generates tremendous pressure from a little amount of external force. For these reasons,

piezoelectric properties of semiconductor nanowires, such as ZnO and GaN, have been studied extensively for fabricating nanogenerators or pressure sensors. However, to the objectives for manufacturing pressure sensing devices using semiconductor nanowires, there is still an obstacle from controllability and combining with a flexible substrate.

The difficulties accompanied by solid single crystal substrates can be circumvented by using graphene films as growth templates. The graphene films are extremely flexible and stretchable due to their excellent mechanical strength, perfect for flexible device application. Importantly, its thermal and chemical stability, as well as a hexagonal structure, made it possible for their use as a crystal growth template. Recently, we successfully achieved to grow ZnO nanotube arrays on CVD-graphene films with vertical manner, precisely controlled shape and individually controlled positions. The CVD-graphene films are not only a growth buffer but also work as a bottom electrode which forms a flexible Ohmic channel between ZnO nanotubes and metal interconnectors.

This chapter describes the fabrication process and demonstration of piezoelectric pressure sensors with flexibility and stretchability. The device is based on ZnO nanotube arrays grown on CVD-graphene films. When an external pressure is applied, their electrical resistivity is increased. Meanwhile, longer ZnO nanotubes are more sensitive to incident pressure; thus the change ratio of flowing current can also be manipulated by preparing a different length of ZnO nanotubes. In addition, their controlled high height-to-diameter ratio enables to respond not only to perpendicular pressure but also to horizontally induced force to the nanosensors.

6.2. Piezoelectric pressure sensor using ZnO nanostructures

6.2.1. Experimental design and procedures

The basic strategy for the fabrication of flexible piezoelectric pressure sensors using ZnO nanotubes is illustrated in Fig. 6.1. The first step is the preparation of ZnO nanotube arrays on CVD-graphene films by using a catalyst-free MOCVD system as described in section 5.3. First, the nanotubes were grown

with precisely controlled dimension and positions, such as 10 μm of mean length, 200 nm of diameter, and 4-μm-pitched hexagonal array. After preparing the nanotube array, the gap between the nanotubes was filled with an insulating flexible polymer layer, polyimide (PI, VTEC PI-080-051), as shown in Fig. 6.1b. Then, the PI layer was cured at 300 °C for 3 min in nitrogen mood, to enhance the mechanical strength and chemical resistance of the layer. After curing process, short oxygen plasma ashing was processed onto the nanostructures to expose the tip of ZnO nanotubes, and a 100-nm-thick gold film was deposited as a top electrode to form Schottky junction with ZnO nanotubes (Fig. 6.1c).[63]

The flexible pressure sensor is prepared by mechanical lift-off of the nanosystems from the host substrate (Fig. 6.1d), by exploiting the weak bonding between graphene and the host substrate, Si wafer. The freestanding form of ZnO/graphene hybrid dimension nanomaterials, supported by PI film, enabled the deposition of a metal electrode at the bottom graphene layer. Finally, chromium/gold bilayer metal electrode was deposit at the graphene films to form

Ohmic electrode junction (Fig. 6.1e), then the flexible piezoelectric nanostructure pressure sensor was formed as Fig. 6.1f.

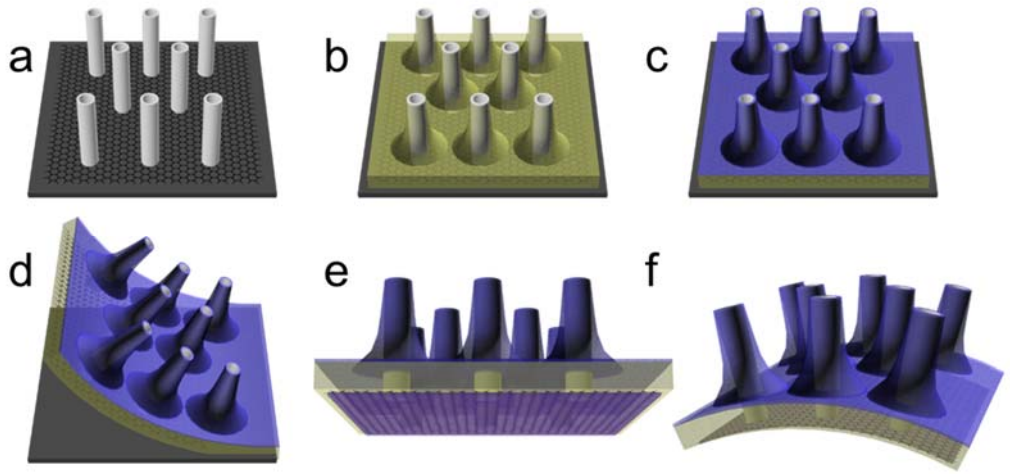

Fig. 6.1. Schematics of the overall process for piezoelectric pressure sensor using ZnO nanotubes grown on CVD-graphene films. (a) preparation of position-selectively grown ZnO nanotubes on CVD-graphene film. (b) Spin-coating of polyimide layer coating onto the nanostructures and (c) deposit top metal electrode layer onto the nanostructure surface after oxygen plasma ashing to expose the tip of ZnO nanotubes. (d) Mechanical lift-off the ZnO nanotubes to expose the bottom graphene layer and to give flexibility to the nanosystem. (e) Deposit bottom electrode (commonly Cr/Au) to form an Ohmic junction and (f) a concept image of the flexible pressure sensor.

Conceptual illustration of the final device structure is schematically illustrated in Fig. 6.2a, where the top gold electrode and bottom graphene/chromium/gold electrode are separated by Pi layer, which fills void among nanotubes. The SEM image in Fig. 6.2b reveals the highly-ordered vertical nanotube array after the full process to fabricate a flexible pressure sensor following the above procedures. The exposed length of nanotubes over PI layer was near 8 μm, while the average diameter of exposed nanotubes was smoothly tapered from 150 nm to needle.

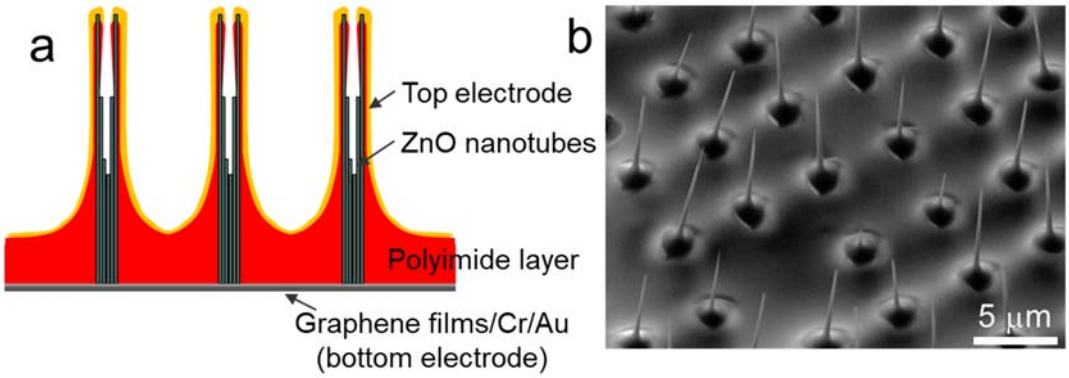

Fig. 6.2. (a) A schematic illustration of cross-sectional image of ZnO nanotube-based piezoelectric pressure sensor and (b) the corresponding SEM image of the surface of the sensor.

6.2.2 Electric properties of ZnO nanotube array grown on graphene films and proper device structure for pressure sensors

The electrical characteristics of the ZnO nanodevice array were investigated by measuring their current–voltage (*I–V*) characteristics curves. Figure 6.3a shows the typical *I–V* curves of the nanodevices composed of both Schottky junction (Au/ZnO) and Ohmic junction (Au/Ti/ZnO) at the electrode. The *I–V* characteristics curves show clean rectifying behavior from Au/ZnO Schottky junction and linear shape from Au/Ti/ZnO Ohmic junction. This result indicates that the ZnO nanotube array grown on graphene films is an excellent template for manufacturing nanoelectronics for both Ohmic (Au/Ti/ZnO) and Schottky (Au/ZnO) nanodevices while the bottom electrode (ZnO/graphene/Cr/Au) provides a good Ohmic junction for electron injection.

To evaluate which device structure is proper for fabricating pressure sensors using the ZnO nanostructures, the pressure response of the two electronic device structures was investigated by measuring decrease ratio of flowing current

through the ZnO nanotubes by the applied force from 0 to 2000 mN. Figure 6.3b reveals the drastically different current change ratio from the two electrode junctions. 1.7% current decrease was observed from the Ohmic device while 20% decrease was observed from the Schottky device with 500 mN applied force. Based on this result, we fabricated piezoelectric pressure sensors using an Au/ZnO Schottky junction to maximize the pressure response of the device in following experiments.

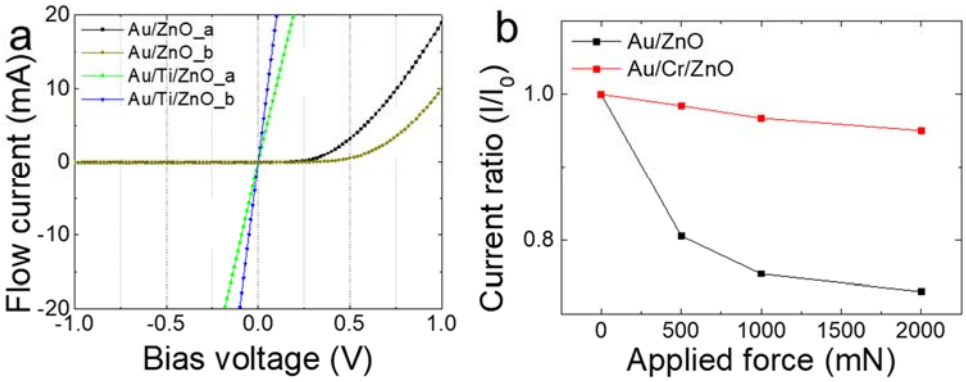

Fig. 6.3. (a) *Current–voltage* curves of ZnO nanotube array grown on graphene films with different top electrodes. (b) Plot showing the current decrease ratio of Schottky (black) and Ohmic (red) nanodevices.

6.2.3. Pressure response

The typical current–voltage characteristics of pressure sensors, using the Au/ZnO Schottky diode, are shown in Figs. 6.4a and b. Flowing current through ZnO nanotubes was decreased with increasing applied force, and recovered to the original amount with force decreasing, at both reverse and forward bias voltage showed the same tendency. The sensitivity (current varying ratio per applied force, $[\Delta I/I_0]/F$) was 1.0 to 1.8 N^{-1}, which was changed with the applied bias voltage, as shown in Fig. 6.4c.

The presumed pressure sensing mechanism of the gold/ZnO nanotube array is illustrated in Fig. 6.4d. A free status of ZnO nanotubes have Schottky contacts at the junction with a gold electrode (Au/ZnO) the Schottky barrier height is Φ_B. When an external force applied, a piezoelectric field is induced inside the ZnO nanotubes. The internal field modulates potential in the ZnO, and charges (e-) are induced at the Au/ZnO Schottky junction, and then the concentrated electric charge increases the Schottky barrier height (ΔE_p). The change in band structure leads the

piezoresistance effect, which leads decrease of flow current through ZnO nanotubes.[73]

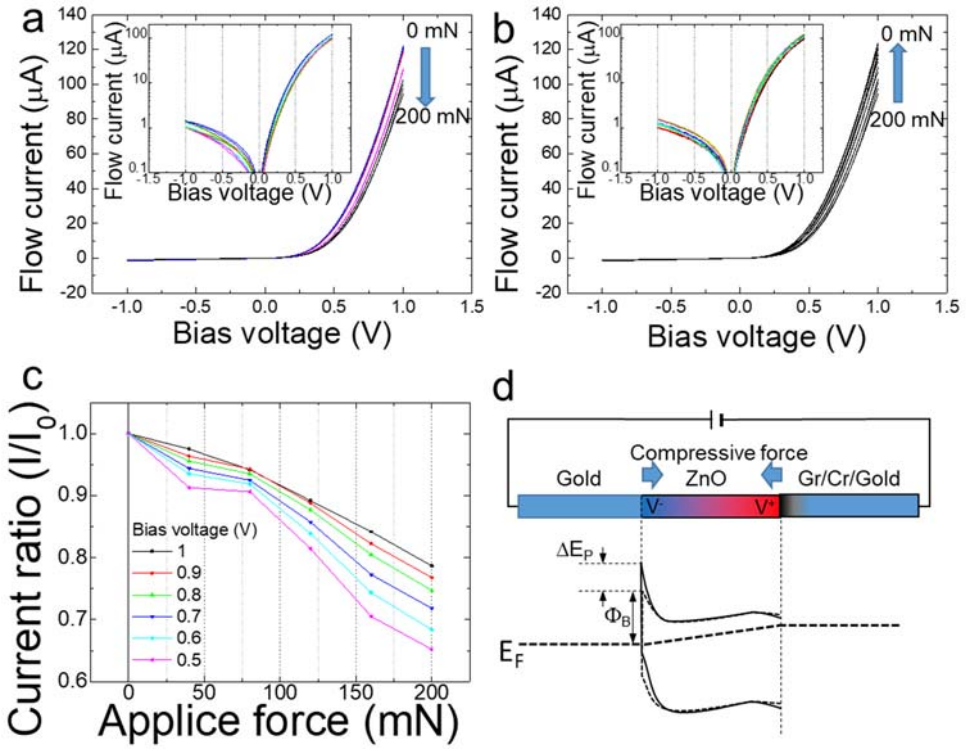

Fig. 6.4. (a, b) Current-voltage characteristics curves of the gold/ZnO Schottky diode pressure sensor under different load conditions. (a) Increasing and (b) decreasing applied force from 0 to 200 mN. (c) The relation of flowing current through ZnO nanotubes and applied force with under bias voltages. (d) Schematic diagram of pressure sensing mechanism showing the change of Schottky barrier height by applied force compressive direction).

The reliability and physical robustness of the ZnO nanotube-based pressure sensor were investigated by measuring the current under dynamic force loading conditions with a fixed bias voltage. For this work, we could precisely control the applied force, directly induced onto the ZnO nanostructures, using a voice-coil motor (V-275.431, PI GmbH & Co. KG). As shown in Fig. 6.5a, the flowing current through ZnO nanotubes was decreased and increased sequentially with modulating applied force. The sensor showed a fast response at every force changing points under 100 ms, same flowing current for the same force, and recovered to the original status after removing the applied force. Figure 6.5b present the relation between the flowing current and applied force with a small hysteresis in the curve. Remarkably, there was a one-to-one correspondence between the flowing current and applied force with a negligible hysteresis to the repeated force.

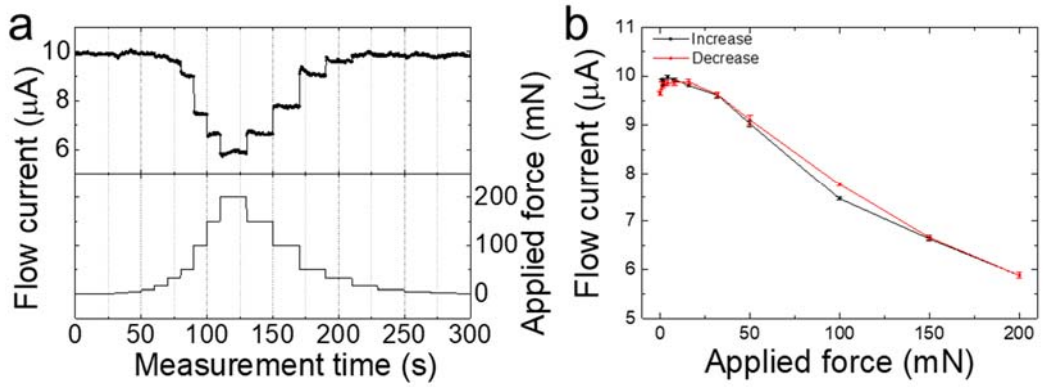

Fig. 6.5. *Current−time* (*I−T*) curves of the ZnO nanotube pressure sensor under various forces at a fixed bias voltage of 0.4 V. (a) A graph showing the relation between current and applied force. The black line shows the flowing current through ZnO nanotubes and the blue line shows applied force ranged from 0 to 200 mN. (b) Current−force curves represent current change with (black) increasing and (red) decreasing applied force.

Nowadays, wearable electronic devices have attracted great attention for medical care, which is enabled to monitor continuously by using wearable medical devices. For instance, atherosclerosis, a kind of critical cardiovascular diseases, is asymptomatic in the early stage, while it leads to a small change of heart pulse.[76] For early diagnosis of these kinds of cardiovascular diseases, wrist pulse is a key indicator of arterial blood pressure and heart rate that provides a lot of information with a non-invasive diagnosis. In this work, the ZnO nanotube-based pressure sensor was attached to the wrist using a 3M Scotch tape to enable the monitoring of the wrist pulse in a real time. Figure 6.6a shows wrist pulse measurement results using the ZnO nanotube pressure sensor before and after running of an adult male (30 years old). The amplitude and period clearly show before and after exercise as shown in Fig.s 6.6b and c.

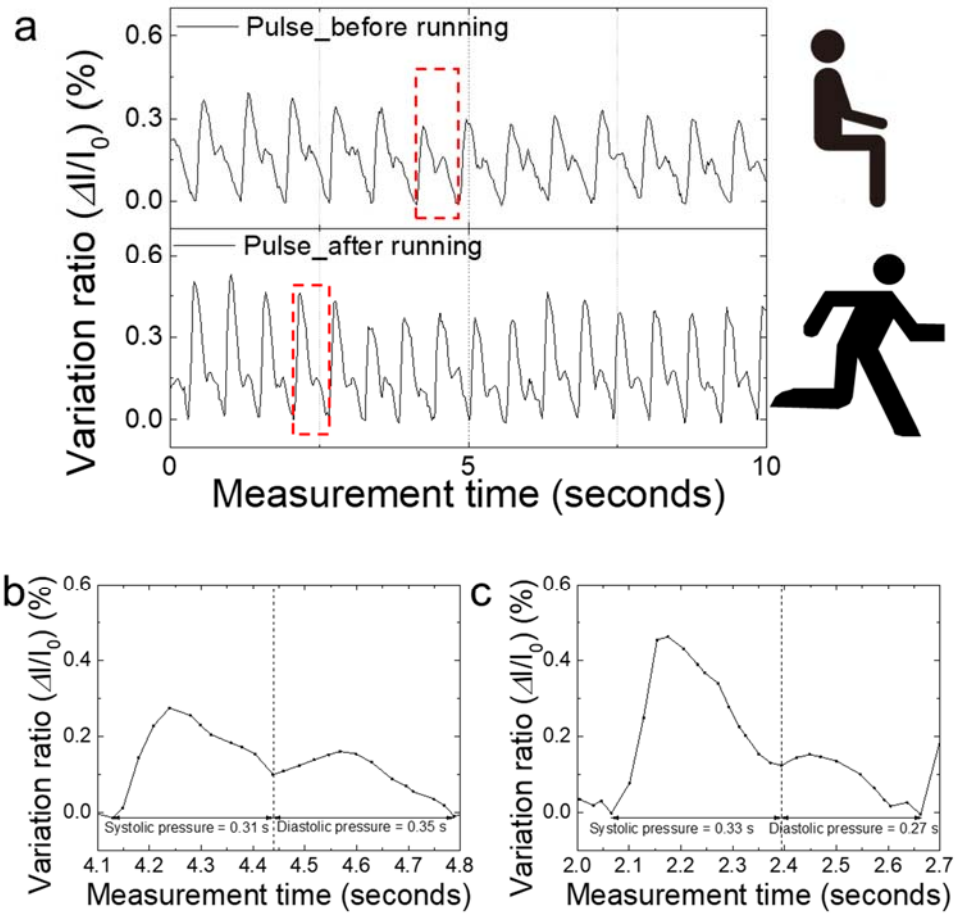

Fig. 6.6. Wrist pulse measurement result. (a) *Current—time* (*I—T*) curves of wrist pulse measured by using ZnO nanotube pressure sensor before and after running of an adult male. (b, c) Single pulse waveform from (a). (b) Before running and (c) after running.

Nanotube pressure sensors have an excellent sensitivity which is able to detect even the slightest movement of air. Fig. 6.7a illustrates the detection method of airflow using the nanotube pressure sensors. Nitrogen flow comes from a nozzle connected to a dry nitrogen cylinder, and the flowing incident area is designated through a pinhole (4.5 mm diameter circle). The applied pressure was calculated by measuring the weight difference using an electronic scale under the pressure sensor. Figure 6.7b shows the sharp and reliable airflow sensing results using the measurement result using the system at 0.4 V of bias voltage. A plot in Fig. 6.7c shows the reliable pressure response of the nanotube pressure sensor that can detect only 1 Pa of air flow.

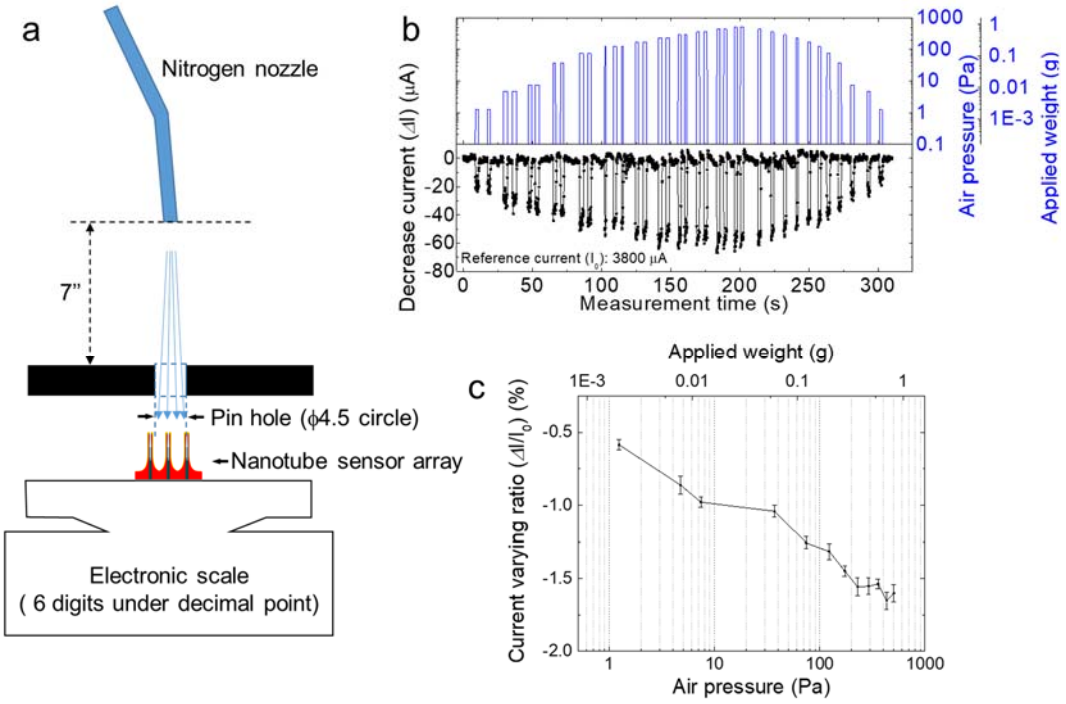

Fig. 6.7. (a) Schematic of air-pressure sensing for the ZnO nanotube pressure sensor. (b) A current response of the ZnO nanotubes with different air flow. (c) Corresponding current variation ratio-air pressure curve.

Measuring human breath pattern is a non-invasive and sustainable monitoring method that makes it possible to diagnosis cardiovascular and pulmonary diseases at an early stage. Traditionally, thermal mass flow sensors have been used to de observe personal human breath to monitor the kinds of disorders, such as sleep apnea. However, the sensors are large and consuming high energy, therefore not suitable for coming under wearable applications such as electronic skin or mobile electronics. These highly-sensitive nanotube pressure sensors, which can detect airflow under 1 Pa of pressure, could be applied for detecting human breath by attaching onto philtrum as shown in Fig. 6.8a. Figure 6.8b shows the investigation to demonstrate the potential use of the nanotube pressure sensor for breath detection. We could observe periodic breath waveform that is a stable and reliable change of flowing current. The result also shows the amount of exhaling and inhaling of human breath.

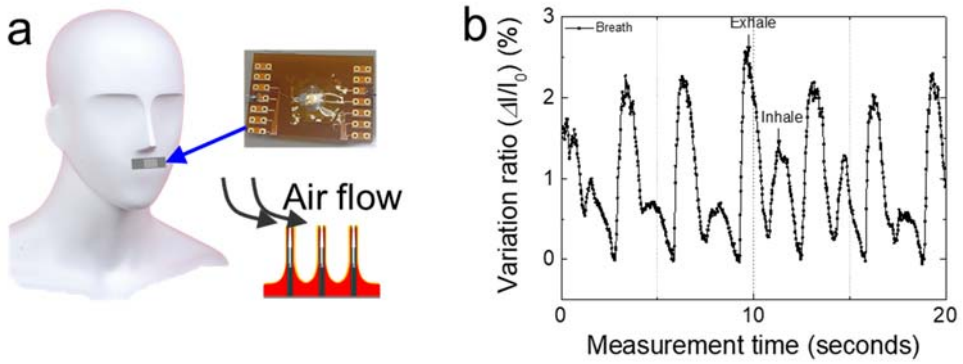

Fig. 6.8. Monitoring of human breathing. (a) A schematic illustration of breath measurement experiment and (b) corresponding measurement result that shows reliable change of flow current in response to human breathing.

6.3. Summary

This chapter described the fabrication process and characteristics of pressure sensing application using ZnO nanotubes grown on graphene layers. The nanotube pressure sensor showed excellent pressure response that can detect a few millinewtons of applied force, and even can detect small airflow near 1 Pa. Additionally, the sensors exhibit a high sensitivity of 4.5 kPa^{-1} and fast response time near 10 ms. Furthermore, the sensors can be used as an electronic skin that measures various personal signal including wrist pulse and human breath by attaching on the human body.

Concluding remark and outlook

7

7.1. Summary

This thesis started with the hypothesis that the position-controlled selective grown one-dimensional (1D) nanostructures combined with two-dimensional (2D) layered nanomaterials provide a novel material system for transferable, flexible, and integrable electronics and optoelectronic device applications. High-quality wide bandgap semiconductor nanostructures were directly grown on graphene by using metal-organic vapor phase epitaxy (MOVPE), with controlled growth manner. The nanostructures were employed to fabricate various nanodevices, such as piezoelectric pressure sensors and light-emitting diodes. The details of achievements are summarized as follow.

1) One-dimensional nanostructure growth on CVD-graphene films

- One-dimensional GaN and ZnO nanostructures were successfully grown on CVD-graphene layers and their structural and optical characteristics

were investigated. The shape of GaN nanostructures was controlled by employing different thicknesses of nickel films as catalyst layer for VLS process, while the same of ZnO nanostructures was controlled by tuning process temperature. Structural analysis using TEM reveals that both nanostructures have highly-ordered atomic structures without defects. However, Optical investigation using a low temperature photoluminescence revealed different defect density of the two nanostructures synthesized by different methods.

2) Position-controlled growth of 1D ZnO nanostructures on CVD-graphene films.

- A novel growth method for precisely-controlled one-dimensional ZnO nanostructure array on graphene films was developed and presented. The ZnO nanostructures had precisely controlled shapes and highly crystalline structures as examined by SEM and TEM. The ZnO nanotubes exhibited promising optical characteristics for lasing device applications. Additionally, the nanostructures were easily detached with negligible

damage from the host substrate using a simple mechanical lift-off to form flexible nanomaterial systems. This method presents a versatile means for the preparation of one-dimensional (1D) nanostructures as functional components in various applications by allowing vertically aligned growth of 1D nanostructures even on amorphous, metallic, or flexible substrate materials, with individually controlled positions and designed dimensions over a wafer-scale area. All these features show that ZnO nanotubes grown on CVD-graphene films are desirable for fabricating three-dimensional integrated nanodevices.

3) Fabrication of piezoelectric pressure sensor using ZnO/graphene hybrid nanosystems

- Furthermore, as a representative demonstration for device application using the ZnO/graphene hybrid nanosytems, piezoelectric pressure sensor based on the ZnO nanotubes grown on graphene films. The nanotube pressure sensor showed excellent pressure response that can detect a few millinewtons of applied force, and even can detect small

airflow near 1 Pa. Additionally, the sensors exhibit a high sensitivity of 4.5 kPa^{-1} and fast response time near 10 ms. Furthermore, the sensors can be used as an electronic skin that measures various personal signal including wrist pulse and human breath by attaching on the human body.

7.2. Future works and outlook.

1D-2D hybrid dimension nanomaterials have many advantages for fabricating nanoelectronics and optoelectronics with flexibility, transferability, and integration with conventional electric circuitry. As an example, this dissertation showed selective growth of ZnO nanotube arrays on CVD-graphene films and demonstrated piezoelectric pressure sensors and LED applications. Thanks to the scalability of CVD-graphene films, this novel material system is very promising blocks for next-generation large-area flexible electronics such as wearable and body-embedded applications. Nevertheless, this field is still in the early stage and remaining large room for improvements as follow.

1) Integrating nanodevices with traditional Si-CMOS devices and flexible circuitry

- The controlled nanomaterials grown on graphene films could be employed as a building block for making integrated device applications with other electronics, such as traditional Si-CMOS or flexible circuitry. The most significant advantage of nanostructure growth on graphene layer is the possibility to apply on arbitrary substrates, including a metal electrode for interconnector, an amorphous oxide for the passivation layer, or even plastics films. By exploiting this, we can combine the two elements into one application to open up a new field of nanodevices.

2) Finding a different way to prepare graphene films on the target substrate

- The primary obstacle which prevents the use of CVD-graphene films in the industrial field is the complex and challenging transfer method through wet-chemical etching the metal foil, used as a catalyst for graphene CVD process. The direct deposition method to prepare a graphene layer would be a solution to circumvent this problem.

References

1. M. S. Gudiksen, L. J. Lauhon, J. Wang, D. C. Smith, and C. M. Lieber, Nature **415** (6872), 617 (2002).

2. J. Xiang, W. Lu, Y. J. Hu, Y. Wu, H. Yan, and C. M. Lieber, Nature **441** (7092), 489 (2006).

3. Z. Y. Fan, D. W. Wang, P. C. Chang, W. Y. Tseng, and J. G. Lu, Applied Physics Letters **85** (24), 5923 (2004).

4. X. D. Wang, J. Zhou, J. H. Song, J. Liu, N. S. Xu, and Z. L. Wang, Nano Letters **6** (12), 2768 (2006).

5. Ruoxue Yan, Daniel Gargas, and Peidong Yang, Nature Photonics **3**, 569 (2009).

6. C. Thelander, P. Agarwal, S. Brongersma, J. Eymery, L. F. Feiner, A. Forchel, M. Scheffler, W. Riess, B. J. Ohlsson, U. Gosele, and L. Samuelson, Materials Today **9** (10), 28 (2006).

7. A. M. Morales and C. M. Lieber, Science **279** (5348), 208 (1998).

8. W. I. Park, D. H. Kim, S. W. Jung, and G. C. Yi, Applied Physics Letters **80** (22), 4232 (2002).

9. W. I. Park, G. C. Yi, M. Y. Kim, and S. J. Pennycook, Advanced Materials **14** (24), 1841 (2002).

10. H. T. Ng, J. Han, T. Yamada, P. Nguyen, Y. P. Chen, and M. Meyyappan, Nano Letters **4** (7), 1247 (2004).

11. J. Goldberger, A. I. Hochbaum, R. Fan, and P. D. Yang, Nano Letters **6** (5), 973 (2006).

12. G. F. Zheng, W. Lu, S. Jin, and C. M. Lieber, Advanced Materials **16** (21), 1890 (2004).

13. W. I. Park, J. S. Kim, G. C. Yi, M. H. Bae, and H. J. Lee, Applied Physics Letters **85** (21), 5052 (2004).

14. J. Kong, N. R. Franklin, C. W. Zhou, M. G. Chapline, S. Peng, K. J. Cho, and H. J. Dai, Science **287** (5453), 622 (2000).

15. P. G. Collins, K. Bradley, M. Ishigami, and A. Zettl, Science **287** (5459), 1801 (2000).

16. M. W. Ahn, K. S. Park, J. H. Heo, J. G. Park, D. W. Kim, K. J. Choi, J. H. Lee, and S. H. Hong, Applied Physics Letters **93** (26) (2008).

17. G. K. Mor, K. Shankar, M. Paulose, O. K. Varghese, and C. A. Grimes, Nano Letters **6** (2), 215 (2006).

18. K. Zhu, N. R. Neale, A. Miedaner, and A. J. Frank, Nano Letters **7** (1), 69

(2007).

19. Q. Wan, Q. H. Li, Y. J. Chen, T. H. Wang, X. L. He, J. P. Li, and C. L. Lin, Applied Physics Letters **84** (18), 3654 (2004).

20. Z. L. Wang and J. H. Song, Science **312** (5771), 242 (2006).

21. S. Xu, B. J. Hansen, and Z. L. Wang, Nature Communications **1** (2010).

22. Y. Gao and Z. L. Wang, Nano Letters **7** (8), 2499 (2007).

23. C. Kim, W. I. Park, G. C. Yi, and M. Kim, Applied Physics Letters **89** (11) (2006).

24. W. I. Park, G. C. Yi, M. Kim, and S. J. Pennycook, Advanced Materials **15** (6), 526 (2003).

25. Y. J. Hong, J. M. Jeon, M. Kim, S. R. Jeon, K. H. Park, and G. C. Yi, New Journal of Physics **11** (2009).

26. C. H. Lee, J. Yoo, Y. J. Hong, J. Cho, Y. J. Kim, S. R. Jeon, J. H. Baek, and G. C. Yi, Applied Physics Letters **94** (21) (2009).

27. K. Tomioka and T. Fukui, Journal of Physics D-Applied Physics **47** (39) (2014).

28. A. R. Gao, N. Lu, P. F. Dai, T. Li, H. Pei, X. L. Gao, Y. B. Gong, Y. L. Wang, and C. H. Fan, Nano Letters **11** (9), 3974 (2011).

29. W. Z. Wu, X. N. Wen, and Z. L. Wang, Science **340** (6135), 952 (2013).

30. Y. J. Hong, H. S. Jung, J. Yoo, Y. J. Kim, C. H. Lee, M. Kim, and G. C. Yi, Advanced Materials **21** (2), 222 (2009).

31. Y. J. Kim, C. H. Lee, Y. J. Hong, G. C. Yi, S. S. Kim, and H. Cheong, Applied Physics Letters **89** (16) (2006).

32. S. D. Hersee, X. Y. Sun, and X. Wang, Nano Letters **6** (8), 1808 (2006).

33. Y. J. Kim, J. Cho, Y. J. Hong, J. M. Jeon, M. Kim, C. Liu, and G. C. Yi, Nanotechnology **21** (5) (2010).

34. A. I. Hochbaum, R. Fan, R. R. He, and P. D. Yang, Nano Letters **5** (3), 457 (2005).

35. K. Tomioka, M. Yoshimura, and T. Fukui, Nature **488** (7410), 189 (2012).

36. S. Roddaro, K. Nilsson, G. Astromskas, L. Samuelson, L. E. Wernersson, O. Karlstrom, and A. Wacker, Applied Physics Letters **92** (25) (2008).

37. F. L. Lu, T. T. D. Tran, W. S. Ko, K. W. Ng, R. Chen, and C. Chang-Hasnain, Optics Express **20** (11), 12171 (2012).

38. X. J. Feng, K. Shankar, O. K. Varghese, M. Paulose, T. J. Latempa, and C. A. Grimes, Nano Letters **8** (11), 3781 (2008).

39. J. A. Jiang, Y. Y. Li, J. P. Liu, and X. T. Huang, Nanoscale **3** (1), 45 (2011).

40. Y. J. Kim, J. H. Lee, and G. C. Yi, Applied Physics Letters **95** (21) (2009).

41. A. M. Munshi, D. L. Dheeraj, V. T. Fauske, D. C. Kim, A. T. J. van Helvoort, B. O. Fimland, and H. Weman, Nano Letters **12** (9), 4570 (2012).

42. Z. H. Zhang, Y. Y. Liu, Y. Yang, and B. I. Yakobson, Nano Letters **16** (2), 1398 (2016).

43. C. Gomez-Navarro, R. T. Weitz, A. M. Bittner, M. Scolari, A. Mews, M. Burghard, and K. Kern, Nano Letters **7** (11), 3499 (2007).

44. S. Das Sarma, S. Adam, E. H. Hwang, and E. Rossi, Reviews of Modern Physics **83** (2), 407 (2011).

45. A. A. Balandin, S. Ghosh, W. Z. Bao, I. Calizo, D. Teweldebrhan, F. Miao, and C. N. Lau, Nano Letters **8** (3), 902 (2008).

46. R. R. Nair, P. Blake, A. N. Grigorenko, K. S. Novoselov, T. J. Booth, T. Stauber, N. M. R. Peres, and A. K. Geim, Science **320** (5881), 1308 (2008).

47. Q. K. Yu, J. Lian, S. Siriponglert, H. Li, Y. P. Chen, and S. S. Pei, Applied Physics Letters **93** (11) (2008).

48. X. S. Li, W. W. Cai, J. H. An, S. Kim, J. Nah, D. X. Yang, R. Piner, A. Velamakanni, I. Jung, E. Tutuc, S. K. Banerjee, L. Colombo, and R. S. Ruoff, Science **324** (5932), 1312 (2009).

49. S. Bae, H. Kim, Y. Lee, X. F. Xu, J. S. Park, Y. Zheng, J. Balakrishnan, T.

Lei, H. R. Kim, Y. I. Song, Y. J. Kim, K. S. Kim, B. Ozyilmaz, J. H. Ahn, B. H. Hong, and S. Iijima, Nature Nanotechnology **5** (8), 574 (2010).

50. L. Samuelson, M. T. Bjork, K. Deppert, M. Larsson, B. J. Ohlsson, N. Panev, A. I. Persson, N. Skold, C. Thelander, and L. R. Wallenberg, Physica E-Low-Dimensional Systems & Nanostructures **21** (2-4), 560 (2004).

51. F. Qian, S. Gradecak, Y. Li, C. Y. Wen, and C. M. Lieber, Nano Letters **5** (11), 2287 (2005).

52. M. H. Huang, S. Mao, H. Feick, H. Q. Yan, Y. Y. Wu, H. Kind, E. Weber, R. Russo, and P. D. Yang, Science **292** (5523), 1897 (2001).

53. M. Law, L. E. Greene, J. C. Johnson, R. Saykally, and P. D. Yang, Nat. Mater. **4** (6), 455 (2005).

54. Y. Cui, Z. H. Zhong, D. L. Wang, W. U. Wang, and C. M. Lieber, Nano Letters **3** (2), 149 (2003).

55. W. Guo, M. Zhang, A. Banerjee, and P. Bhattacharya, Nano Letters **10** (9), 3355 (2010).

56. Y. Li, J. Xiang, F. Qian, S. Gradecak, Y. Wu, H. Yan, H. Yan, D. A. Blom, and C. M. Lieber, Nano Letters **6** (7), 1468 (2006).

57. Y. B. Tang, Z. H. Chen, H. S. Song, C. S. Lee, H. T. Cong, H. M. Cheng, W. J. Zhang, I. Bello, and S. T. Lee, Nano Letters **8** (12), 4191 (2008).

58. K. Chung, C. H. Lee, and G. C. Yi, Science **330** (6004), 655 (2010).

59. C. H. Lee, Y. J. Kim, Y. J. Hong, S. R. Jeon, S. Bae, B. H. Hong, and G. C. Yi, Advanced Materials **23** (40), 4614 (2011).

60. P. K. Mohseni, A. Behnam, J. D. Wood, C. D. English, J. W. Lyding, E. Pop, and X. L. Li, Nano Letters **13** (3), 1153 (2013).

61. Y. J. Kim, H. Yoo, C. H. Lee, J. B. Park, H. Baek, M. Kim, and G. C. Yi, Advanced Materials **24** (41), 5565 (2012).

62. W. M. Choi, K. S. Shin, H. S. Lee, D. Choi, K. Kim, H. J. Shin, S. M. Yoon, J. Y. Choi, and S. W. Kim, Nano Research **4** (5), 440 (2011).

63. W. I. Park, G. C. Yi, J. W. Kim, and S. M. Park, Applied Physics Letters **82** (24), 4358 (2003).

64. J. B. Park, N. J. Kim, Y. J. Kim, S. H. Lee, and G. C. Yi, Current Applied Physics **14** (11), 1437 (2014).

65. J. Yoo, Y. J. Hong, S. J. An, G. C. Yi, B. Chon, T. Joo, J. W. Kim, and J. S. Lee, Applied Physics Letters **89** (4) (2006).

66. M. A. Reshchikov and H. Morkoc, Journal of Applied Physics **97** (6) (2005).

67. H. Z. Xu, Z. G. Wang, I. Harrison, A. Bell, B. J. Ansell, A. J. Winser, T. S. Cheng, C. T. Foxon, and M. Kawabe, Journal of Crystal Growth **217** (3), 228 (2000).

68. H. Park, S. Chang, J. Jean, J. J. Cheng, P. T. Araujo, M. S. Wang, M. G. Bawendi, M. S. Dresselhaus, V. Bulovic, J. Kong, and S. Gradecak, Nano Letters **13** (1), 233 (2013).

69. Y. J. Hong, J. W. Yang, W. H. Lee, R. S. Ruoff, K. S. Kim, and T. Fukui, Advanced Materials **25** (47), 6847 (2013).

70. K. S. Novoselov, A. K. Geim, S. V. Morozov, D. Jiang, Y. Zhang, S. V. Dubonos, I. V. Grigorieva, and A. A. Firsov, Science **306** (5696), 666 (2004).

71. S. R. Na, J. W. Suk, L. Tao, D. Akinwande, R. S. Ruoff, R. Huang, and K. M. Liechti, Acs Nano **9** (2), 1325 (2015).

72. A. D. Rakic, A. B. Djurisic, J. M. Elazar, and M. L. Majewski, Applied Optics **37** (22), 5271 (1998).

73. Z. L. Wang, Journal of Physical Chemistry Letters **1** (9), 1388 (2010).

74. C. H. Wang, W. S. Liao, Z. H. Lin, N. J. Ku, Y. C. Li, Y. C. Chen, Z. L. Wang, and C. P. Liu, Advanced Energy Materials **4** (16) (2014).

75. Y. S. Zhou, R. Hinchet, Y. Yang, G. Ardila, R. Songmuang, F. Zhang, Y. Zhang, W. H. Han, K. Pradel, L. Montes, M. Mouis, and Z. L. Wang, Advanced Materials **25** (6), 883 (2013).

76. G. L. WOOLAM, P. L. SCHNUR, C. VALLBONA, and H. E. HOFF, Circulation **25** (3), 533 (1962).

77. H. S. Jung, Y. J. Hong, Y. Li, J. Cho, Y. J. Kim, and G. C. Yi, Acs Nano **2** (4), 637 (2008).

78. K. Maeda, T. Takata, M. Hara, N. Saito, Y. Inoue, H. Kobayashi, and K. Domen, Journal of the American Chemical Society **127** (23), 8286 (2005).

79. J. Bae, J. Bin Han, X. M. Zhang, M. Wei, X. Duan, Y. Zhang, and Z. L. Wang, Journal of Physical Chemistry C **113** (24), 10379 (2009).

Appendix

Flexible photocatalyst applications using GaN nanowires grown on graphene films

A.1. Introduction

In this section, the flexible potocatalyst applications using GaN nanowires grown on graphene through VLS method as described in the chapter 4. The GaN nanowires grown on graphene films were transferred onto polymer substrates using a simple lift-off method for applications as flexible photocatalysts. Photocatalysis activities of the GaN nanowires prepared on the flexible polymer substrates were investigated under bending conditions.

A.2. Experimental method

The GaN nanowires grown on the graphene films were released from the Si substrates and transferred onto the PET substrates for applications as flexible photocatalysts. The gaps between the GaN nanowires on graphene films were filled

using the polymer PMMA, which is flexible, easy to remove, and supported the nanostructures and the graphene films during the layer-transfer process. Following spin-coating with PMMA, the films were released from the 300-nm-thick SiO_2/Si substrate by etching the sacrificial SiO_2 layer using a buffered oxide etchant. Complete release required a few hours, where the exact time depended on the sample size. The GaN nanowires released from the supporting substrate were readily transferred onto the PET substrates using deionized water. Subsequently, the PMMA layer was removed via rinsing with acetone and methanol to expose the nanowires.

The photocatalytic activity of the GaN nanowires was characterized by measuring the decoloration of 3 mL of 0.05 mM Orange II solution in a quartz cell. The GaN nanowire/graphene structure on the SiO_2/Si substrate was used to investigate the effects of varying the thickness of the Ni layer and of varying the pH. A quartz substrate was used as a reference to investigate the effects of varying the direction of the ultraviolet (UV) irradiation. To measure the photocatalytic activity of GaN nanowires as the pH was varied, a buffer solution was used. For

each set of photocatalytic experiments, a series of samples and a control (with no photocatalyst) were simultaneously irradiated with UV light using a halogen lamp (Osram Ultra-Vitalux 230V E27/EX), which had a spectrum similar to that of daylight. A UV/near-infrared spectrophotometer (Varian Cary 5000) was used to measure the optical absorption in the range of 300–800 nm.

A.3. Photocatalyst characteristics of GaN nanowires

The photocatalytic activity of the GaN nanowires was determined by measuring the decoloration of the dye Orange II under irradiation with UV light using a halogen lamp. To investigate the effects of the GaN surface morphology on the photocatalytic activity, we measured the amount of dye solution that was photodegraded using the GaN nanostructures grown using different thicknesses of Ni, as the morphology of the GaN depended strongly on the thickness of the Ni layer. As shown in Figure A1a, following 90 minutes of UV irradiation, the optical absorption of the dye decreased by 44% when the GaN nanowires grown on the 2-nm-thick Ni layer were used, whereas absorption decreased by 35% when the GaN

structures grown using the 0.5-nm-thick Ni layer were used. The GaN nanowires exhibited excellent stability in acidic conditions (see Fig. A2). Following UV irradiation for 10 hours, the absorption of the dye with pH values of 4 and 2 was 21% and 29% of the initial absorption, respectively, which was larger than the 7% with pH 7. The increase in the photocatalytic activity in acidic conditions is consistent with previous report.[77] Furthermore, as shown by the SEM images in the inset, the morphology of the GaN nanowires did not change following the photocatalysis experiments at pH 2. Thus, GaN nanowires exhibited excellent stability in acidic conditions, which suggests some important advantages over oxide nanostructures, which are not stable in acidic environments.[78,79] Furthermore, we investigated the degradation of the dye as a function of time. Figure A1b shows that $\ln(C/C_0)$ is linear with time, where C is the absorption of the dye solution as a function of time and C_0 is initial absorption, which indicates that the photocatalytic activity follows first-order kinetics. The rate constants for GaN grown on 2-, and 0.5-nm-thick Ni layers were 0.0063, and 0.0048 min^{-1}, respectively, as determined from the gradient of the curve shown in Figure A1b. The larger photocatalytic

activity of the GaN nanowires is attributed to the increased surface-to-volume ratio [4,20].

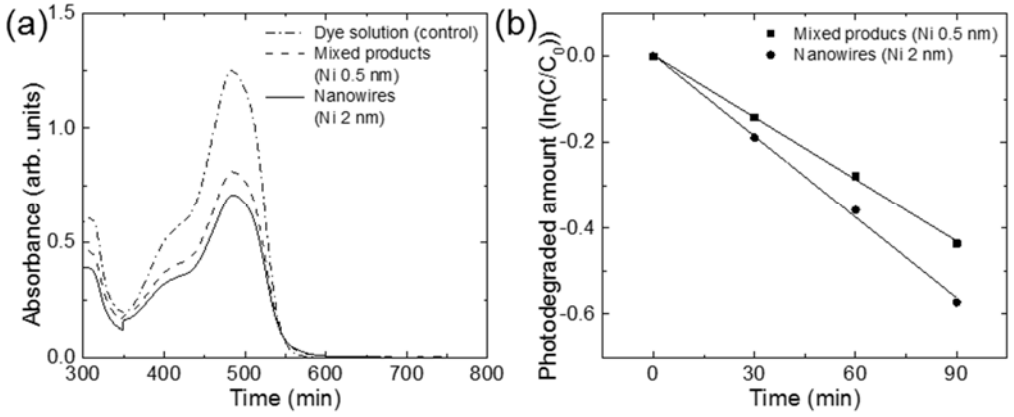

Fig. A1. (a) Absorption spectra of the dye solution photodegraded using GaN nanowires grown on Ni layers with different thicknesses. (b) A plot of the degradation as a function of the irradiation time.

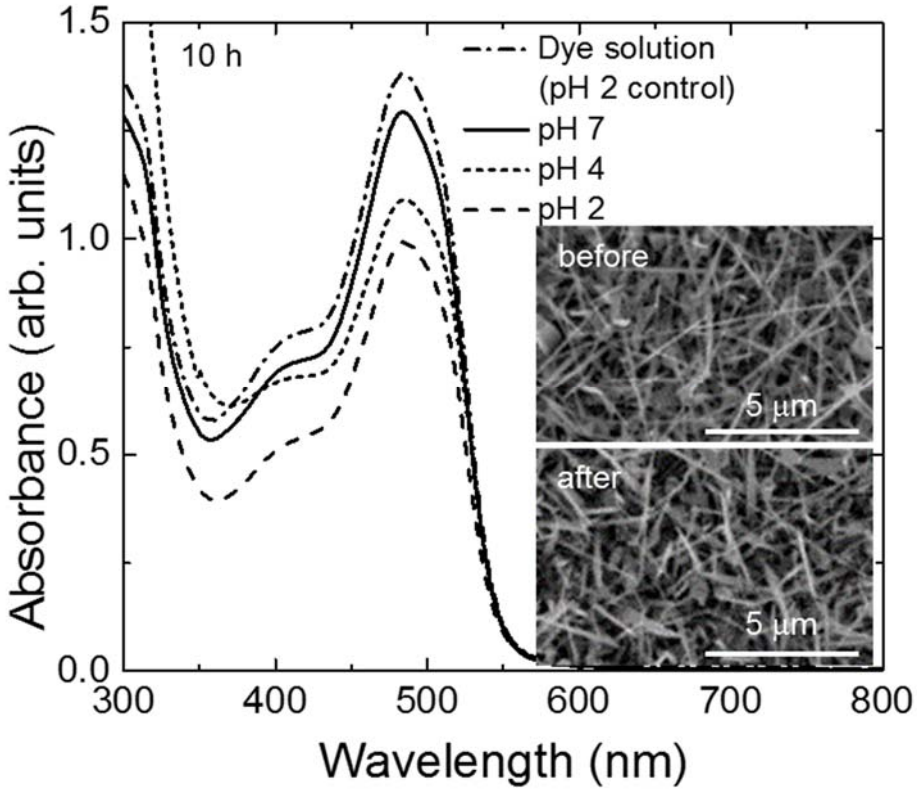

Figure A2. Absorption spectra of organic dye solution photodegraded by GaN nanowires under pH conditions of 2, 4, and 7.

In addition to the investigation of stable photocatalysis, GaN nanowires grown on the graphene substrate were transferred onto a 100-μm-thick PET film. PET is a common material that is widely used in the manufacture of plastic bottles. Figure A3a shows the photocatalytic activity of the GaN nanowires transferred onto the PET substrate, which was subsequently bended (inset of Fig. A3a), as well as the GaN nanowires on the SiO_2/Si substrate; both structures were of the same size (0.5 cm^2). The GaN nanowires that were transferred onto the PET substrate exhibited 34% photodegradation of the organic dye, whereas the GaN nanowires that remained on the SiO_2/Si substrate exhibited 45% photodegradation. This variation was attributed to differences in the angle of incidence of the UV light, due to the curvature. It appears that the GaN nanowires maintained their photocatalytic characteristics after transfer onto the PET substrate and deformation.

To evaluate the possibility of photocatalyst applications in which light is incident either from the front or back, the GaN nanowires were transferred onto a quartz substrate, which exhibited transmittance of approximately 90% at visible and UV wavelengths. Figure A3b shows the absorption spectra of the dye solutions that

were photodegraded with the light incident on the front side and the back side. The control here was a reference dye solution, which was degraded with no photocatalyst. Front-side UV irradiation resulted in degradation of 41% of the dye after 12 hours, whereas back-side illumination resulted in degradation of 27% of the dye (see Table A1). The reduced photocatalytic activity in the case of back-side illumination was most likely due to absorption by the graphene layer, which had a transmittance of less than 80%. This may be improved by using a thinner graphene layer. Although the photocatalytic activity under back-side illumination was reduced, this result suggests that the GaN nanowires grown on the graphene layer may be used to form photocatalytic devices that can be illuminated from multiple directions. Consequently, these GaN/graphene hybrid materials have potential applications in photocatalysts that can be illuminated from any direction with long-term stability and mechanical flexibility.

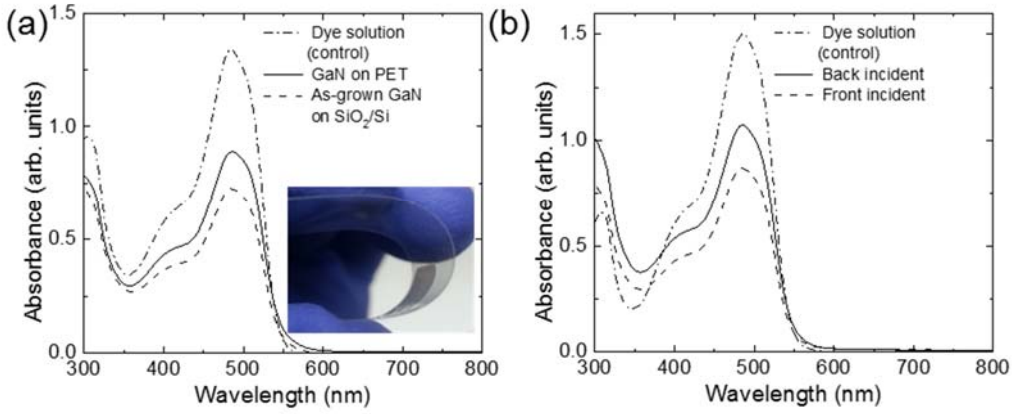

Fig. A3. (a) Typical absorption spectra of the organic dye solution photodegraded using GaN nanowires on a flat SiO_2/Si substrate and bended PET substrate. Inset of (a) is a photograph showing a bended specimen on PET substrates. (b) Typical absorption spectra of the organic dye solution photodegraded using GaN nanowires on quartz substrate under front and back side illumination.

TABLE 1. The photocatalytic activity of the GaN nanowires as the incident direction of the UV light was varied.

Sample description	**Absorbance at 486 nm (arbitrary unit)**	**Amount of dye photodegraded (%)**
Control	1.5	0
Front incident	0.88	41
Back incident	1.1	27

A.4. Summary

We have described a process to achieve the growth of GaN nanowires, together with a layer-transfer method, to produce flexible photocatalysts on polymer substrates. GaN nanowires were grown directly on large-area CVD-grown graphene and exhibited a high aspect ratio and large areal density, which was shown to depend strongly on the thickness of Ni catalyst layer used during the growth. The GaN nanostructures exhibited a single-crystal structure, with favorable structural properties, and PL measurements revealed well-resolved exciton emission peaks. The GaN nanowires exhibited photocatalytic activity that depended on the geometry and areal density. The photocatalytic activity was enhanced in an acidic environment, and transparent, flexible photocatalytic devices were demonstrated. These results show that the GaN nanowire and graphene hybrid nanostructures have potential applications in photocatalysis.

Summary in Korean

국문 요약문

반도체 나노소재의 단결정 소재 제작의 용이함과 고밀도 집적소자 제조로의 응용 가능성은 최근 십 수년간 많은 주목을 받아왔다. 그 중 1차원 나노소재는 높은 종횡비와 축방향 및 동축방향의 양자구조 제작 기술 발달에 힘입어 양자소자 제조에 있어 중요한 실험적 근거가 되어준다. 특히 쌓아가기 방식의 1차원 나노소재 배열 제조기술의 발견은 고밀도 소자 제조에 있어 기존 박막식각 방식에서는 해결하지 못했던 높은 종횡비와 고품질 단결정 확보 방법의 해결책을 제시했다. 쌓아가기 방식으로 제조되는 1차원 나노소재의 이러한 장점들인 3차원 입체 구조의 소자 제조 및 전통적인 실리콘 기반의 전자소자와의 결합에 있어 많은 시도를 유도했고, 이는 지금까지 이루어진 많은 실험적 증거의 원천이 되어왔다. 하지만, 기존의 나노소재 제조 방법은 실리콘과 사파이어로 대표되는 단결정 웨이퍼 상에서만 가능하다는 기술적 한계가 존재했고, 이는 유연성, 높은 전기 및 열 전도성, 광학적 투명성 등을 갖는 소재로의 응용에 큰 장애물이 되어왔다. 본 논문에서는 나노소재를 성장하기 위한 성장층으로 기존의 단결정 기판 대신 그래핀을 사용함으로써 위의 다양한 특성들을 갖는 나노소재 배열에 대한 배경기술을 개발하고자 하였다. 나노구조 화합물 반도체를 그래핀 위에 에피탁시 성장을 함으로써 형태와 위치가 정교하게 제어 된 고품질 반도체 나노소재를 다양한 기판 위에 성장할 수 있었으며, 이를 이용해 광소자 및 압력감지 소자 응용이 가능함을 입증했다.

연구의 과정으로는, 우선 다양한 방법으로 성장되는 서로 다른 반도체

나노구조의 그래핀 위에서의 성장형태를 관찰했다. 산화아연 나노구조와 질화갈륨 나노구조를 각각 비촉매 유기금속화학증착법 (MOCVD)와 금속 촉매를 이용한 기체-액체-고체 (VLS) 방식으로 그래핀 위에 성장해 봤으며, 그들의 결정구조와 광학적 특성을 각각 투과전자현미경 (TEM)과 광 발광분석 (photoluminescence, PL) 측정을 통해 분석했다. 그래핀 위에 성장된 산화아연 나노구조의 우수한 구조적 및 광학적 특성에 주목하여 이의 위치 및 형태조절 방법 개발에 집중하였으며, 비정질 산화막을 그래핀 위에 패턴하여 성장제어층으로 사용함으로써 수직으로 성장된 나노소재의 위치 및 형태를 정교하게 조절하는 것에 성공했다. 이렇게 성장된 1차원 나노소재/그래핀의 복합차원 물질은 기판에서 쉽게 탈착이 가능하고 임의의 기판으로 전사가 되면서도 높은 물리적 내구성을 보유하고 있어 유연성 소재의 제작이 가능하게 되었다. 이 새로운 나노소재의 소자로써의 응용 가능성을 확인하기 위해 산화아연의 압전특성을 이용한 압력감지 센서의 제작을 시도하였으며, 결과적으로 1차원 압전 나노구조물을 이용한 매우 높은 감도의 압력센서 제조에 성공하였다. 나노구조의 작은 단면적에 기반한 높은 압력반응 특성 및 높은 종횡비의 휘어지는 특성을 이용하여 1 Pascal 미만의 매우 작은 압력의 공기흐름마저 측정 가능한 민감한 압력센서의 제작이 가능했다. 이러한 발견은 단순히 압력센서 제작으로 귀결되는 것이 아니라, 다양한 나노소재 응용의 원천기술이 되는 새로운 플랫폼이 될 것이다.

Acknowledgements

24살의 갓 학사를 받고 연구를 시작한 제가 31살이 되어서 학위를 마치게 되었습니다. 학위과정에 많은 어려움이 있었고 내가 왜 이 길을 왔을까 후회도 많이 했지만, 주변 많은 분들의 도움으로 끝까지 올 수 있었습니다. 가장 먼저 이규철 교수님께 감사드립니다. 8년이 넘는 오랜 시간 동안 이쯤에서 포기할까 생각할 정도로 많은 어려움이 있었는데, 교수님의 지도 하에 여기까지 올 수 있었습니다. 여전히 많이 부족하지만, 앞으로도 노력하겠습니다. 김남중 교수님 감사합니다. 논문 한 줄 제대로 쓸 줄 모르던 제가 이나마 할 수 있게 된 것은 교수님의 친절한 가르침 덕분이었습니다. 매번 부탁만 드리는데도 항상 친절하게 도움 주셔서 정말 감사하면서도 죄송한 마음을 가지고 있습니다. 연구실 선배이신 유진경 박사님, 홍영준 교수님, 김용진 박사님, 이철호 교수님, 그리고 그 이전에 연구실에 계셨던 모둔 선배님들께 감사드립니다. 선배님들께서 마련해 두신 기반이 있었기에 이렇게 연구를 해올 수 있었습니다. 특히 실험적으로 많은 도움을 주신 홍영준 교수님과 이철호 교수님께 크게 감사드립니다. 같이 연구실 생활을 한 건욱이형, 재혁이형, 재현이형, 그리고 현준형, 실험에 대한 기초가 전혀 없던 저에게 많은 도움을 준 것에 대해 감사드립니다. 연구실 후배이자 동료들인 홍석이형, 민호형, 영빈형, 근동이, 준영이, 종우, 지영이, 동하, 그리고 근수형, 효빈이형, 장현이에게 감사합니다. 긴 시간동안 여러분들이 있었기에 그래도 버틸 수 있었던 것 같습니다. 혜진누나, 희나씨, 현주씨도 실험에 많은 도움을 받았습니다. 마지막으로 긴 박사과정동안 항상 응원을 주고 휴식이 되어준 가족들에게 진심으로 감사의 말씀을 전합니다.

Curriculum Vitae

PERSONAL INFORMATION

Name: Jun Beom Park
Born: Seoul, Korea (April 24, 1988)
E-mail: s.jbpark@gmail.com, junbumi@snu.ac.kr

EDUCATION

Seoul National University, Seoul, Korea
Ph.D. in Physics (M.S/Ph.D. combined course)
* Advisor: Prof. Gyu-Chul Yi — Mar. 2010 – Aug.2018

Seoul National University, Seoul, Korea
B.A. in Physics
Mar. 2006 – Feb. 2010

AWARD AND SCHOLARSHIP

Seoul Science Fellowship — Mar. 2011 – Feb.2013
Korea Physics Society Encouragement Award — Sep. 2017

RESEARCH INTERESTS

- Semiconductor nanostructure growth on CVD-graphene films
- Piezoelectric properties of ZnO nanostructures
- Applications of semiconductor nanostructures and its heterostructures for LED, capacitors, and sensors
- Flexible devices based on 1D nanostructures/graphene hybrid system.

EXPERIMENTAL EXPERIENCE AND SKILLS

• **Material Growth**

1) Metal-organic chemical vapor deposition (MOCVD)

- ZnO nanostructures (non-catalytic method) on graphene and sapphire substrates
- GaN nanowires (VLS method) on graphene and sapphire substrates

2) Wet-chemical method (hydrothermal)

- ZnO nanorods on glass and plastic substrates

• **Material Characterizations**

- Surface morphological characterizations: SEM, AFM, FIB
- Optical characterization: PL, EL,
- Structural characterization: XRD, TEM
- Nano-electrical characterization: c-AFM & impedance analyzing for single-nanotube capacitor and piezoelectric nanowires.

• **Semiconductor processing**

- Lithography process: Photo & e-beam lithography machine, reactive ion etch
- CMOS process: RIE, RTA, metallization, ALD, sputtering, PECVD

PUBLICATIONS

"Scalable ZnO nanotube arrays grown on CVD-graphene films"
J. B. Park, H. Oh, J. Park, N.-J. Kim, H. Yoon, and G.-C. Yi, APL Materials, **4**, 106104 **2016**

"Metal-catalyst-assisted growth of GaN nanowires on graphene films for flexible photocatalyst applications"

J. B. Park, N.-J. Kim, Y.-J. Kim, S.-H. Lee, G.-C. Yi, *Current Applied Physics*, 14, 111437 **2014**

“Vertical ZnO Nanotube Transistor on Graphene Film for Flexible Inorganic Electronics”
H. Oh**, J. B. Park**, W. Choi, H. Kim, Y. Tchoe, A. Agrawal and G.-C. Yi, *Small*, 14, 1800240 (2018)

“ZnO nanolasers on graphene films”
H. Baek, **J. B. Park**, J. Park, J. K. Hyun, H. Yoon, H. Oh, and J. Yoon, *Applied Physics Letters*, 108, 263102 **2016**

“Microtube Light-Emitting Diode Arrays with Metal Cores”
Y. Tchoe, C.-H. Lee, **J. B. Park**, H. Baek, K. Chung, J. Jo, M. Kim, G.-C. Yi, *ACS Nano*, 10, 3, 3114, **2016**

"Controlled growth of inorganic nanorod arrays using graphene nanodot seed layers"
Y.-J. Kim, S.-S. Kim, **J. B. Park**, B.-H. Sohn, and G.-C. Yi, *Nanotechnology,* 25, 135609 **2014**

"High-Resolution Observation of Nucleation and Growth Behavior of Nanomaterials Using a Graphene Template"
J. Jo, H. Yoo, S.-I. Park, **J. B. Park**, S. Yoon, M. Kim, G.-C. Yi, *Advanced Materials,* 26, 132011 **2014**

"GaN nanowire/thin film vertical structure p-n junction light-emitting diodes"
Y. J. Hong, C.-H. Lee, **J. B. Park**, S. J. An, G.-C. Yi, *Applied Physics Letters,* 103, 261116 **2013**

"Geometry Induced Dislocations in Coaxial Heterostructural Nanotubes"

A. Yoon, J. Y. Park, J.-M. Jeon, Y. Cho, **J. B. Park**, G.-C. Yi, K. H. Oh, H. N. Han, M. Kim, *Small*, 9, 132255 **2013**

"Position- and Morphology-Controlled ZnO Nanostructures Grown on Graphene Layers"
Y.-J. Kim, H. Yoo, C.-H. Lee, **J. B. Park**, H. Baek, M. Kim, G.-C. Yi, *Advanced Materials*, 24, 415565 **2012**

"*Gallium nitride nano structures for light-emitting diode applications*"
M. S. Kang, C.-H. Lee, **J. B. Park**, H. Yoo, G.-C. Yi, *Nano Energy*, 1(3), 391 **2012**

INTERNATIONAL CONFERENCE PRESENTATIONS

[Talk] "F*lexible shear force sensor arrays using position- and morphology-controlled ZnO nanotubes grown on graphene films*", **J. B. Park**, Y. Tchoe, H.-H. Kim, and G.-C. Yi, 59th Electronic Materials Conference, Southbend, IN, USA, 2017

[Talk] *"Scalable ZnO Nanotube Arrays Grown on CVD-graphene Films for Flexible Device Applications"*, **J. B. Park**, J. Park, J. Yoon, and G.-C. Yi, IWZnO2016, Taipei, Taiwan **2016**

[Talk] *"Scalable ZnO nanotube array on CVD-graphene "*, **J. B. Park**, H. Oh, J. Park, N.-J. Kim, H. Yoon, and G.-C. Yi, KPS, Daejeon, Korea **2016**

[Talk] *"Position- and Morphology-Controlled ZnO Nanostructures Grown on Graphene Layers"*, **J. B. Park**, Y.-J. Kim, H. Yoo, C.-H. Lee, H. Baek, M. Kim, G.-C. Yi, ISPSA-XVI, Jeju, Korea **2013**

[Poster] "*Individually addressable nanotube pressure sensor array*", **J. B. Park** and G.-C. Yi, ICAMD2015, Jeju, Korea, 2017

[Poster] "*Scalable ZnO nanotube arrays grown on CVD-graphene films*", **J. B. Park,** J. Park, N.-J. Kim, H. Yoon, and G.-C. Yi, MRS Fall, Boston, USA, 2016

[Poster] "*Position-controlled semiconductor nanotube arrays grown on graphene films for integrated devices*", **J. B. Park** and G.-C. Yi, ICAMD2015, Jeju, Korea, 2015

PATENTS (REGISTERED)

"SEMICONDUCTOR LIGHT EMITTING DEVICE", 1013359450000

"PHOTOCATALYST INCLUDING CARBON LAYER SUBSTRATE", 1013196610000

"촉각정보 제공 장치", KR 10-2016-0057600